ABSTRACT

PORTER, HUGH LAWSON, IV. Thin film growth and doping characteristics of ZnO and β-Ga_2O_3. (Under the direction of Professors Jagdish Narayan and John F. Muth)

ZnO films have been prepared through both pulsed laser deposition (PLD) and pulsed electron deposition (PED). The films grown through PLD have been co-doped with tellurium and nitrogen to compensate for ZnO's natural *n*-type behavior and have been shown to be highly resistive. A discussion of the isoelectronic impurity, tellurium, and the *p*-type impurity, nitrogen, and their compensating mechanisms is given. A Kaufman ion source was used to incorporate atomic nitrogen into ZnO films, and the impact of N_2^+ ions with the ZnO film is proposed as the cause of breaking the nitrogen molecules into individual atoms. Tellurium has been incorporated into the films by mixing a small amount of ZnTe in the source material. The films are not strongly *p*-type, but resistivity and photoconductive responsivity have been shown to increase with doping concentration, suggesting donor compensation and more intrinsic films. There appears to be an optimal percentage of incorporated tellurium of 0.5%, at which both of these properties are at a maximum, and this is suggested to be a solubility limit for this process. Time-resolved photoluminescence shows a much shorter excess carrier life-time in the doped films, which implies that the enhanced photoconductivity is indeed due to the films being more intrinsic.

Epitaxial β-Ga_2O_3 has been prepared through pulsed electron deposition. The epitaxial growth relationship is given, and shown to be due to domain matching epitaxy. X-ray diffraction (XRD), and high resolution transmission electron microscopy (HR-TEM) confirm the relationship between film and substrate. Finally, optical absorption measurements provide an optical band gap of 4.96 eV.

THIN FILM GROWTH AND DOPING CHARACTERISTICS OF ZnO AND β-Ga_2O_3

By

Hugh L. Porter

A dissertation submitted to the Graduate Faculty of North Carolina State University in partial fulfillment of the requirements for the Degree of Doctor of Philosophy

DEPARTMENT OF ELECTRICAL AND COMPUTER ENGINEERING

Raleigh, NC
2005

Approved By:

_____	_____
Professor John F. Muth Co-chair of Advisory Committee	Professor Jagdish Narayan Co-chair of Advisory Committee
_____	_____
Professor Robert M. Kolbas	Professor Veena Misra

DEDICATION

For my parents,

Hugh and Louise Porter,

And for my wife,

Ailing Cai

BIOGRAPHY

Hugh Lawson Porter, IV, was born on August 28, 1968, in Neptune, New Jersey. In May of 1991, he received a Bachelor's of Science in Mechanical Engineering from Rennselaer Polytechnic Institute in Troy, New York. After graduation, he worked as a mechanical engineer for a while, but returned to graduate school in August of 1998 to study materials science. In May of 2000, he received a Master's of Science in Materials Science from Southwest Missouri State University in Springfield, Missouri. Hugh began his Ph.D. studies at North Carolina State University in August of 2000. His research has been performed under the advisement of Dr. J. Narayan of the Department of Materials Science and Engineering, and Dr. J. Muth of the Department of Electrical and Computer Engineering. Hugh defended his thesis in January of 2005.

ACKNOWLEDGMENTS

I would like to thank Drs. Narayan and Muth for guiding my research, and helping give me an inside view of the research process. The many hours they have spent with me, and the patience they have shown throughout the process, have been fundamental to my education and development as a scientist. I am also grateful for the support and guidance I have received from Dr. Kolbas and Dr. Misra over the last few years. Also, Dr. Henry Everitt of Duke University has been very generous with his time and resources. I would also like to thank my fellow graduate students—Ailing Cai, Mason Reed, Meredith Reed, Amit Chugh, Abhishek Gupta, Thomas Rawdanowicz, Jason Haverkamp, Shivaraman Ramachandran, Chunming Jin, Honghui Zhou, Haiyan Wang, Christian Mion, Andrew Oberhofer, Xiyao Zhang, and John Foreman—for their friendship and support. In particular, much gratitude is owed to my wife, Ailing Cai, for always being with me throughout the process, and enduring the times when I have been less than inspired. And finally I would like to thank the faculty, technicians, post-docs, and administrative staff at North Carolina State University for their time and expertise.

TABLE OF CONTENTS

Page

LIST OF TABLES

Page

LIST OF FIGURES

Page

1.0 Introduction

In this thesis, the wide band gap semiconductors, ZnO and β-Ga_2O_3, will be investigated. Most of the work will focus on ZnO, and its doping and photoconductive characteristics. There will also be a short discussion on epitaxial growth of β-Ga_2O_3, and its role in future wide band gap semiconductor applications. Together these materials represent examples of wide band gap semiconductors that are frequently considered for applications to ultraviolet (UV) opto-electronic devices.

The first semiconductor device was a transistor built in 1947 by William Shockley, John Bardeen, and Walter Brattain at AT&T's Bell Laboratories in New Jersey. The device was built out of germanium, and for several years afterwards, germanium was the dominant semiconductor material.

In the early 1960's silicon replaced germanium as the semiconductor of choice for most applications. The reason was that silicon had a slightly larger band gap, which lowered the leakage current in the device. Also, with silicon it is possible to grow an atomically abrupt oxide layer. This cannot be done with germanium, and it is critical for many device applications.

For opto-electronic devices, none of the first three Group IV elements are suitable. The reason is because they all have indirect band gaps, and indirect band gaps do not make efficient light emitters. Direct band gaps are needed for opto-electronic devices, and semiconductors with direct band gaps usually must be formed from III-V or II-VI compound materials.

The first light emitting diode to emit light in the visible spectrum was invented in 1962 by Nick Holonyak.[1-2] To get the right band gap to emit red light, gallium arsenide was alloyed with gallium phosphide.

In subsequent decades, the desire to produce light throughout the visible spectrum motivated research into materials with wider and wider band gaps, such as GaP for amber and yellow LED's, and InGaN for green LED's. Eventually the visible spectrum was completed, as it became possible to make blue and ultraviolet LED's and laser diodes out of the III-V compound, GaN.[3]

ZnO is a II-VI semiconductor compound with many properties, such as band gap and wurtzite crystal structure similar to GaN. In recent years, ZnO has not received the same attention as GaN, however, due to recent advances in fabricating *p*-type GaN, compared to the difficulty in doping ZnO *p*-type. However, ZnO has been useful in its polycrystalline form.[4] Such polycrystalline applications include surface acoustic wave devices, varistors, phosphors, and transparent conducting films. ZnO is probably best known for its use in some cosmetic products, such as sunscreen and baby powder.

Recent advances in growing single-crystal, epitaxial ZnO have sparked new interest in this material for opto-electronic applications.[5-8] There are a variety of methods for growing single-crystal ZnO, such as molecular beam epitaxy (MBE),[9] metal-organic chemical vapor deposition (MOCVD),[10] vapor transport,[11] and finally pulsed laser deposition (PLD).[5-8] But for the present work, and the cited studies, we will focus mostly on pulsed laser deposition (PLD).

The types of applications for which GaN and ZnO are receiving this attention include bipolar opto-electronic devices operating in the near UV, such as light-emitting

diodes (LED's), laser diodes for CD-ROM and DVD memories, laser printers, and UV photo-detectors.[12] The wide band gaps of these materials make them particularly suited for these types of applications, since with shorter wavelengths smaller spots can be formed, resulting in a higher bit density on optical storage media. Also, because of the wide band gap, these materials typically have high break down voltages, and high electron mobility, and are potentially good for fabricating high power transistors.[13-14]

ZnO is an inorganic compound formed from a Zn^{2+} cation reacted with an O^{2-} anion. Thus, it is often referred to as a II-VI compound, since its cation, zinc, is a Group II element on the periodic table, and its anion, oxygen, is a Group VI element on the periodic table.

With lattice constants of a = 3.25 Å and c = 5.21 Å, zinc oxide grows in the wurzitic crystalline state.[15] (See Figure 1-1). Thus, its crystal structure is composed of two inter-penetrating hexagonal close-packed (HCP) lattices, off-set by some fraction of lattice constant in the c-direction. One of the HCP lattices is populated entirely by zinc atoms, and the other is populated entirely by oxygen atoms. Thus, each atom in the crystal has a coordination number of four, with each of its four nearest neighbors being an atom of the opposite type.

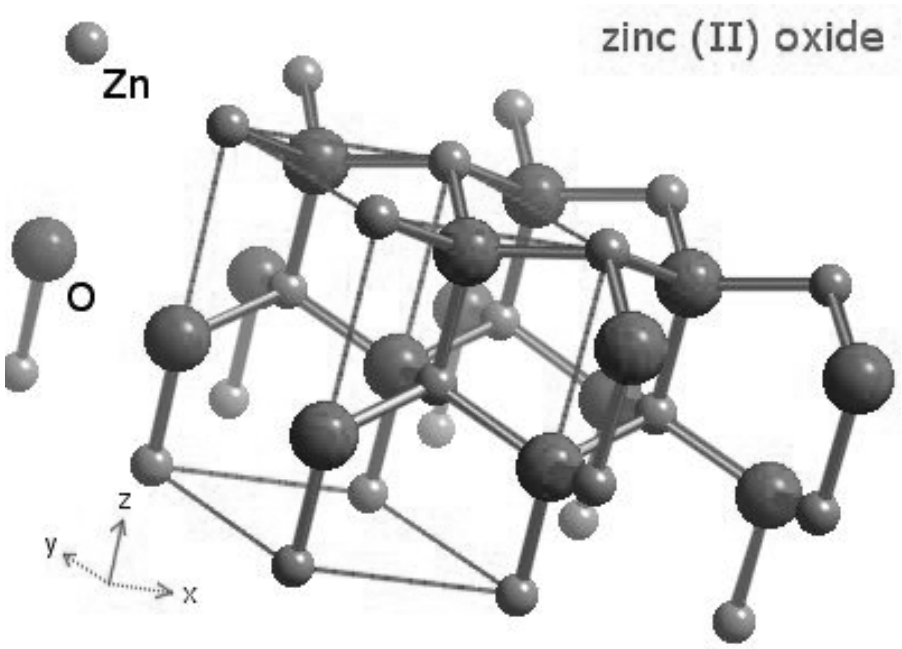

Fig. 1-1 The wurzite crystal structure of zinc oxide.[16] Due to the ionic nature of zinc oxide, the O^{2-} atoms are slightly larger than the Zn^{2+} atoms.

ZnO is often compared to GaN, because of their similar properties. (See Table 1-1). Thus, they are considered for similar applications. ZnO has a number of advantages over GaN including a higher excitonic binding energy, (60 meV as compared to 24 meV for GaN), which makes ZnO a brighter light emitter. Unlike GaN, ZnO can be grown in bulk, and can be used as its own substrate. Also, ZnO is compatible with wet etchants, and does not need dry etching, like GaN does. And finally, ZnO has a high radiation resistance.[17]

Parameter	GaN	AlN	InN	6H-SiC	Si	GaAs	Sapphire	ZnO
Symmetry	Wurtzite	Wurtzite	Wurtzite	Wurtzite	Diamond	Cubic	Corundum	Wurtzite
Native Substrate	No	No	No	Yes	Yes	Yes	---	Yes
Lattice Constant (a)	3.189	3.112	3.548	3.081	5.431	5.653	4.758	3.252
Lattice Constant (c)	5.185	4.982	5.76	15.117	---	---	12.99	--
Band Gap Energy (eV)	3.4	6.2	1.89	3.03	1.12	1.42	9.0	3.34
Band Gap Transition	Direct	Direct	Direct	Indirect	Indirect	Indirect		Direct
	ε_{xy} = 10.4	8.5	15.3	9.66	11.99	13.1	10	ε_0 = 8.59
	ε_z = 9.5							$\varepsilon_{infinity}$ = 4.0
Break Down Field (MV/cm)	>3	---	---	3	0.3	0.4	--	--
Electron Effective Mass	0.22	0.33	0.11	0.45	0.98	0.067	---	1
Hole Effective Mass	0.8	---	---	1.2	0.49	0.45	---	0.59
Exciton Effective Radius (Ang)	32	---	---	---	---	125	---	~17
Exciton Reduced Mass	0.173-0.180 m_0	---	---	---	---	0.058 m_0	---	~0.1437 m_0
LO Phonon Energy (meV)	91	---	---	---	---	36	---	72
electron mobility (cm^2/(V-sec)		---	---	---	---	8500	--	--
Saturation Velocity (10^7 cm/s)	2.5	---	2.5	2	1	2	--	--
	cf 8	---	---	---	---	degenerate	---	cf 39.5
	so 21	---	---	---	---	350	---	so -3.5
Melting Point °C	>1700	3000	1100	2830	1414	1238	2050	1975
Density (g/cm^3)	6.15	3.23	6.81	3.21	2.33	5.32	3.98	5.61
Index of Refraction	2.33	2.2	2.85-3.0	2.6-2.7	4	3.43	1.77	1.85

Table 1-1 A comparison of several of the fundamental properties of various materials used in wide band gap, optoelectronic applications.

GaN is the dominant material for blue opto-electronic devices with millions of LED's produced monthly.[18] Repeatable, high-quality *p*-type ZnO, that could be considered device-quality, has only recently been reported.[19] This lack of understanding of the *p*-type behavior of ZnO is what has motivated much of present study, and will be discussed in greater detail in the next chapter.

A complimentary material for GaN and ZnO is β-Ga_2O_3, which is currently being investigated for use as a transparent conductor for electrical contacts in opto-electronic devices.[20] With its wide band gap of nearly 5 eV,[21] it is transparent to any light generated by ZnO or GaN devices, and it can therefore be used as a transparent conducting electrode to many wide band gap devices.

The as grown material is usually very high in resistivity, but doping with tin has produced very conductive *n*-type material with conductivities around 8 S cm^{-1}.[22-23] The crystal structure is monoclinic with $a = 12.23 \pm 0.02$ Å, $b = 3.04 \pm 0.01$ Å, $c = 5.80 \pm 0.01$ Å, and $\beta = 103.7 \pm 0.3^{o}$, and the space group is C2/*m*(C_{2h}^3).[24]

1.1 References

1. J. Holonyak, N. and S. F. Bevacqua, "Coherent (visible) light emission from $GaAs_{1-x}P_x$ junctions," *Applied Physics Letters*, vol. 1, pp. 82-83, 1962.
2. N. J. Holonyak, "From transistors to light emitters," *IEEE Journal on Selected Topics in Quantum Electronics*, vol. 6, pp. 1190-1200, 2000.
3. S. Nakamura, G. Fasol, and S. J. Pearton, *The Blue Laser Diode*, 1st ed.: Springer-Verlag Telos, 1997.

4. D. C. Look, "Recent advances in ZnO materials and devices," *Materials Science and Engineering B-Solid State Materials for Advanced Technology*, vol. 80, pp. 383-387, 2001.

5. A. K. Sharma, K. Dovidenko, S. Oktyabrsky, D. E. Moxey, J. F. Muth, R. M. Kolbas, and J. Narayan, "Growth of high quality single, crystal ZnO films on sapphire by pulsed laser ablation," presented at Advances in Laser Ablation of Materials. Symposium, 13-16 April 1998, San Francisco, CA, USA, 1998.

6. R. D. Vispute, V. Talyansky, Z. Trajanovic, S. Choopun, M. Downes, R. P. Sharma, T. Venkatesan, M. C. Woods, R. T. Lareau, K. A. Jones, and A. A. Iliadis, "High quality crystalline ZnO buffer layers on sapphire (001) by pulsed laser deposition for III-V nitrides," *Applied Physics Letters*, vol. 70, pp. 2735, 1997.

7. J. Narayan, K. Dovidenko, A. K. Sharma, and S. Oktyabrsky, "Defects and interfaces in epitaxial ZnO/α-Al_2O_3 and AlN/ZnO/α-Al_2O_3, heterostructures," *Journal of Applied Physics*, vol. 84, pp. 2597-2601, 1998.

8. Y. Segawa, A. Ohtomo, M. Kawasaki, and H. Koinuma, "Growth of ZnO Thin Film by Laser MBE: Lasing of Exciton at Room Temperature," *Physica Status Solidi (B): Basic Research*, vol. 202, pp. 669, 1997.

9. Y. Chen, D. M. Bagnall, H.-j. Koh, K.-t. Park, K. Hiraga, Z. Zhu, and T. Yao, "Plasma assisted molecular beam epitaxy of ZnO on c-plane sapphire: growth and characterization," *Journal of Applied Physics*, vol. 84, pp. 3912, 1998.

10. Y. Liu, C. R. Gorla, S. Liang, N. Emanetoglu, Y. Lu, H. Shen, and M. Wraback, "Ultraviolet detectors based on epitaxial ZnO films grown by MOCVD," *Journal of Electronic Materials*, vol. 29, pp. 69-74, 2000.

11. D. C. Look, D. C. Reynolds, J. R. Sizelove, R. L. Jones, C. W. Litton, G. Cantwell, and W. C. Harsch, "Electrical properties of bulk ZnO," *Solid State Communications*, vol. 105, pp. 399-401, 1998.

12. D. C. Look, D. C. Reynolds, C. W. Litton, R. L. Jones, D. B. Eason, and G. Cantwell, "Characterization of homoepitaxial p-type ZnO grown by molecular beam epitaxy," *Applied Physics Letters*, vol. 81, pp. 1830-1832, 2002.

13. K. Shiojima, T. Makimura, T. Kosugi, S. Sugitani, N. Shigekawa, H. Ishikawa, and T. Egawa, "High-power AlGaN/GaN dual-gate high electron mobility transistor mixers on SiC substrates," *Electronics Letters*, vol. 40, pp. 775-776, 2004.

14. W. Saito, Y. Takada, M. Kuraguchi, K. Tsuda, I. Omura, and T. Ogura, "Design and demonstration of high breakdown voltage GaN high electron mobility transistor (HEMT) using field plate structure for power electronics applications," *Japanese Journal of Applied Physics, Part 1: Regular Papers and Short Notes and Review Papers*, vol. 43, pp. 2239-2242, 2004.

15. D. P. Norton, Y. W. Heo, M. P. Ivill, K. Ip, S. J. Pearton, M. F. Chisholm, and T. Steiner, "ZnO: Growth, doping and processing," *Materials Today*, vol. 7, pp. 34-40, 2004.

16. http://www.webelements.com, "zinc (II) oxide," 2004.

17. D. C. Look, C. Coskun, B. Claflin, and G. C. Farlow, "Electrical and optical properties of defects and impurities in ZnO," *Physica B-Condensed Matter*, vol. 340, pp. 32-38, 2003.

18. S. Nakamura, T. Mukal, M. Senoh, and N. Iwasa, "Thermal annealing effects on P-type Mg-doped GaN films," *Japanese Journal of Applied Physics, Part 2: Letters*, vol. 31, pp. 139-142, 1992.

19. D. C. Look and B. Claftin, "P-type doping and devices based on ZnO," *Physica Status Solidi B-Basic Research*, vol. 241, pp. 624-630, 2004.

20. N. Ueda, H. Hosono, R. Waseda, and H. Kawazoe, "Synthesis and control of conductivity of ultraviolet transmitting β-Ga_2O_3 single crystals," *Applied Physics Letters*, vol. 70, pp. 3561-3563, 1997.

21. H. H. Tippins, "Optical Absorption and Photoconductivity in the Band Edge of β-Ga_2O_3," *Physical Review*, vol. 140, pp. A316-A319, 1965.

22. M. Orita, H. Hiramatsu, H. Ohta, M. Hirano, and H. Hosono, "Preparation of highly conductive, deep ultraviolet transparent β-Ga_2O_3 thin film at low deposition temperatures," *Thin Solid Films*, vol. 411, pp. 134-139, 2002.

23. J. Frank, M. Fleischer, and H. Meixner, "Gas-sensitive electrical properties of pure and doped semiconducting Ga_2O_3 thick films," *Sensors and Actuators, B: Chemical, Proceedings of the 1997 Eurosensors XI Conference. Part 4 (of 4), Sep 21-24 1997*, vol. B48, pp. 318-321, 1998.

24. S. Geller, "Crystal Structure of β-Ga_2O_3," *The Journal of Chemical Physics*, vol. 33, pp. 676-684, 1960.

2.0 Review of the Literature

2.1 Problem of doping ZnO *p*-type

For elemental semiconductors, such as silicon or germanium, pure semiconductor materials tend to be electrically intrinsic. Only after adding an extrinsic dopant, such as boron or phosphorous, does it become *n*-type or *p*-type. The doping behavior of these types of materials is widely understood, and easily controlled. Also, a wide variety of doping methods exist, including diffusion, ion implantation, and *in situ* doping with epitaxial growth. In fact, it is very common in bipolar devices, for example, to dope and redope the same silicon crystal from *n*-type to *p*-type and back again during the processing of the device.

However, compound semiconductors, especially those with wide band gaps, pose special challenges. Dopants for these materials can be amphoteric, meaning the position of the dopant atom on the cation or anion lattice site can result in it acting as either an *n*-type or *p*-type impurity. Also, compound semiconductor materials almost always have very small stoichiometry imbalances between their cation constituent and anion constituent which result in the material tending to be *n*-type or *p*-type, even before the introduction of extrinsic impurities.[1] This tendency for the material to be *n*-type or *p*-type, as grown, can make it very difficult to dope the material for the opposite type.

In the case of ZnO, the crystal almost always has a deficiency of oxygen, because oxygen is the lighter of the two materials, and has a higher vapor pressure during crystal growth. ZnO is partially ionic, as are all compound semiconductors. Charge balance

thus requires the resulting zinc rich material to be *n*-type. This is illustrated in Figure 2-1-a, where a diagram is given of a charge-balanced ZnO crystal that has a perfect balance in its stoichiometry. Such a material would be intrinsic in its electrical behavior. In Figure 2-1-b, a diagram is drawn with one oxygen atom removed. The requirement for the crystal to be charge-balanced must still be met. Since the oxygen had negative charge associated with it when it was in the ionic crystal, that same negative charge must be left behind after the oxygen leaves the crystal. The left-behind negative charge has no localized state confining it, and will therefore end up in the conduction band, making the crystal *n*-type.

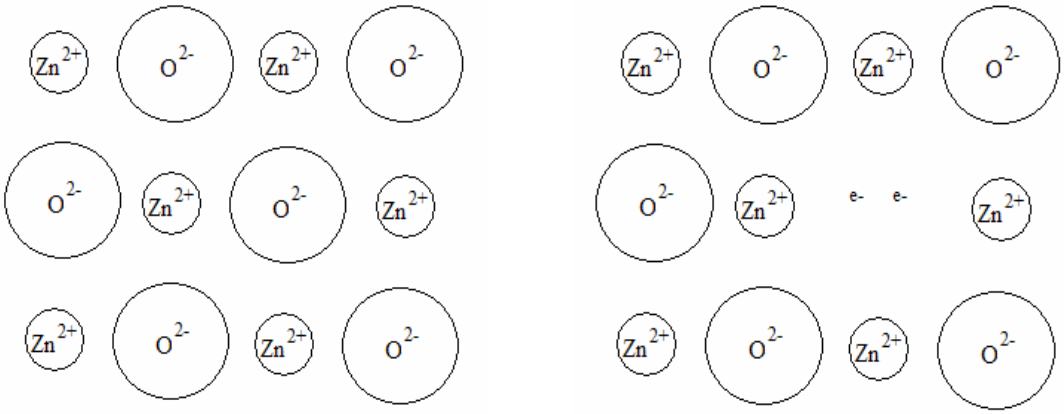

Fig. 2-1. A two-dimensional schematic representation of a ZnO crystal, a) with perfect stoichiometry, and b) with an oxygen vacancy.[2]

Nevertheless, stoichiometric imbalances are not an insurmountable challenge. GaAs has a natural stoichiometric imbalance, but it has been feasible to grow both *n*-type and *p*-type GaAs for decades.[3] The difference with materials such as ZnO is the very wide band gap. Wider band gap materials are harder to dope for several reasons. First, the Fermi levels must be shifted from the intrinsic, or undoped, level, by a larger amount than they do in narrower band gap materials. The large amount by which the Fermi level

must be shifted makes it energetically favorable for self-compensating defects to form. These self-compensating defects offset the extrinsic dopant, and keep the Fermi level from moving too much from its natural position.[4] The chemical potential of adding each additional charge carrier to the doped material adds to the total energy of the system, and that energy can be relaxed with the formation of a self-compensating defect. We can express this mathematically by writing:[5]

$$\Delta H(\alpha, q) = (Const.) \pm qE_f$$

where $\Delta H(\alpha,q)$ represents the formation energy of a self-compensating defect; E_f is measured from the valence band maximum; the constant is some amount of energy associated with each particular type of self-compensating defect; and the sign on q depends on whether an acceptor-like defect is forming or a donor-like defect is forming. Thus if the constant term is on the order of the band gap of the material there may be a point at which the formation energy of a self-compensating defect falls to zero, and the material may not be doped further. (For ZnO the Zn-O bond strength is a modest 1.65 eV per bond. Thus, the energy of formation for a defect need not be very high for self-compensating defects to form.) The energy at which this happens is labeled E_{pin}. Thus we can write:[5]

$$E_{pin}^{p} \leq E_f \leq E_{pin}^{n}$$

which suggests that the actual Fermi energy, E_f, may not exceed the limits of the E_{pin}. These theoretical extrema for the Fermi energy are illustrated for a variety of II-VI semiconductors in Figure 2-2. Here it is shown that the materials where the conduction band is closer to the vacuum level tend to be the materials that are hard to dope *n*-type, and the materials where the valence band is farther from the vacuum level tend to be the

materials that are hard to dope *p*-type. Thus it is suggested that the theoretical extrema for the Fermi energies are independent of the material.

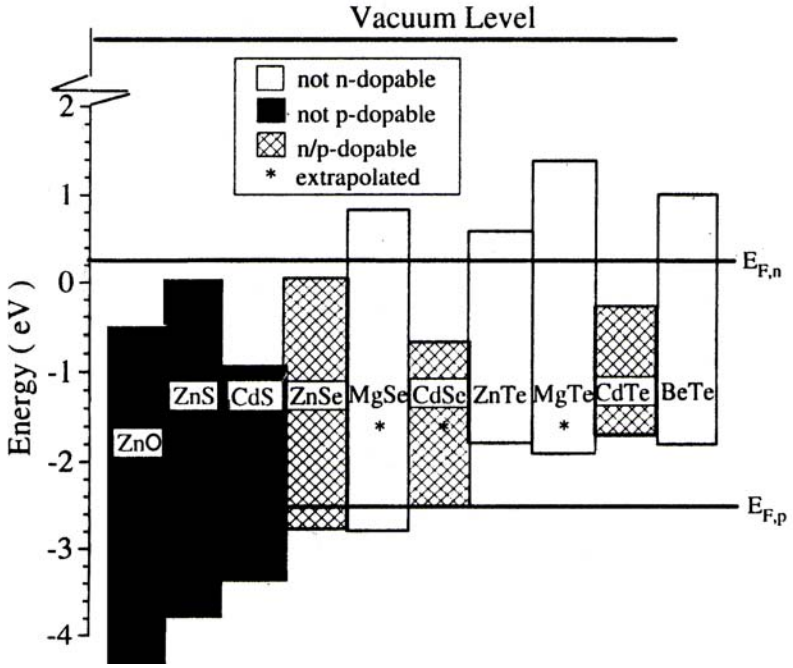

Fig. 2-2. The band gaps of several II-VI compounds, as compared with the vacuum level.[6] The energy reference is taken as the conduction band minimum of ZnS. The solid lines, labeled $E_{f,n}$ and $E_{f,p}$, represent the theoretical limits at which self-compensating defects should form if the Fermi level could be shifted to that level.

To make silicon either *n*-type or *p*-type, the Fermi level need only be moved by about 0.5 eV, either up or down. For ZnO, however, since the pure material is already *n*-type, the Fermi level is already near the conduction band. And since the band gap of 3.4 eV is three times greater than that of silicon, the Fermi level must move about 3 eV, or almost six times as far as is necessary in silicon, to make the material *p*-type. Even in the hypothetical case, if a perfectly constructed ZnO crystal could exist, with a Fermi level right in the center of the band gap, a 1.5 eV shift in Fermi energy would still be required

to make the material *p*-type. All of this extra energy will give the crystal more of a thermodynamic incentive to form self-compensating defects to resist the change.

A second way to view the challenge of doping wide band gap semiconductors is to consider what the wider band gap is doing to the impurity levels within the band gap. In Figure 2-3, a graphic illustration is given of what tends to happen to acceptor levels in wider band gap materials. The wider band gap will tend to result in everything within the band gap being spaced further apart, including the space between the valence band and the acceptor levels. Silicon provides an example of a narrow gap material, where E_g = 1.1 eV, and E_A = 45 meV (boron). And GaN provides an example of a wide gap material, where E_g = 3.4 eV and E_A = 200 meV (magnesium). Also, the *p*-type carrier concentration has an exponential relationship with the acceptor level/valence band energy difference, demonstrating that wider gap materials will tend to have only a small percentage of carriers thermalized for a given impurity concentration.

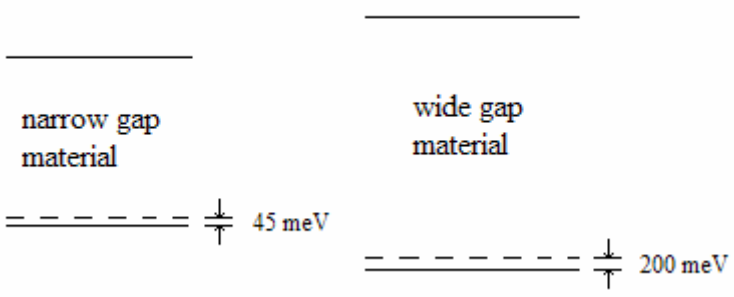

Fig. 2-3. A comparison of a typical narrow band gap material with a wider band gap material illustrating a proportionally increased difference between the acceptor level and the valence band.

This relationship is also observed experimentally.[7] In Figure 2-4, the measured electron concentrations are plotted versus the aluminum concentration in $Al_xGa_{(1-x)}N$ alloys that were grown under identical conditions. Since the band gap is close to being a

linear function of aluminum concentration, and since the y-axis is plotted logarithmically, we can see that the doping efficiency is exponentially related to band gap.

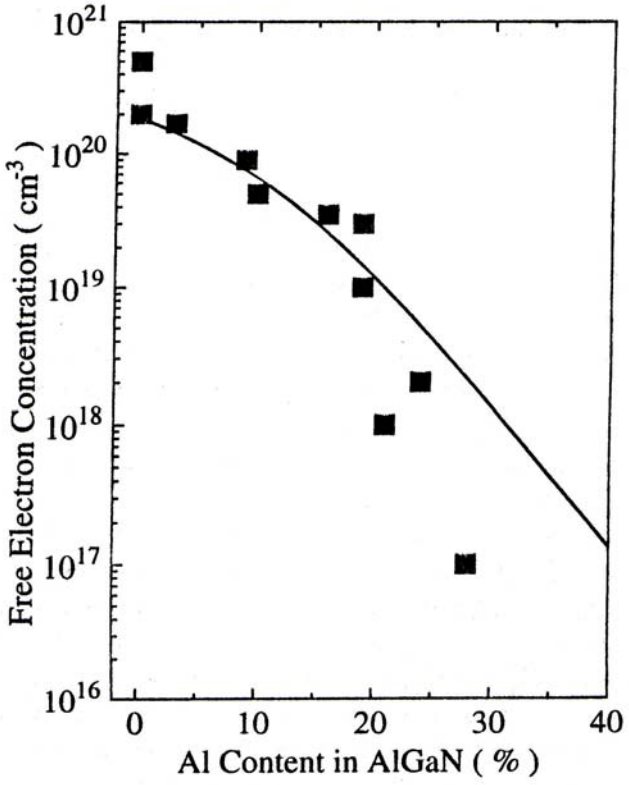

Fig. 2-4. A plot of the electron concentration in identically prepared *n*-type AlGaN thin films.[5,7]

In spite of the theoretical difficulty of doping ZnO *p*-type there have been a number of reported successes.[8] One report, involving the co-doping of ZnO with both Ga and N, indicates *p*-type film resistivities of about 0.5 Ω cm.[9] It remains to be seen, however, whether these materials can demonstrate the stability, through many thousands of hours of usage, needed for commercial success.

2.2 Isoelectronic Impurities

Normally when two compound semiconductors are alloyed with each other, the objective is to take advantage of Vegard's Law to shift the band gap, and normally it is the cation constituents that are substituted for each other. An example is $In_xGa_{(1-x)}N$, where some indium has been added to GaN to make the band gap smaller. Cation-substituted alloys are normally chosen for this purpose, since they are experimentally easier to work with. The cation solubility is usually larger than the anion solubility. Cations also have favorable physical properties that make them more compatible with growth temperature and pressure conditions. However, the growth of quaternary alloys, that substitute both cations and anions, is sometimes investigated for the purpose of simultaneously engineering the band gap and lattice constants of materials.[10]

Nevertheless, the goal of alloying two materials is not always for the purpose of band gap engineering or lattice constant engineering, and a large solubility is not always required. The goal may be to change the electrical or optical properties of the material. Often only a small amount of the alloy material is needed. Linearity of the material properties, such as band gap with alloy composition, is no longer desired. Since the alloy is very dilute, it is sometimes referred to as an "isoelectronic impurity." The word "isoelectronic" is meant to emphasize the fact that the impurity material comes from the same column on the periodic table as the host material, and as such, is not a dopant in the traditional sense of the word. Thus we are talking about materials that are not entirely dopants, but they are not entirely alloys either.

Several isoelectronic impurity systems have been investigated throughout the last few decades. Examples include $Al_xGa_{(1-x)}As:N$,[11] ZnSe:O,[12] ZnTe:O,[13] ZnO:Te,[14] ZnO:Hg,[15] $CdS_{(1-x)}Se_x:Te$,[16] and GaP:N.[17]

The goal of isoelectronic impurity research is to determine what energy states may be introduced into the crystal with the impurity, and what effect those energy states will have on the opto-electronic properties of the material. A number of phenomena have been attributed to isoelectronic impurities in semiconductors, including recombination centers,[13,18,19] bound excitons,[15,17,20,21] excitonic molecules,[22] band gap bowing,[23-25] isoelectronic donors and acceptors,[12,26] enhancement of *p*-type dopability,[14] and finally the increase of nitrogen solubility in forming p-type behavior.[27]

One of the main theories as to how isoelectronic impurities work involves differences in electronegativity between the isoelectronic impurity and the host element it replaces. It has been suggested that a highly electronegative element such as oxygen, doped into ZnSe or ZnTe can act as an "isoelectronic acceptor", since it will tend to bind electrons more than tellurium or selenium.[12,13]

2.3 Growth methods and defect structures for ZnO

There has been renewed interest in single-crystal ZnO in recent years, and a number of growth techniques have emerged, including molecular beam epitaxy (MBE),[28] metal-organic chemical vapor deposition (MOCVD),[29] vapor transport,[30] and finally pulsed laser deposition (PLD).[31-34] The focus of this discussion will be on PLD, because

that is the apparatus used in the present study. It also worth noting that PLD was the growth technique used for the most successful report, so far, of fabricating *p*-type ZnO.[9]

The basic schematic of a pulsed laser deposition chamber is shown in Figure 2-5. A pulsed laser deposition chamber consists of a target and heated substrate facing each other inside a high vacuum chamber. Pulses, about 25 ns in duration, of high-powered light, between 0.8 and 1.0 joules, are generated by an external excimer laser, (often KrF at 248 nm), and focused on the target through an ultraviolet laser window in the chamber. These pulses of light are absorbed by the target. A small amount of the target ablates resulting in a plasma of energetic atoms that impinge on the substrate, where the material is reabsorbed as a film. The high energy of the vaporized atoms in the laser plume is advantageous because the kinetic energy of the impinging atoms is transferred to the growing film resulting in high surface atom mobility for incorporating into the crystal structure. This affords somewhat lower growth temperatures for pulsed laser deposition than for other techniques.

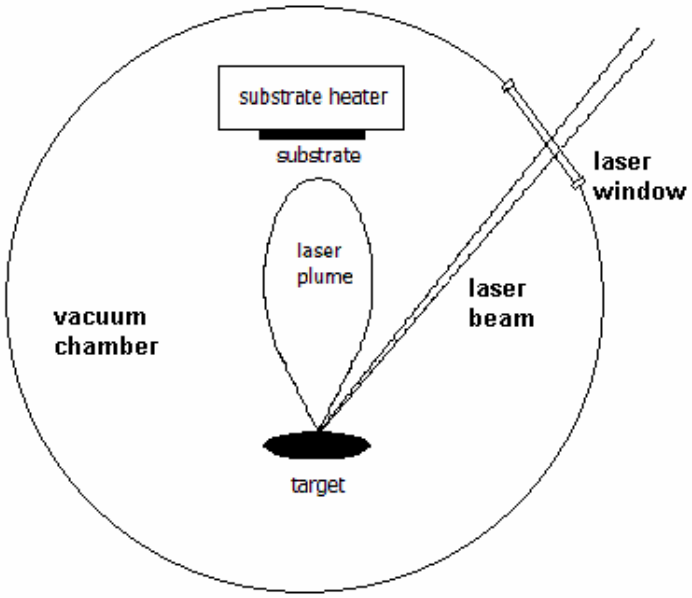

Fig. 2-5. A schematic of a pulsed laser deposition chamber.

Pulsed laser deposited ZnO can either be achieved through ablating Zn metal in an oxygen environment, and letting the Zn metal oxidize during growth, or it can be achieved through ablating a target that is already formed from ZnO.[35] In either case, a partial pressure of oxygen of between 10^{-6} and 10^{-3} Torr is typically maintained in the chamber, with optimum pressures depending on growth temperature.[36] ZnO film growth rates are usually around 1 μ per hour, and it is customary to cool down slowly in an oxygen environment after growth, to prevent desorption of oxygen at higher temperatures, and to give the crystal time to relax dislocations induced by different coefficients of thermal expansion in ZnO compared to sapphire.

Sapphire (0001) is typically chosen as a substrate material, because of the lattice matching consideration. It is also transparent into the deep UV, and it is electrically insulating.

The growth mode for ZnO on sapphire (0001) is domain matching epitaxy,[37] where six lattice planes of ZnO in the $[2\bar{1}\bar{1}0]$ direction match with seven lattice planes of sapphire in the $[01\bar{1}0]$ direction. What this means is that the periodicity of the heterojunction is not achieved through the convention lattice matching paradigm, in which individual lattice planes are matched 1:1 due to their similar spacing, but rather through the periodicity of "domains" wherein an integer multiple of lattice planes of one material matches closely with an integer multiple of lattice planes of the other material. For ZnO on sapphire, since the lattice constant of ZnO in the $[2\bar{1}\bar{1}0]$ direction multiplied by 6 is approximately equal to the lattice constant of sapphire in the $[01\bar{1}0]$ direction multiplied by 7, the growth is energetically favorable to take place with a 30^{o} rotation in the basal plane, under the paradigm of domain matching epitaxy. Thus,

$$1domain \approx 6 \cdot a_{ZnO} = 6 \cdot 0.3252nm = 1.9512nm$$
$$\approx 7 \cdot a_{sapphire} = 7 \cdot 0.2747nm = 1.9229nm$$

resulting in a 1.471% mismatch. Were the materials to grow in the conventional lattice matching paradigm, the mismatch would be 18%, and would result in numerous defects. The in-plane orientation of ZnO on sapphire, and cross-sectional image are shown in Figure 2-6.

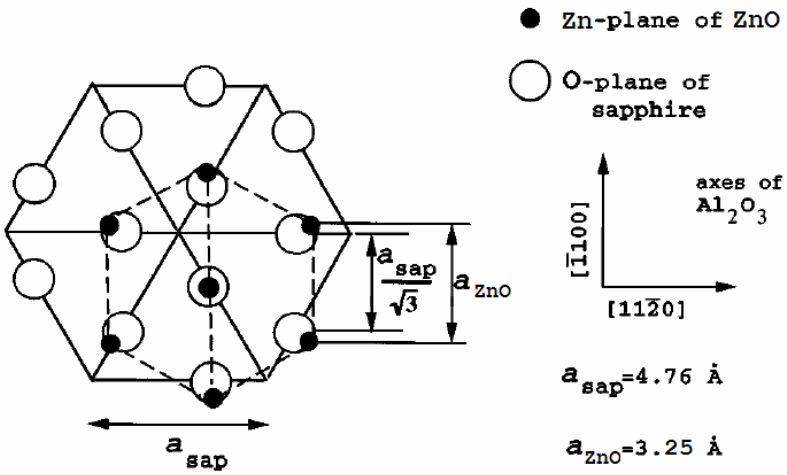

a)

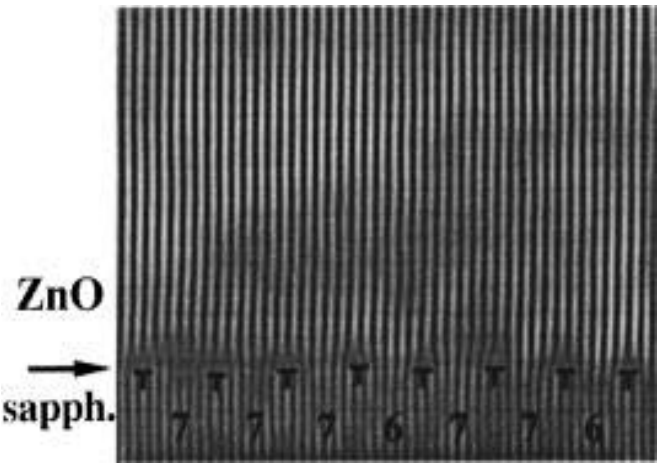

b)

Fig. 2-6. a) An in-plane diagram of the 30° rotation of ZnO on the basal plane of sapphire,[38] and b) a Fourier filtered cross-sectional transmission electron micrograph (TEM) showing the periodic termination of half planes of sapphire at the interface with ZnO.[33]

Dislocation studies on ZnO grown on sapphire have shown that threading dislocations have mostly 1/3<11$\bar{2}$0> Burgers vectors.[33] Stacking faults are also very common, and inversion domains have been observed. Dislocation densities as low as 10^7 cm^{-2} have been achieved.

2.4 Nitrogen doping of II-VI semiconductors and Kaufman ion sources

Until 1990, the only wide band gap II-VI semiconductor compound that could be doped both *n*-type and *p*-type was CdTe.[4] This changed with the introduction of nitrogen plasma as a *p*-type source for the molecular beam epitaxial growth of *p*-type ZnSe.[39]

Operating *in situ* with a molecular beam epitaxial growth chamber, these nitrogen sources are also called free-radical sources (FRS). They consist of electrodeless high-frequency (13.5 MHz) discharge cells, which take high purity N_2 gas from a cylinder and crack a very small percentage of it (~1%) into atomic nitrogen. The atomic and molecular nitrogen impinges on the growing film, and it is suggested that the atomic nitrogen is more reactive than the molecular nitrogen, and is therefore much more likely to be incorporated in the film.[39]

The obvious drawback of this technique is the very small atomization efficiency of the plasma source. Although the atomic nitrogen is more reactive than the molecular nitrogen, it is inevitable that some molecular nitrogen will be incorporated into the film, introducing non-substitutional nitrogen, and providing a mechanism for self-compensating defects in the film.

Also, the very low flux of atomic nitrogen necessitates fairly low growth rates, (~0.5 μ/hr), which make the technique somewhat less productive than one would hope to achieve with such techniques as pulsed laser deposition (PLD), or low-pressure chemical vapor deposition (LPCVD). Thus, the plasma source technique, which is itself a costly technique, has been typically used with molecular beam epitaxy (MBE).

Another technique that has been used for doping II-VI compounds *p*-type is ion implantation of nitrogen.[40,41] The biggest drawback to this method is that the defects introduced during the ion implantation process are not easily annealed out of compound semiconductors, such as ZnO. Ion implantation has enjoyed much success with silicon, only because the defect physics of silicon, and the post-implant annealing processes are well established.[42] The deliberate amorphization of silicon during the implant process, and the subsequent solid-phase epitaxial regrowth during annealing, are not practical for compound semiconductors, because of the different vapor pressures and self-diffusion characteristics of the two constituent elements.

In this thesis, a novel method of doping ZnO with nitrogen is investigated. A Kaufman-type ion source is used to impinge N_2^+ upon the ZnO crystal during growth. The molecular nitrogen is broken into atomic species upon impact with the film, and is incorporated substitutionally during growth.

A Kaufman ion source is a low-voltage DC ion source that is small enough to be mounted *in situ* with a high vacuum growth chamber, such as a PLD chamber. A drawing of a Kaufman ion source is shown in Figure 2-7-a, along side of the schematic circuit diagram shown in Figure 2-7-b.

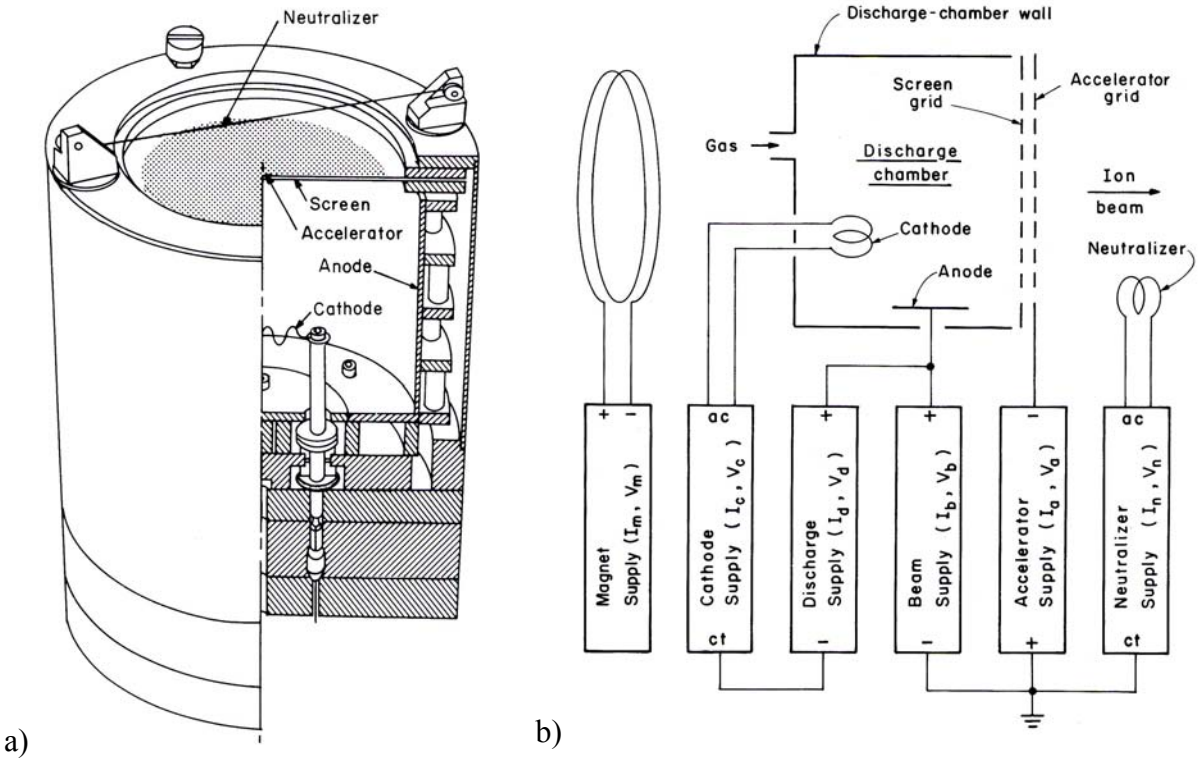

Fig. 2-7. a) A cut-out drawing of a Kaufman ion source, and b), a schematic circuit diagram of a Kaufman ion source.[43]

A hot cathode boils off electrons, which are then accelerated to the anode. Nitrogen gas that is leaking in through the gas inlet is impacted with the electrons and becomes ionized. The ionized N_2^+ molecules are then accelerated out through the accelerator grid, with a potential of about 1 kV. Finally, the accelerated ions with kinetic energies of around 1 kV impinge upon the substrate.

A typical application of a Kaufman source is to incorporate nitrogen into a nitride film which might otherwise be deficient in nitrogen.[44-47] Kaufman ion sources are also used to increase density and improve adhesion during thin films growth.[48-50] These techniques are sometimes called ion-beam assisted deposition.

Perhaps because of the availability and success of plasma sources, there has been considerably less work done on Kaufman ion sources being used as a source of dopants in thin films.[51] While the Kaufman source produces a large dose of the ion material, the Kaufman ion source produces an unanalyzed beam of ions, and is therefore considered a somewhat "dirty" process. This issue, and other issues, will be addressed in the present work.

2.5 Photoconductivity

In the quest to produce *p*-type ZnO, and finally to produce bipolar ZnO devices, it is necessary to characterize the thin films for their electrical properties. Hall effect and capacitance-voltage (CV) measurements, for example, are standard techniques for semiconductors. However, for the case of wide band gap semiconductors on an insulating substrate with film thicknesses of less than a micron, these techniques, while not impossible, are difficult to implement reliably with high confidence in the results. This suggests that alternate methods should be investigated. Other methods include hot-point probe, Seebeck measurements, deep-level transient spectroscopy (DLTS), and photoconductivity. In particular, it has been suggested that non-equilibrium carrier transport properties, such as photoconductivity (PC), will be a necessary supplement to the work towards making bipolar ZnO devices.[52] In comparison with the other techniques, photoconductivity is simple to set up, and the spectra obtained are easier to interpret.

Very little is known about the photoconductive characteristics of doped ZnO.[53] Only a handful of papers have addressed this issue,[54,55] yet it could potentially provide a wealth of information towards developing *p*-type ZnO. The photoconductivity measurement is very sensitive to deep levels,[2,52] and for highly intrinsic material, which can not be measured with Hall effect, we expect photosensitivity to be enhanced, providing qualitative information about carrier mobility.

Besides being useful for developing *p*-type ZnO, photoconductivity of ZnO is worth studying for its own sake, because of the usefulness of fabricating solar-blind photodetectors from ZnO.[53,56,57] Applications from these photodetectors include *in situ* gas monitoring, missile plume detection, and poison gas detection.[58]

2.6 Photoluminescence

Photoluminescence is another popular technique for revealing information about ZnO. It has been employed to investigate a number of different properties, including band structure and doping issues.[59-66]

Due to its large excitonic binding energy (~60 meV), ZnO is among the brightest luminescent materials. Excitons increase luminescent efficiency by reducing the likelihood of non-radiative recombination. Photoluminescence measures all radiative recombination processes,[67] and as such, is a direct and useful means to determine the brightness of a particular film of ZnO, and its potential brightness if applied to fabricating a device.

It is expected that near-band-edge luminescence should dominate the photoluminescent spectrum of ZnO,[59] and the extent to which deep level luminescence is observed is normally considered a sign of poor quality material. As such, it is typical to use photoluminescence as a measure of film quality.

The brightness of ZnO is normally observed in spontaneous emission, but if lasers are to be fabricated from ZnO, it is also necessary to observe stimulated emission. This is achieved by increasing the pumping power of the exciting laser, until there is population inversion between the conduction band and valence band. For pure ZnO, it has become relatively common to observe stimulated emission, even at room temperature.[60,64,68]

Temperature dependent photoluminescence can give greater information about the different types of near-band-edge luminescence in the material. This is because the lower thermal energy in the crystal reduces interference from phonons, and makes the energy transitions sharper and better resolved from one another. Work has been done on low temperature photoluminescence of ZnO to reveal different types of transitions, including free exciton, and donor and acceptor bound exciton recombination.[65,66,68]

Time-resolved photoluminescence has been employed to measure recombination times for any of the processes observed in pulsed or steady-state photoluminescence. Time-resolved photoluminescence has been used to measure recombination times for exciton-exciton scattering-induced stimulated emission in ZnO.[68] It has also been used to compare the recombination times of films grown by different methods.[69] This is taken to be a measure of film quality, since higher quality films should have slower recombination times. Also, time resolved photoluminescence can be used to compare the recombination speeds of different peaks in photoluminescence to verify if one of them is a phonon

replica of the other, since a parent peak and its phonon replica should have similar decay times.[62]

2.7 Gallium oxide

There are other wide band gap transparent conducting oxides (TCO's), besides ZnO. β-Ga_2O_3, is a TCO that is naturally *n*-type, also due to oxygen vacancies, and has a band gap of ~4.7 eV,[70] which is among the largest values of any of the known TCO's to date.[71] It has received attention recently as a very promising material for fabricating a variety of opto-electronic devices operating in the deep UV.[72] The fact that it is both transparent and conducting make it an attractive contact material for opto-electronic devices operating in the near UV to the visible spectrum. The crystal structure is monoclinic with $a = 12.23 \pm 0.02$ Å, $b = 3.04 \pm 0.01$ Å, $c = 5.80 \pm 0.01$ Å, and $\beta = 103.7 \pm 0.3^{o}$, and the space group is $C2/m(C_{2h}^{3})$.[73]

β-Ga_2O_3 bulk single crystals have been grown through the floating zone method,[72,74] and through the Verneuil method.[75] Thin films of β-gallium oxide have been grown through pulsed laser deposition,[76] and electron-beam evaporation.[77] Pulsed laser deposition has the advantage of non-equilibrium processing, with film stoichiometry closely matched with that of the target. For wide band gap materials, such as gallium oxide, the photon energy of the typical eximer laser used for pulsed laser deposition (KrF laser operating at 248 nm) is not high enough to be greatly absorbed by the target material. This suggests the possible alternative growth method, pulsed election deposition (PED), which will be investigated in this thesis.

When β-Ga_2O_3 is grown on sapphire (0001), the gallium oxide is oriented in the [$\bar{2}$01] direction.[76,78] For the in-plane orientation, it has been shown though cross-sectional transmission electron microscopy (TEM) that the crystal orients itself such that (010) β-Ga_2O_3 // (01$\bar{1}$0) α-Al_2O_3, and (201) β-Ga_2O_3 // (2$\bar{1}\bar{1}$0) α-Al_2O_3.[78]

Its native *n*-type behavior is another characteristic it shares with ZnO. However, the method of conduction is not exactly the same with gallium oxide as it is with ZnO. Unlike ZnO, the undoped, as grown gallium oxide is usually highly resistive. Nevertheless, Ga_2O_3 can be doped with SnO_2, making it n-type, with resulting resistivities of around 0.1 ohm cm.[76,79]

2.8 References

1. N. K. Abrikosov, V. F. Bankina, L. V. Poretskaya, L. E. Sheliova, and E. V. Skudnova, *Semiconducting II-VI, IV-VI, and V-VI Compounds*, 1st ed. New York: Plenum Press, 1969.
2. R. H. Bube, *Photoconductivity of Solids*, 1st ed. New York, NY: Robert E. Krieger Publishing Co., Inc., 1960.
3. J. Holonyak, N. and S. F. Bevacqua, "Coherent (visible) light emission from $GaAs_{1-x}P_x$ junctions," *Applied Physics Letters*, vol. 1, pp. 82-83, 1962.
4. S. J. Pearton, *Processing of Wide Band Gap Semiconductors*, 1st ed: Noyes Publications, 2000.

5. S. B. Zhang, S.-H. Wei, and A. Zunger, "A phenomenological model for systematization and prediction of doping limits in II-VI and I-II-VI2 compounds," *Journal of Applied Physics*, vol. 83, pp. 3192, 1998.

6. W. Faschinger, S. Ferreira, H. Sitter, R. Krump, and G. Brunthaler, *Materials Science Forum*, vol. 29, pp. 182-184, 1995.

7. S. Yoshida, S. Misawa, and S. Gonda, *Journal of Applied Physics*, vol. 53, pp. 6844, 1982.

8. D. C. Look and B. Claftin, "P-type doping and devices based on ZnO," *Physica Status Solidi B-Basic Research*, vol. 241, pp. 624-630, 2004.

9. M. Joseph, H. Tabata, H. Saeki, K. Ueda, and T. Kawai, "Fabrication of the low-resistive p-type ZnO by codoping method," presented at Yanada Conference LIV. 9th International Conference on Shallow-Level Centers in Semiconductors, Sep 24-27 2000, Awaji Island, Hyogo, 2001.

10. K. Shim, H. Rabitz, J.-H. Chang, and T. Yao, "Energy band gap of the alloy $Zn_{1-x}Mg_xSe_yTe_{1-y}$ lattice matched to ZnTe, InAs and InP," *Journal of Crystal Growth. The 9th International Conference on II-VI Compounds, Nov 1-Nov 5 1999*, vol. 214, pp. 350-354, 2000.

11. Y. Makita, H. Ijuin, and S. Gonda, "Composition-ratio dependence of formation of bound states in nitrogen-implanted $Al_xGa_{1-x}As$," *Applied Physics Letters*, vol. 28, pp. 287-289, 1976.

12. K. Akimoto, T. Miyajima, and Y. Mori, "Photoluminescence spectra of oxygen-doped ZnSe grown by molecular-beam epitaxy," *Physical Review B*, vol. 39, pp. 3138-3144, 1989.

13. J. L. Merz, "Isoelectronic Oxygen Trap in ZnTe," *Physical Review*, vol. 176, pp. 961-968, 1968.

14. H. L. Porter, C. Jin, J. Narayan, A. L. Cai, J. F. Muth, and O. W. Holland, "Structural, optical and electrical properties of the novel semiconductor alloy $ZnO_xTe_{(1-x)}$," presented at Quantum Confined Semiconductor Nanostructures, Dec 2-5 2002, Boston MA, United States, 2002.

15. T. Agne, M. Dietrich, H. J., S. Lany, H. Wolf, and T. Wichert, "Optical properties of the isoelectronic trap Hg in ZnO," *Applied Physics Letters*, vol. 82, pp. 3448-3450, 2003.

16. O. Goede and W. Heimbrodt, "Isoelectronic Impurity Te in CdS/1-x/Se/x/ Mixed Crystals," *Physica Status Solidi B*, vol. 110, pp. 175-182, 1982.

17. D. G. Thomas and J. J. Hopfield, "Isoelectronic Traps Due to Nitrogen in Gallium Phosphide," *Physical Review*, vol. 150, pp. 680-689, 1966.

18. H. P. Hjalmarson and C. B. Norris, "A phenomenological model of the red luminescence kinetics in ZnTe:O," *Journal of Applied Physics*, vol. 61, pp. 734, 1986.

19. J. D. Cuthbert and D. G. Thomas, "Fluorescent Decay Times of Excitons Bound to Isoelectronic Traps in GaP and ZnTe," *Physical Review*, vol. 154, pp. 763-771, 1967.

20. O. Goede, W. Heimbrodt, T. Lau, G. Matzkeit, and B. Selle, "Optical and RBS Studies of ZnS:Te Thin Films," *Physica Status Solidi A*, vol. 94, pp. 259, 1986.

21. O. Goede, W. Heimbrodt, and R. Muller, "$CdS_{1-x}Te_x$ as Persistence-Type Semiconductor Mixed Crystals," *Physica Status Solidi B*, vol. 105, pp. 543-550, 1981.

22. J. L. Merz, R. A. Faulkner, and P. J. Dean, *Physical Review*, vol. 188, pp. 1228-1239, 1969.

23. Y. Nabetani, T. Mukawa, Y. Ito, T. Kato, and T. Matsumoto, "Epitaxial growth and large band-gap bowing of ZnSeO alloy," *Applied Physics Letters*, vol. 83, pp. 1148-1150, 2003.

24. M. Weyers, M. Sato, and H. Ando, "Red shift of photoluminescence and absorption in dilute GaAsN alloy layers," *Japanese Journal of Applied Physics, Part 2: Letters*, vol. 31, pp. 853-855, 1992.

25. M. Kondow, K. Uomi, K. Hosomi, and T. Mozume, "Gas-source molecular beam epitaxy of GaN_xAs_{1-x} using a N radical as the N source," *Japanese Journal of Applied Physics, Part 2: Letters*, vol. 33, pp. 1056-1058, 1994.

26. K. Akimoto, T. Miyajima, and Y. Mori, "Injection luminescence in oxygen-doped ZnSe grown by molecular beam epitaxy," *Journal of Crystal Growth. Proceedings of the 4th International Conference on II-VI Compounds 1989, Sep 17-22 1989*, vol. 101, pp. 1009-1012, 1990.

27. Y. Fan, J. Han, R. L. Gunshor, J. Walker, N. M. Johnson, and A. V. Nurmikko, "The Study of Nitrogen Doping in ZnSe and ZnSe:Te," *Journal of Electronic Materials*, vol. 24, 1995.

28. Y. Chen, D. M. Bagnall, H.-j. Koh, K.-t. Park, K. Hiraga, Z. Zhu, and T. Yao, "Plasma assisted molecular beam epitaxy of ZnO on c-plane sapphire: growth and characterization," *Journal of Applied Physics*, vol. 84, pp. 3912, 1998.

29. Y. Liu, C. R. Gorla, S. Liang, N. Emanetoglu, Y. Lu, H. Shen, and M. Wraback, "Ultraviolet detectors based on epitaxial ZnO films grown by MOCVD," *Journal of Electronic Materials*, vol. 29, pp. 69-74, 2000.

30. D. C. Look, D. C. Reynolds, J. R. Sizelove, R. L. Jones, C. W. Litton, G. Cantwell, and W. C. Harsch, "Electrical properties of bulk ZnO," *Solid State Communications*, vol. 105, pp. 399-401, 1998.

31. A. K. Sharma, K. Dovidenko, S. Oktyabrsky, D. E. Moxey, J. F. Muth, R. M. Kolbas, and J. Narayan, "Growth of high quality single, crystal ZnO films on sapphire by pulsed laser ablation," presented at Advances in Laser Ablation of Materials. Symposium, 13-16 April 1998, San Francisco, CA, USA, 1998.

32. R. D. Vispute, V. Talyansky, Z. Trajanovic, S. Choopun, M. Downes, R. P. Sharma, T. Venkatesan, M. C. Woods, R. T. Lareau, K. A. Jones, and A. A. Iliadis, "High quality crystalline ZnO buffer layers on sapphire (001) by pulsed laser deposition for III-V nitrides," *Applied Physics Letters*, vol. 70, pp. 2735, 1997.

33. J. Narayan, K. Dovidenko, A. K. Sharma, and S. Oktyabrsky, "Defects and interfaces in epitaxial ZnO/α-Al_2O_3 and AlN/ZnO/α-Al_2O_3, heterostructures," *Journal of Applied Physics*, vol. 84, pp. 2597-2601, 1998.

34. Y. Segawa, A. Ohtomo, M. Kawasaki, and H. Koinuma, "Growth of ZnO Thin Film by Laser MBE: Lasing of Exciton at Room Temperature," *Physica Status Solidi (B): Basic Research*, vol. 202, pp. 669, 1997.

35. J. Bruncko, M. Michalka, and F. Uherek, "Pulsed laser deposition of ZnO: Comparison between deposition from Zn and ZnO target," presented at Laser and Laser Information Technologies, Sep 27-Oct 1 2003, Smolyan, Bulgaria, 2004.

36. S. Choopun, R. D. Vispute, W. Noch, A. Balsamo, R. P. Sharma, T. Venkatesan, A. Iliadis, and D. C. Look, "Oxygen pressure-tuned epitaxy and optoelectronic properties of laser-deposited ZnO films on sapphire," *Applied Physics Letters*, vol. 75, pp. 3947, 1999.

37. J. Narayan and B. C. Larson, "Domain epitaxy: A unified paradigm for thin film growth," *Journal of Applied Physics*, vol. 93, pp. 278-285, 2003.

38. K. Dovidenko, S. Oktyabrsky, J. Narayan, and M. Razeghi, "Aluminum nitride films on different orientations of sapphire and silicon," *Journal of Applied Physics*, vol. 79, pp. 2439, 1996.

39. R. M. Park, M. B. Troffer, C. M. Rouleau, J. M. DePuydt, and M. A. Haase, "p-type ZnSe by nitrogen atom beam doping during molecular beam epitaxial growth," *Applied Physics Letters*, vol. 57, pp. 2127-2129, 1990.

40. A. N. Georgobiani, A. N. Gruzintsev, V. T. Volkov, M. O. Vorobiev, V. I. Demin, and V. A. Dravin, "P-Type ZnO:N obtained by ion implantation of nitrogen with post-implantation annealing in oxygen radicals," presented at Proceedings of the 4th International Conference on Radiation (RESMDDo2), Jul 10-12 2002, 2003.

41. A. N. Georgobiani, A. N. Gruzintsev, V. T. Volkov, M. O. Vorob'ev, and V. A. Dravin, "ZnO thin films with hole conduction produced by N^+ ion implantation and oxygen-radical annealing," *Mikroelektronika*, vol. 33, pp. 204-209, 2004.

42. J. Narayan, O. W. Holland, W. H. Christie, and J. J. Wortman, "Rapid thermal and pulsed laser annealing of boron fluoride-implanted silicon," *Journal of Applied Physics*, vol. 57, pp. 2709-2716, 1984.

43. H. R. Kaufman and R. S. Robinson, *Operation of Broad-Beam Sources*, 1st ed. Alexandria, Virginia: Commonwealth Scientific Corporation, 1984.

44. J.-E. Doering, L. Guangnan, and H.-R. Stock, "Influence of ion beam assisted deposition parameters on the properties of boron nitride thin films," *Diamond and Related Materials. Proceedings of the 1998 6th International Conference on New Diamond Science and Technology (ICNDST-6), Aug 31-Sep 4 1998*, vol. 8, pp. 1697-1702, 1999.

45. J.-H. Huang, C.-H. Lin, and H. Chen, "Ion beam assisted deposition of TiN thin film on Si (100)," *Materials Chemistry and Physics*, vol. 59, pp. 49-56, 1999.

46. C.-W. Jeon and S.-H. Kim, "Growth behavior of GaN film on Si (111) substrate by an ion-beam assisted evaporation process," *Materials Science & Engineering B: Solid-State Materials for Advanced Technology*, vol. B57, pp. 110-115, 1999.

47. H. Jiang, K. Tao, and H. D. Li, "Structure and magnetic properties of Fe-N films deposited on heated substrates by ion-beam-assisted deposition," *Journal of Magnetism and Magnetic Materials*, vol. 149, pp. 358-362, 1995.

48. S.-K. Koh, S.-K. Song, W.-K. Choi, H.-J. Jung, and S.-N. Han, "Improving wettability of polycarbonate and adhesion with aluminum by Ar^+ ion irradiation," *Journal of Materials Research*, vol. 10, pp. 2390-2394, 1995.

49. R. A. Erck, "Pin-pull adhesion measurements of copper films on ion-bombarded alumina," *Thin Solid Films. Proceedings of the 21st International Conference on Metallurgical Coatings and Thin Films, Apr 25-29 1994*, vol. 253, pp. 362-366, 1994.

50. D. A. Kotov, "Broad beam low-energy ion source for ion-beam assisted deposition and material processing," *Review of Scientific Instruments*, vol. 75, pp. 1934-1936, 2004.

51. S. Bhattacharyya, K. Walzer, M. Hietschold, and F. Richter, "Nitrogen doping of tetrahedral amorphous carbon films: Scanning tunneling spectroscopy," *Journal of Applied Physics*, vol. 89, pp. 1619-1624, 2001.

52. J. W. Tomm, B. Ullrich, X. G. Qiu, Y. Segawa, A. Ohtomo, M. Kawasaki, and H. Koinuma, "Optical and photoelectrical properties of oriented ZnO films," *Journal of Applied Physics*, vol. 87, pp. 1844-1848, 2000.

53. P. Sharma, K. Sreenivas, and K. V. Rao, "Analysis of ultraviolet photoconductivity in ZnO films prepared by unbalanced magnetron sputtering," *Journal of Applied Physics*, vol. 93, pp. 3963-3970, 2003.

54. J. C. Simpson and J. F. Cordaro, "Photocapacitance and photoconductance of Bi-doped ZnO," *Journal of Applied Physics*, vol. 69, pp. 4011-4016, 1991.

55. A. N. Gruzintsev, V. T. Volkov, and E. E. Yakimov, "Photoelectric properties of ZnO films doped with Cu and Ag acceptor impurities," *Semiconductors*, vol. 37, pp. 259-262, 2003.

56. D. Basak, G. Amin, B. Mallik, G. K. Paul, and S. K. Sen, "Photoconductive UV detectors on sol-gel-synthesized ZnO films," *Journal of Crystal Growth*, vol. 256, pp. 73-77, 2003.

57. P. Schreiber, T. Dang, T. Pickenpaugh, G. Smith, P. Gehred, and C. Litton, "Solar blind UV region and UV detector development objectives," *Proceedings of SPIE - The International Society for Optical Engineering. Proceedings of the 1999 Photodetectors: Materials and Devices IV, Jan 27-Jan 29 1999*, vol. 3629, pp. 230-248, 1999.

58. M. Razeghi and A. Rogalski, "Semiconductor ultraviolet detectors," *Journal of Applied Physics*, vol. 79, pp. 7433-7473, 1996.

59. S. Bethke, H. Pan, and B. W. Wessels, "Luminescence of heteroepitaxial zinc oxide," *Applied Physics Letters*, vol. 52, pp. 138-140, 1988.

60. Z. K. Tang, G. K. L. Wong, P. Yu, M. Kawasaki, A. Ohtomo, H. Koinuma, and Y. Segawa, "Room-temperature ultraviolet laser emission from self-assembled ZnO microcrystallite thin films," *Applied Physics Letters*, vol. 72, pp. 3270-3272, 1998.

61. Y. R. Ryu, S. Zhu, J. D. Budai, H. R. Chandrasekhar, P. F. Miceli, and H. W. White, "Optical and structural properties of ZnO films deposited on GaAs by pulsed laser deposition," *Journal of Applied Physics*, vol. 88, pp. 201-204, 2000.

62. R. E. Sherriff, D. C. Reynolds, D. C. Look, B. Jogai, J. E. Hoelscher, T. C. Collins, G. Cantwell, and W. C. Harsch, "Photoluminescence measurements from

the two polar faces of ZnO," *Journal of Applied Physics*, vol. 88, pp. 3454-3457, 2000.

63. H. J. Ko, Y. F. Chen, Z. Zhu, T. Yao, I. Kobayashi, and H. Uchiki, "Photoluminescence properties of ZnO epilayers grown on CaF_2 (111) by plasma assisted molecular beam epitaxy," *Applied Physics Letters*, vol. 76, pp. 1905-1907, 2000.

64. Y. Chen, N. T. Tuan, Y. Segawa, H.-j. Ko, S.-k. Hong, and T. Yao, "Stimulated emission and optical gain in ZnO epilayers grown by plasma-assisted molecular-beam epitaxy with buffers," *Applied Physics Letters*, vol. 78, pp. 1469-1471, 2001.

65. A. Zeuner, H. Alves, D. M. Hofmann, B. K. Meyer, M. Heuken, J. Blasing, and A. Krost, "Structural and optical properties of epitaxial and bulk ZnO," *Applied Physics Letters*, vol. 80, pp. 2078-2080, 2002.

66. T. Makino, K. Tamura, C. H. Chia, Y. Segawa, M. Kawasaki, A. Ohtomo, and H. Koinuma, "Photoluminescence properties of ZnO epitaxial layers grown on lattice-matched $ScAlMgO_4$ substrates," *Journal of Applied Physics*, vol. 92, pp. 7157-7159, 2002.

67. D. K. Schroder, *Semiconductor Material and Device Characterization*, 2nd ed. New York, NY: John Wiley & Sons, Inc., 1998.

68. U. Ozgur, A. Teke, C. Liu, S.-J. Cho, H. Morkoc, and H. O. Everitt, "Stimulated emission and time-resolved photoluminescence in rf-sputtered ZnO thin films," *Applied Physics Letters*, vol. 84, pp. 3223-3225, 2004.

69. K.-S. Sohn, D.-K. Hwang, and J.-M. Myoung, "Time Integrated/Resolved Photoluminescence of ZnO Films Deposited on Sapphire and GaAs," *Japanese*

Journal of Applied Physics, Part 1: Regular Papers and Short Notes and Review Papers, vol. 42, pp. 7376-7378, 2003.

70. H. H. Tippins, "Optical Absorption and Photoconductivity in the Band Edge of β-Ga_2O_3," *Physical Review*, vol. 140, pp. A316-A319, 1965.

71. M. R. Lorenz, J. F. Woods, and R. J. Gambino, "Some electrical properties of the semiconductor β-Ga_2O_3," *Journal of Physics and Chemistry of Solids*, vol. 28, pp. 403-404, 1967.

72. N. Ueda, H. Hosono, R. Waseda, and H. Kawazoe, "Synthesis and control of conductivity of ultraviolet transmitting β-Ga_2O_3 single crystals," *Applied Physics Letters*, vol. 70, pp. 3561-3563, 1997.

73. S. Geller, "Crystal Structure of β-Ga_2O_3," *The Journal of Chemical Physics*, vol. 33, pp. 676-684, 1960.

74. N. Ueda, H. Hosono, R. Waseda, and H. Kawazoe, "Anisotropy of electrical and optical properties in β-Ga_2O_3 single crystals," *Applied Physics Letters*, vol. 71, pp. 933-935, 1997.

75. M. Ueltzen, "The Verneuil flame fusion process: substances," *Journal of Crystal Growth*, vol. 132, pp. 315-328, 1993.

76. M. Orita, H. Hiramatsu, H. Ohta, M. Hirano, and H. Hosono, "Preparation of highly conductive, deep ultraviolet transparent β-Ga_2O_3 thin film at low deposition temperatures," *Thin Solid Films*, vol. 411, pp. 134-139, 2002.

77. M. Passlack, E. F. Schubert, W. S. Hobson, M. Hong, N. Moriya, S. N. G. Chu, K. Konstadinidis, J. P. Mannaerts, M. L. Schnoes, and G. J. Zydzik, "Ga_2O_3 films for

electronic and optoelectronic applications," *Journal of Applied Physics*, vol. 77, pp. 686-693, 1995.

78. H. Ohta, M. Orita, M. Hirano, K. Ueda, and H. Hosono, "EPITAXIAL GROWTH OF TRANSPARENT CONDUCTIVE OXIDES," *International Journal of Modern Physics B*, vol. 16, pp. 173-180, 2002.

79. J. Frank, M. Fleischer, and H. Meixner, "Gas-sensitive electrical properties of pure and doped semiconducting Ga_2O_3 thick films," *Sensors and Actuators, B: Chemical. Proceedings of the 1997 Eurosensors XI Conference. Part 4 (of 4), Sep 21-24 1997*, vol. B48, pp. 318-321, 1998.

3.0 Experimental methods

3.1 Target preparation

Thin films of ZnO can be grown either through the ablation of pure Zn targets in an oxygen environment, or through the ablation of pure ZnO targets.[1] For the present study, sintered polycrystalline ZnO targets were used.

High purity target materials can be purchased through companies such as Alfa-Aesar or Cerac. Online catalogs can be searched at www.alfa.com and www.cerac.com. It is best to choose powdered material with a mesh size of 200 or better. According to standard sieve charts, this corresponds to an average particle size of 75 μm or smaller. Smaller particles means that there is more surface area, and more surface area means that there are more opportunities for atoms to diffuse out to neighboring particles, which is how the sintering process works.

The purity of the target material also needs to be considered carefully. For most pulsed energy deposition methods, impurities in the target material are the most significant source of contamination for the process.

Typically, powdered ZnO purities of around 99.995% are easily found. Purities of 99.9995% can also be found, but they are much more expensive. To determine if a certain purity is sufficient, it is a good idea to express it in terms of impurities per cubic centimeter. For example, ZnO that is 99.995% pure has 0.005% impurities. Thus, if we make the assumption that the impurities have the same density and atomic mass as the ZnO we can see that:

$$\frac{0.00005g}{1g} * \frac{5.67g}{cm^3} * \frac{1mole}{81.39g} * \frac{12.04 \times 10^{23} atoms}{1mole} = 4.2 \times 10^{18} cm^{-3}$$

Due to the mining process, most of these impurities are isoelectronic, and therefore they are not electrically active, but nevertheless, this provides an idea of how significant the target impurities could potentially be. (As a point of comparison, in chemical vapor deposition (CVD), commercial producers of bubbler sources claim electrical activity of source impurity levels to be as low as 10^{14} cm^{-3}).

Another useful calculation related to target purity is to consider how much these impurities weigh compared to the typical target of 15 grams. Using the same assumptions as above, we see that the impurities make up less than a milligram of target material. This is useful to know, because throughout the target preparation process, there will be many opportunities for more impurities to be introduced, and the operator must keep this in mind, because a sloppy target preparation procedure could defeat the purpose of buying the more expensive, higher purity powder. Thus, if using ZnO powder that is 99.995% pure, the operator must remember that if additional impurities are only on the order of a fraction of a milligram, then the powder purity has not been wasted.

If target powders need to be mixed, such as in the formation of an alloy, this mixing can usually be done by pouring the powders into a beaker, and then adding alcohol, and a magnetic stirrer. The mixture should then be stirred for several minutes, or several hours, depending on how well the powders tend to mix. Some Teflon coated magnetic stirrers are not chemically resistant to certain solvents, so care should be taken.

After the powder has had sufficient time to dry, usually over-night in a fume hood, it is ready to press. It is not a good idea to press wet powders, because the moisture will be squeezed out of the powder, and it will deliver small amounts of the powder into the

sliding surfaces of the die, causing the die to freeze up. Nevertheless, some operators prefer a very slight amount of moisture in the powder to help the powder stay together after pressing. The humidity in the air may be enough for this purpose.

The die should be clean, and should be lubricated with a very small amount of oleic acid. Oleic acid works best, because it is carbon-based, and carbon impurities will have the least negative effect on the resulting target.

After about 10 to 15 grams of powder are poured into the die, the powder can be pressed. The amount of pressure is typically around 5000 PSI, but this is not always the case. If, after pressing at 5000 PSI, the powder still does not hold together, sometimes it is useful to try a lower pressure. The reason is because after pressing at a higher pressure, it takes more force to get the resulting mass out of the die, and the added vibration can shake the powders loose again. (This is why some die are made tapered, so that the pressed powder does not have to slide against the walls of the die for very long while it is being removed.)

After a mass of pressed powder is removed from the die, it will have a small amount of oleic acid on its surface. Very gently rubbing it on a Kim-wipe will remove a small amount of material from the target, as it removes the oleic acid.

A clean alumina crucible is typically used to sinter the target. Some loose ZnO powder can be added inside the crucible to further protect the target from impurities in the furnace.

Typical sintering temperatures are around two thirds the melting point of the material.[2] (This is, of course, assuming the material doesn't have a sublimation point below its melting point. Some materials are dangerous to sinter, and the operator should

very carefully read the materials safety data sheets (MSDS) for the material, prior to sintering.) Temperatures above 1000^{o} C to 1200^{o} C, for about 10 to 12 hours, work well with ZnO.

The resulting target (ZnO) should be yellowish, or white, in appearance, and very hard. It is a good idea to polish the resulting target before the first use, and after each successive use. A diagram showing how the powder is effected by the entire process is shown in Figure 3-1.

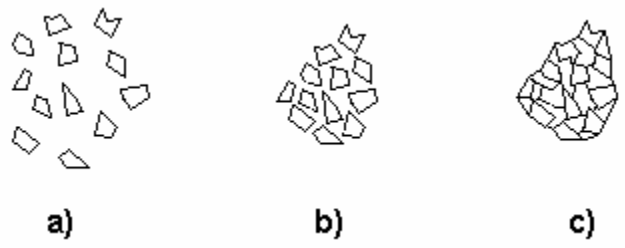

Fig. 3-1. The microscopic view of a) ZnO powder, b) pressed ZnO powder, and c) sintered polycrystalline target.

3.2 Film growth

3.2.1 Pulsed laser deposition (PLD)

The pulsed laser deposition (PLD) technique, a high energy ablation technique,[3] was introduced in chapter 2. For the present study, this technique was slightly modified, but the general idea is the same.

Small pieces of *c*-axis (0001) oriented sapphire, approximately 1 cm on the edge, are degreased in ultrasonic baths of first acetone, and then methanol, for five minutes

each. The sample is then silver-pasted to a sample holder which is then mounted into the chamber. The polycrystalline ZnO target is also mounted into the chamber.[4]

For the present study, the chamber is slightly modified. In Figure 3-2, a diagram of the modified chamber is given.

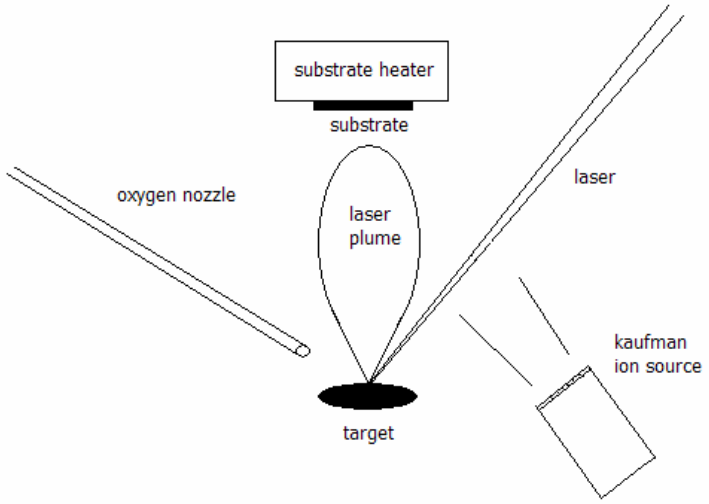

Fig. 3-2. A schematic of the pulsed laser deposition chamber used for the present study. A Kaufman ion source and an oxygen nozzle have been added.

A Kaufman ion source has been added to dope the films with nitrogen. Also, an oxygen nozzle has been added, which directs oxygen directly onto the target.

With nitrogen leaking directly into the Kaufman ion source, and oxygen leaking in through the nozzle into the chamber, the cathode in the Kaufman ion source is protected from oxidation.

The nitrogen valve was opened until the ion gauge for the growth chamber indicated about 3.5×10^{-4} Torr. The pressure in the chamber after opening the oxygen valve was about 9×10^{-4} Torr. This ratio of pressures has been reported elsewhere.[5]

Thus, there was somewhat more oxygen in the chamber than nitrogen, but since the nitrogen was leaked directly into the Kaufman ion source discharge chamber, it was expected that more nitrogen than oxygen was accelerated at the sample. Some oxygen, of course, will diffuse into the discharge chamber, against the flow of ions, but this is somewhat undesirable, as it will greatly reduce cathode lifetime.

The ideal location of the oxygen nozzle was another topic of investigation. Singh, *et al*, investigated the use a nozzle to direct the flow of oxygen towards the sample and towards the substrate during the pulsed laser deposition of YBCO thin films.[6] The best incorporation of oxygen was observed when the nozzle was pointed directly at the sample. However, for Singh's experiment, the chamber pressure was in the 10^{-2} Torr regime. In this pressure regime, laminar flow is observed, and it is reasonable to expect that the oxygen molecules will flow over the entire surface of the sample as they impinge upon it. Our pressure range, however, is around 10^{-4} Torr, which suggests molecular flow, and a very long mean free path of about a half a meter. Oxygen molecules are not likely to flow over a wide surface, but rather they are expected to bounce off of whatever they impinge upon. Thus, for our experiment it was observed that the best oxygen incorporation was found when the oxygen nozzle pointed directly at the point on the target where the laser pulses ablated the surface. Thus, the high energy density in this location was able to contribute to the dissociation of oxygen molecules into atomic species that can be incorporated more efficiently into the film.

The Kaufman-type ion source was a 3 cm broad beam ion source with focused molybdenum optics from Commonwealth Scientific Corporation. It was powered by an Advanced Energy ID 2501 Ion-Beam Drive. A Faraday cup was used to calibrate the

flux of ions impinging on the sample from the ion source. The challenge of calibrating the ion source is finding the right combination of growth conditions that provides enough energy to atomize the nitrogen, and enough nitrogen to dope the sample, but not so much of either to sputter the film itself. It was observed that a suitable beam current was typically around 3.9 mA, with a beam voltage of 1200 V. This somewhat low beam current was achieved by lowering the cathode current until the discharge current was a little under 0.2 A. It was also observed that the proper functioning of the neutralizer filament was necessary to keep the beam focused on the sample. Films that were grown without the neutralizer did not receive adequate nitrogen flux.

3.2.2 Pulsed electron deposition (PED)

All of the β-Ga_2O_3 films that were grown for this study, and some of the ZnO films, were grown with channelspark pulsed electron deposition (PED). Channelspark pulsed electron deposition is very similar to pulsed laser deposition, except that, instead of using short pulses of light originating from outside of the chamber, pulsed electron deposition uses short pulses of electron current originating from inside the chamber. A schematic of the pulsed electron deposition chamber used for the present study is shown in Figure 3-3.

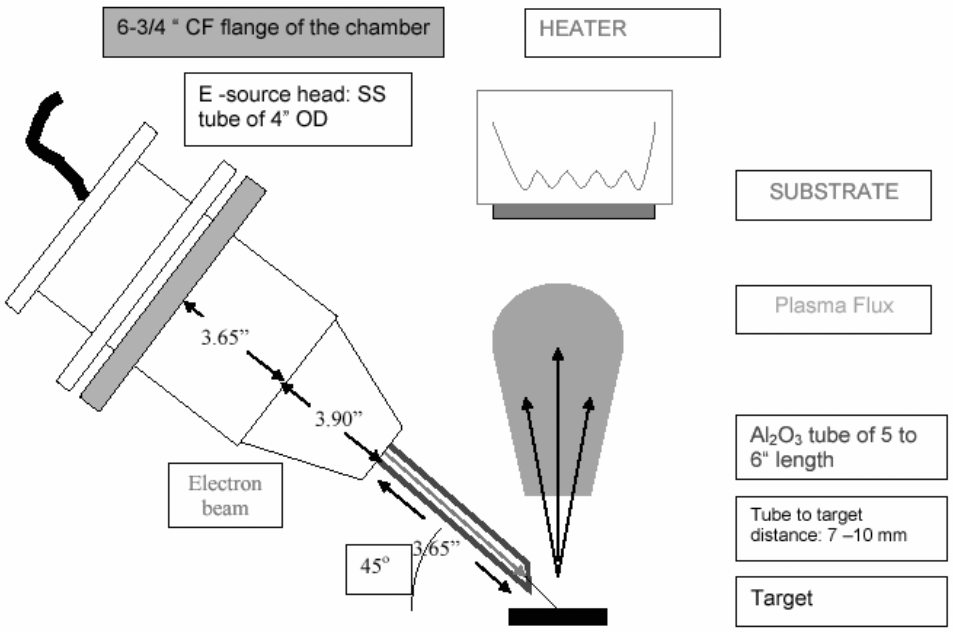

Fig. 3-3. A schematic of a pulsed electron deposition chamber.

In channelspark pulsed electron deposition[7-8] a short pulse of electrons (~70 ns) is produced in a hollow cathode, at a gas pressure between 5 and 30 mTorr. The resulting plasma is confined in the ceramic spark channel, typically an Al_2O_3 or glass hollow tube with an inner diameter of 2 to 4 mm. This permits the charge to be efficiently transferred to the tip of the channel which is placed about 5 mm from the target. The accelerating potential, adjustable from between 8 to 20 kV then results in a discharge to the target surface. The resulting electron beam retains it small dimension due to magnetic self-pinching effects induced by the large instantaneous current of ~1000 A. The electrons penetrate the surface of the target to a depth depending on the accelerating voltage, and approximately 0.8 Joules of energy is deposited in a spot approximately 1-2 mm in diameter. This results in the high energy ablation of the target material. As in PLD, the stoichiometry of the target material is preserved in the film within 1% to 5 % of its

original value in the target. Also similar to PLD, the ionized species are very energetic. Unlike PLD, this method will work with materials that are transparent to ultraviolet photons, and optical reflection effects do not occur since the electrons can penetrate the plume.

Similar to PLD, samples are silver-pasted to a sample holder which heats the sample during growth. The target is rotated and rastered for uniform ablation, and the sample is sometimes rotated for uniform deposition. Growth rates of 1 or 2 μ per hour are observed. The sample is slowly cooled after deposition.

3.3 Pulsed laser annealing

For some of the samples, but not all of them, pulsed laser annealing was attempted to improve the post-growth crystallography and increase the electrical activation of the dopants. The pulsed laser annealing was carried out with a KrF excimer laser operating at 248 nm, with a pulse length of approximately 25 ns.

The pulsed laser annealing technique was first pioneered by J. Narayan, et al., and was originally used for annealing ion-implanted silicon.[9-10] In the studies by Narayan, et al., it is assumed that the laser annealing will very briefly melt the silicon. This melting depth is measured by observing the crystalline/amorphous interface depth under transmission electron microscopy (TEM). For this work, however, melting is not desired, because ZnO is a sublimating compound.

For the present study, samples of nitrogen and tellurium doped ZnO were fastened to glass slides with two-sided tape, and held in the path of the excimer laser beam. The

annealing took place in the air, and sometimes the samples were annealed with the laser impinging on the front side of the sample, and sometimes the samples were annealed from the back side, by first turning the sample face down on the two-sided tape. Figure 3-4 shows how the sample was positioned with respect to the UV lens. For optimum laser intensity, the sample was held at some position, *x*, from the lens' focal point. If the sample were held too close to the focal point, it would be damaged. If held too far from the focal point, it would not get adequate laser intensity to anneal the sample. The annealing process was then carried out with the triggering of the laser by the user.

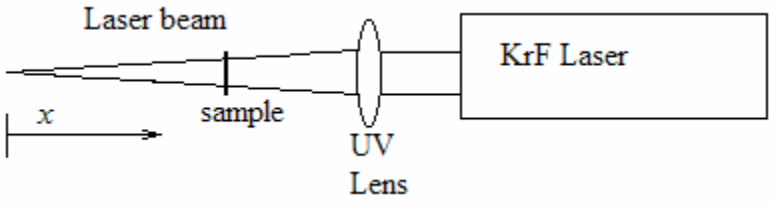

Fig. 3-4. A schematic of the laser annealing process, showing the position of the sample with respect to the UV lens.

3.4 X-ray diffraction (XRD)

Most of the x-ray diffraction (XRD) experiments for this study were carried out on a Rigaku diffractometer equipped with a Cu K_α source and a graphite monochromator. This is a single-crystal diffractometer with resolution high enough for θ-2θ chemical analysis, but not high enough for high-resolution rocking curve measurements. For some of the samples, rocking curve measurements were carried out in a different laboratory.

Samples are mounted to the sample holder with modeling clay to ensure good adhesion and to allow for the sample to settle into a position flush with the 0^o position of

the instrument. After the Cu K_α source is turned on, the experiment is started using the computer interface. Typically, scans are performed from 20^o to 100^o in 0.1^o increments, and 1 second counting time between measurements. Smaller than 0.1^o increments are sometimes attempted, but they are not justified by the resolution of the instrument.

3.5 Transmission electron microscopy (TEM)

3.5.1 Sample preparation

Transmission electron microscopy sample preparation is, by far, the most intensive and specialized skill used in the present study. Especially considering that sapphire is considered one of the most difficult materials to work with; TEM sample preparation was the most time-consuming aspect of the present study.

From the original sample, which is approximately 1 cm on an edge, several small pieces are cleaved. These small pieces are about 1 mm x 3 mm, and they are taken from the sample such that some of them are oriented lengthwise in the $[2\bar{1}\bar{1}0]$ direction, and the others are oriented in the $[01\bar{1}0]$ direction. (Straight lines are drawn on the back of the sample prior to cleaving, so that the orientation is not forgotten, and also so that the film side is not mistaken for the back side of the sample.)

These pieces are then glued together, with permanent glue on the film side of the sample, such that a piece in the $[2\bar{1}\bar{1}0]$ direction is glued to a piece in the $[01\bar{1}0]$ direction. The reason for gluing two pieces together is so that the ZnO films will not chip

off during the polishing process, and also so that the final sample will have ZnO orientations in both low index directions.

After applying the glue, the pieces are pressed together and held on a hot plate until the glue hardens. Then the sample is waxed onto a pyrex cylinder, such that the long edges of the two pieces are facing outward.

The pyrex cylinder is mounted in a sample holder, and the sample is polished smooth on one side with SiC paper, and then finally diamond paper. The wax is melted off, and the sample is turned over, so the now smooth side is touching the pyrex cylinder, and the other side is then polished. The final thickness of the sample should be between 40 μ and 80 μ.

With the sample still in the pyrex cylinder, the sample is mounted into the dimpling machine to polish a crater in the center of the sample. The purpose of this crater is to create a point in the center of the sample where the sample is thinnest. This will hopefully be the point where a hole will form during ion milling.

Before ion milling, the sample must be removed from the pyrex stub, and permanently glued to a tantalum or molybdenum ring. The rings are exactly 3 mm in diameter, and this is the reason for making the sapphire pieces 3 mm long.

The ion milling process bombards the center of the sample with Ar^+ ions which dry etch the sample at an angle of around 5^o from the smooth surface of the sample, and an ion energy of around 5 keV, using two ion guns which alternately aim their ions at the top and the bottom of the sample, as the sample is slowly rotated. Because of the dimple in the sample, a hole eventually forms at the center of the sample near the interface. Figure 3-5 shows the final sample with a small hole in the center. A close-up of the hole

shows the thin area where the ZnO film will actually be imaged. Because of the low angle of ion bombardment, this thin foil of ZnO varies in thickness between 10 nm at the outer surface, and 100 nm near the sapphire interface.

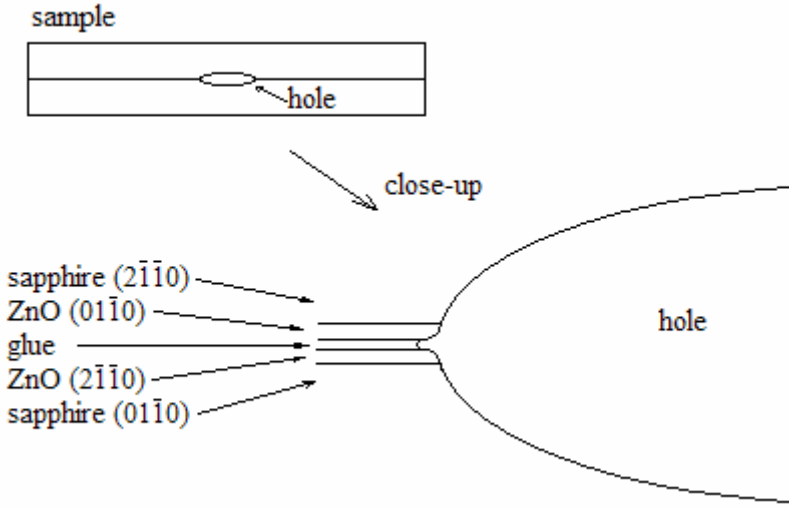

Fig. 3-5. The final sample after polishing and ion milling which is only 3 mm long, and showing a close-up of the edge of the hole where the TEM imaging will actually take place.

3.5.2 Microscopic imaging and diffraction

Most of the transmission electron microscopy performed for this study was done on a 200 kV JEOL 2010F high-resolution transmission electron microscope with point-to-point resolution of 1.8 Å. For some of the samples a Topcon EM002B thermionic emission microscope operating at 200 kV was used.

The sample is mounted to the goniometer with set screws, and cleaned in a plasma cleaner for several minutes prior to being mounted in the microscope. Liquid nitrogen is used to reduce phonon noise in the sample, and improve resolution in high-resolution imaging. After pump-down and alignment of the microscope, the imaging

begins with low-magnification images of the film and substrate. These images are typically taken on photographic film, which is later developed and scanned. Electron diffraction is also typically done at this time.

These low-magnification images can also be used to perform $\mathbf{g}\cdot\mathbf{b}$ analysis on threading dislocations in the film. To do this, the sample must be tilted with the goniometer into the "two-beam condition", wherein only two diffracted beams appear strongly. This improves the contrast between the threading dislocation and the rest of the film.[11] The two-beam condition is then repeated for the other **g** direction, where two different diffracted beams, perpendicular to the first two, appear strongly.

High-magnification images are performed on a CCD camera mounted inside the microscope. The images are saved on the computer in a format that can be analyzed through a fast Fourier transform (FFT) to determine the crystal quality and orientation. The FFT is a type of computer-generated diffraction pattern for high-magnification images.

3.6 Optical absorption

Some of the optical absorption measurements for this study were performed on a dual-beam Perkin-Elmer Lambda 5 (UV-VIS-NIR) absorption spectrophotometer. Other optical absorption measurements were performed on a dual-beam Hitachi spectrophotometer. Most measurements were performed at room temperature.

Using a small piece of two-sided tape, which is carefully placed outside of the optical path, the sample is mounted in one of the beam paths for the spectrophotometer,

while a blank piece of sapphire is sometimes mounted in the other (reference) beam path. The reference beam path is sometimes left open. In fact, leaving the reference beam path open is a preferable way to report some data. Optical absorption/transmission is calculated as a function of wavelength as the monochromated light is scanned through the sample and compared to the light in the reference beam.

3.7 Resistivity and hot-point probe

There were room temperature and low temperature resistivity measurements taken for this study. The room temperature resistivity measurements were carried out with a four-point probe, consisting of four needle probes, equally spaced from each other, directly touching the surface of the ZnO sample. Between the two outer probes, a constant current was driven through the sample using a Keithley 2400 sensitive digital multimeter. The voltage between the two inner probes was monitored using a Keithley 6517A electrometer. Resistivity was then calculated based on sample geometry.

For low temperature studies, gold contacts are evaporated onto the sample with a sputter coater, and gold wires are fastened to these gold contacts with indium dots. The sample is then mounted with vacuum grease onto the cold finger inside a Janis cryostat, connected to a closed-cycle helium refrigerator. The cryostat is pumped down to a few milliTorr with a roughing pump, and the refrigerator is started. Below approximately 150 K, the roughing pump can be closed to prevent oil back-streaming, and the vacuum is maintained due to the cold finger trapping gas molecules.

The temperature of the cold finger is held constant every 10 degrees K by use of an electrical resistance heater and a Lakeshore 331 temperature controller. During this time a measurement is taken.

Measurements are performed by driving current through the outer contacts using a Keithley 220 current source, and measuring the voltage between the inner contacts using a Keithley 182 sensitive digital voltmeter. Through a GPIB interface, the experiment is controlled by a computer, which records each measurement and then allows the sample to cool down another 10 degrees K until the sample reaches the minimum possible temperature the cryostat can reach, which is typically about 5 K.

3.8 Photoconductivity

The photoconductivity experiment consisted of a xenon lamp shining light through a monochromator. The monochromated light then went through a UV lens, and was focused on a small spot on the sample. Two needle probes connected to a Keithley 6517A electrometer were positioned inside this small spot of light. A schematic of the experiment is shown in Figure 3-6.

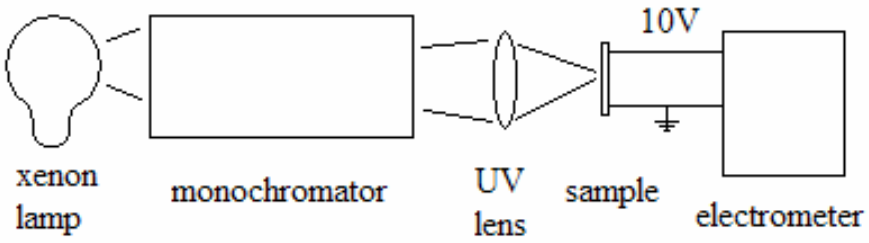

Fig. 3-6. A schematic of the photoconductivity experiment.

The spacing between the two needle probes was optimized according to the size and shape of the spot of light from the UV lens. In order for the light to have the maximum impact on the conductivity of the sample, it is assumed that the light must be evenly distributed over an area of largest current density. The current density was modeled on a computer, and dog-bone shaped areas of constant current density indicated that the needle probes should be spaced from one another at a distance approximately equal to two thirds the diameter of the spot of light. The two-dimensional plot of current density in the sample is given as Figure 3-7.

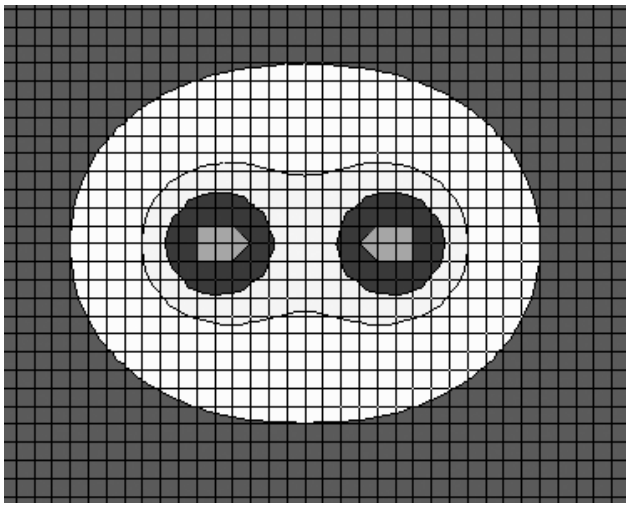

Fig. 3-7. A mathematical model of current density from one needle probe to another.

The Keithley 6517A electrometer applies a constant voltage across the needle probes, while the resulting current is monitored by a computer through a GPIB interface. During wavelength scans, each measurement is taken by the computer, and then the monochromator is moved to the next wavelength. To measure the photosensitivity of the samples, the monochromator is positioned to its zeroth order reflection so that a large amount of polychromatic light impinges on the sample. With this technique it is possible

to compare the photosensitivity of different samples, which may not have exactly the same wavelength dependent spectrum.

3.9 Photoluminescence

Another non-equilibrium technique for characterizing thin films is photoluminescence. Similar to photoconductivity, the technique involves the photo-excitation of a sample and the measurement of its non-equilibrium properties.

In the case of photoluminescence (PL), electron-hole pairs are created through incident radiation, and their subsequent radiative recombination is measured.[12] Only events that emit light can be measured, and the degree to which non-radiative processes are present in the sample is the degree to which photoluminescence will be diminished.

Shallow donors and acceptors usually produce radiative recombination just below the band edge emission, and can be resolved at low temperatures. Deeper level impurities and defects are typically more difficult to resolve. A diagram of the excitation process, as well as two emission processes is given as Figure 3-8. Several other emission processes are also possible, including free exciton emission, and acceptor-bound exciton emission, but are not shown.

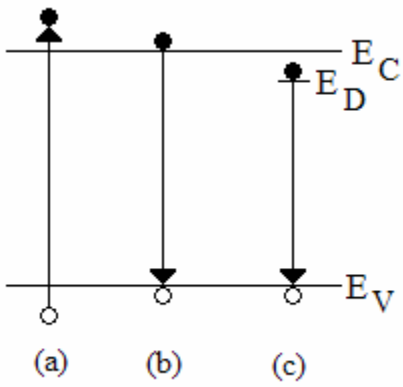

Fig. 3-8. The photoluminescence process involves a) the excitation of an electron-hole pair using a photon energy typically larger than the band gap of the material, and a number of radiative recombination processes are possible including b) band-to-band radiation, and c) donor-bound exciton radiation.

The experimental arrangement for conventional photoluminescence is very basic. It involves shining a laser on a sample, and positioning the detector in such a way that the reflected laser light does not get collected. This takes advantage of the fact that the luminescence is spherically symmetric in its intensity profile, but the laser light is mostly confined to a certain angle of reflection. Of course, because of surface roughness, and other effects, it is impossible to avoid some of the laser light going into the detector, and for this reason, it is standard practice to use a filter in front of the detector that removes the specific wavelength of light which is expected from the excitation source.

The detector is typically a photomultiplier tube, and a spectrometer. This is because the spectrometer can provide very good wavelength resolution, and the photomultiplier tube is very sensitive to small amounts of light. This method requires that the spectrometer be slowly scanned through each of the wavelengths of interest, while the photomultiplier tube counts the photons detected at each wavelength.

With advancements in integrated circuit technology, another method of luminescence detection has emerged. This is a device which combines a spectrometer with a charge-coupled device (CCD) that simultaneously monitors the light intensity from a variety of wavelengths. This gives the researcher an instant image of the luminescent spectrum, which does not require the scanning of the spectrometer from wavelength to wavelength. This makes the experiment faster, and gives the operator the ability to tweak the position of the sample and the mirrors in such a way as to optimize the light collected.

Temperature-dependent photoluminescence involves the use of a cryostat. The sample is mounted in a cryostat, which is equipped with UV windows to allow laser light in and luminescent light out. The cryostat is pumped down to provide thermal insulation, and the cold finger on which the sample is mounted is cooled. The method of cooling may be an open dewar for liquid nitrogen or liquid helium, or it may be a closed-cycle helium pump. Everything else about the experiment is exactly the same as conventional room-temperature photoluminescence.

One method of measuring time-dependent photoluminescence, known as femtosecond excitation correlation (FEC), involves the use of a beam splitter, several mirrors, and a stepper motor to control the position of one of the mirrors.[13] A pulsed femtosecond laser produces a very short excitation pulse, which is split with a beam-splitter into two beams. One of the beams follows a fixed path to the sample. The other beam follows a slightly longer path, controlled by the stepper motor, to the exact same spot on the sample. Thus, the sample is hit with two femtosecond beams, which are separated by any number of picoseconds.

The photons are counted, for the wavelength of interest, using a photomultiplier or CCD, and the data is plotted as a function of the time separation between the two pulses. If the pulses are very far apart, then the number of photons counted should be exactly equal to twice the number of photons that are counted with only one pulse. As the pulses are brought closer and closer together, the sample is re-excited by the second pulse, before it has had time to recover from the first pulse. Thus, if the sample has been excited into a super-linear regime, the net amount of luminescence should be greater than twice the amount of one pulse. A schematic diagram of the process is given as Figure 3-9.

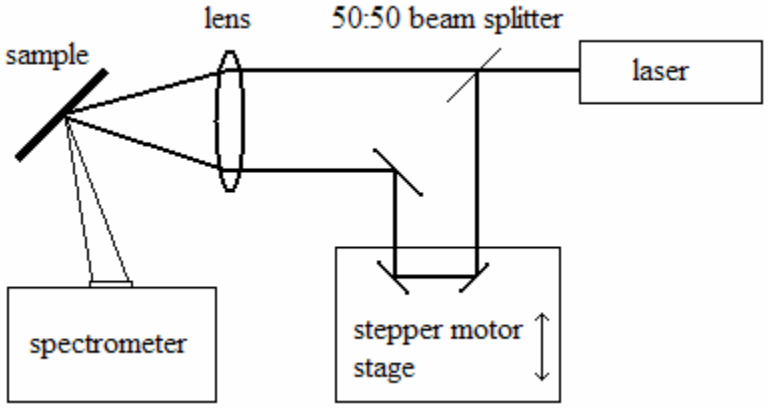

Fig. 3-9. A simplified schematic of a femtosecond excitation correlation (FEC) experiment, showing a beam splitter, a series of mirrors, and a stepper motor, which produce two femtosecond pulses which arrive at a sample at slightly different times.

Another method of measuring time-dependent photoluminescence involves the use of a streak camera.[13] A streak camera works by using the photoelectric effect to convert a time-dependent optical signal into a time-dependent electrical signal. The time-dependent electrical signal is accelerated through a time-dependent voltage, that spreads the signal out and produces a spatially-resolved image that describes the time-dependence of the in-coming signal.[13] The advantage of the streak camera over FEC time-dependent

techniques is that the experiment need not occur in the super-linear regime. However, streak camera speeds are typically not as fast as two-beam measurements.

3.10 References

1. J. Bruncko, M. Michalka, and F. Uherek, "Pulsed laser deposition of ZnO: Comparison between deposition from Zn and ZnO target," presented at Laser and Laser Information Technologies, Sep 27-Oct 1 2003, Smolyan, Bulgaria, 2004.
2. N. Ichinose, *Introduction to Fine Ceramics*. New York, NY: John Wiley & Sons LTD., 1987.
3. R. K. Singh and J. Narayan, "Pulsed-laser evaporation technique for deposition of thin films: Physics and theoretical model," *Physical Review B*, vol. 41, pp. 8843, 1990.
4. J. Narayan, K. Dovidenko, A. K. Sharma, and S. Oktyabrsky, "Defects and interfaces in epitaxial ZnO/α-Al_2O_3 and AlN/ZnO/α-Al_2O_3, heterostructures," *Journal of Applied Physics*, vol. 84, pp. 2597-2601, 1998.
5. A. V. Singh, R. M. Mehra, A. Wakahara, and A. Yoshida, "p-type conduction in codoped ZnO thin films," *Journal of Applied Physics*, vol. 93, pp. 396, 2003.
6. R. K. Singh, L. Ganapathi, P. Tiwari, and J. Narayan, "Effect of processing geometry in oxygen incorporation and in situ formation of $YBa_2Cu_3O_7$ superconducting thin films by pulsed laser evaporation technique," *Applied Physics Letters*, vol. 55, pp. 2351-2353, 1989.

7. G. Muller, M. Konijnenberg, G. Krafft, and C. Schultheiss, *Science and Technology of Thin Films*: World Scientific, 1995.

8. R. Stark, J. Christiansen, K. Frank, F. Mucke, and M. Stetter, "Pseudospark Produced Pulsed Electron Beam for Material Processing," *IEEE Transactions on Plasma Science*, vol. 23, pp. 258, 1995.

9. R. K. Singh and J. Narayan, "A Novel Method for Simulating Laser-Solid Interactions in Semiconductors and Layered Structures," *Materials Science and Engineering B*, vol. 3, pp. 217-230, 1989.

10. J. Narayan, O. W. Holland, W. H. Christie, and J. J. Wortman, "Rapid thermal and pulsed laser annealing of boron fluoride-implanted silicon," *Journal of Applied Physics*, vol. 57, pp. 2709-2716, 1984.

11. D. B. Williams and C. B. Carter, *Transmission electron microscopy: A textbook for materials science*, 1st ed. New York, NY: Plenum Press, 1996.

12. D. K. Schroder, *Semiconductor Material and Device Characterization*, 2nd ed. New York, NY: John Wiley & Sons, Inc., 1998.

13. W. Demtroder, *Laser Spectroscopy*, 3rd Edition ed: Springer-Verlag, 2002.

4.0 Experimental results

4.1 Pulsed laser deposited ZnO

Before the experiments on the doping characteristics of ZnO were carried out, the conditions for growing pure, epitaxial ZnO were optimized. Growth temperature and annealing conditions were varied, and the resulting effect on crystal quality was examined through x-ray diffraction (XRD), and transmission electron microscopy (TEM).

Firstly, a series of films were grown using the pulsed laser deposition (PLD) technique, varying the growth temperature between 600^{o} C and 800^{o} C. The films were then characterized, and the experiment was repeated for a new set of films.

Rocking curve scans were made on a high resolution double-crystal diffractometer outfitted with a channel-cut-collimator and a Si (111) monochromatic crystal set for Cu K_{α} radiation. The resulting plot of x-ray full-width at half-maximum versus growth temperature is shown in Figure 4-1.

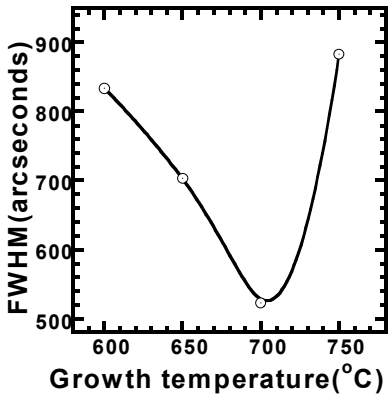

Fig. 4-1. Full width at half maximum of HRXRD of as-grown ZnO samples change as a function of growth temperatures.[1]

It is clear from this data that the best films resulted from a growth temperature of around 700^{o} C. The full-width at half-maximum at this temperature is roughly 0.15^{o}. This compares with 0.16^{o} reported by Narayan, et al.,[2] and 0.12^{o} reported by Bae, et al.[3] Lower growth temperatures result in poorer quality films, because the substrate does not provide enough energy to impinging atoms, while they seek optimal positions in the growing crystals. Higher growth temperatures result in poorer quality films, because the overly oxidizing environment produces poor surface morphology, and thus poor growth morphology.

Both high magnification and low magnification transmission electron microscopy (TEM) was performed using a JEOL-2010F analytical electron microscope with point-to-point resolution of 0.18 nm (TEM) and 0.12 nm (STEM). The cross-sectional high resolution TEM (HRTEM) micrograph of zinc oxide sample prepared at 650^{o}C is shown in Figure 4-2-a. The sample was prepared in the $(01\bar{1}0)$ axis, as evidenced by the close-packed arrangement of sapphire atomic columns. The image shows epitaxial growth, low defect density, and a sharp interface between the sapphire and the zinc oxide film, which is rotated 30^{o} in the c-plane with respect to the substrate. Periodic dark and light bands of strain in the zinc oxide are perpendicular to the interface, and it is suggested that this indicates a successful domain matching epitaxial relationship between the sapphire substrate and the zinc oxide film.[4]

Figure 4-2-b shows the low magnification cross-sectional transmission electron micrograph of a pure ZnO sample grown at 700^{o} C. Again, a low defect density is observed. Dislocation tangles near the interface react to form low density threading dislocations which propagate to the surface of the film. Plan-view samples were not

prepared, so defect densities can not be given with certainty, but the defects are estimated at 10^8 cm^{-2}, which are comparable to high quality films reported in the literature.[2,5,6]

a) b)

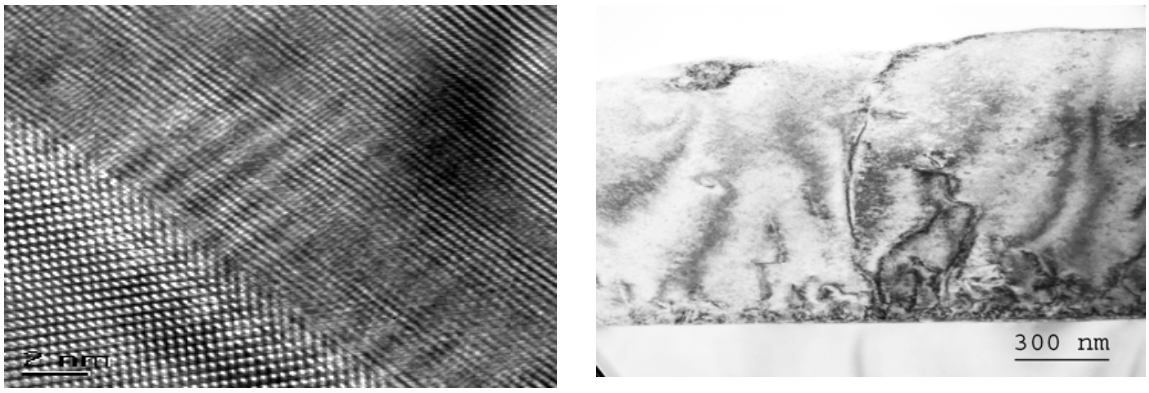

Fig. 4-2. a) The cross-sectional high resolution TEM (HRTEM) micrograph of zinc oxide sample prepared at 650° C.[1] b) The cross sectional low magnification TEM micrograph of zinc oxide sample prepared at 700° C.

Two thermal anneals were performed on the samples. Both anneals were carried out in a programmable quartz tube furnace. The first anneal was with both ends of the quartz tube open to the air. The temperature of the furnace was programmed to increase to 700° C over the course of one hour, the temperature was held at 700° C for an additional hour, before finally slowly cooling back down to room temperature. The second anneal was carried out while flowing high purity oxygen through the quartz tube, and using a temperature of 750° C. Optical measurements were made before and after each of the anneals.

From cathodoluminescence analysis, the sample grown at 750° C has a sharp band-edge emission shown in Figure 4-3-d. However, it has stronger deep level emission than the sample grown at 700° C shown in Figure 4-3-c. Hence, the ratio of the band-edge emission to deep level emission of sample grown at 750° C is less than the

sample grown at 700^{o} C. Based on the x-ray rocking curve data and room temperature CL measurement, we found the sample grown at 700^{o} C has the best crystal and optical quality.

In order to investigate the effects of the annealing atmosphere for improving sample quality, CL spectra were taken after the annealing in air for one hour at 700^{o} C and annealing in oxygen at 750^{o} C for one hour. As shown in Figure 4-3-b, the intensities of the band-edge emission of the sample grown at 650^{o} C increase after annealing in air, but it is much more predominant when annealed in oxygen ambient. For samples grown at 600^{o} C and 750^{o} C, shown in Figure 4-3-a and -d, the intensities of the band-edge emission decrease after annealed in air and oxygen environments. The band-edge emission of the sample grown at 700^{o} C became weaker after annealed in air at 700^{o} C, and then became stronger again after annealed in oxygen at 750^{o} C. Meanwhile, the deep level, green emission of all samples increased to some extent. It became much broader for the sample grown at 600^{o} C after the two anneals. It increased least for the film grown at 700^{o} C, which has the best crystal and optical quality. This green emission of ZnO has previously been reported to be related to oxygen vacancies, interface related defects and impurity mechanisms in the film.[7-9] The above observations suggest that effective annealing conditions are determined in part by the quality of the initial film. In polycrystalline thin films annealing is often associated with grain growth, and individual grains if larger than the exciton radius can be efficient light emitters when excited. The increase of band edge emission in this study is consistent with obtaining better crystallinity and reducing mechanisms that would disrupt the exciton. A decrease in the green luminescence with annealing in air and oxygen would suggest that the number of

oxygen vacancies is being lowered. However, an increase of the green band luminescence is found in films grown above and below the optimum temperature of 700 degrees. This suggests that something more complicated than just the replacement of point defects is occurring. It also suggests that the recombination mechanisms of the exciton and the defect luminescence are decoupled.

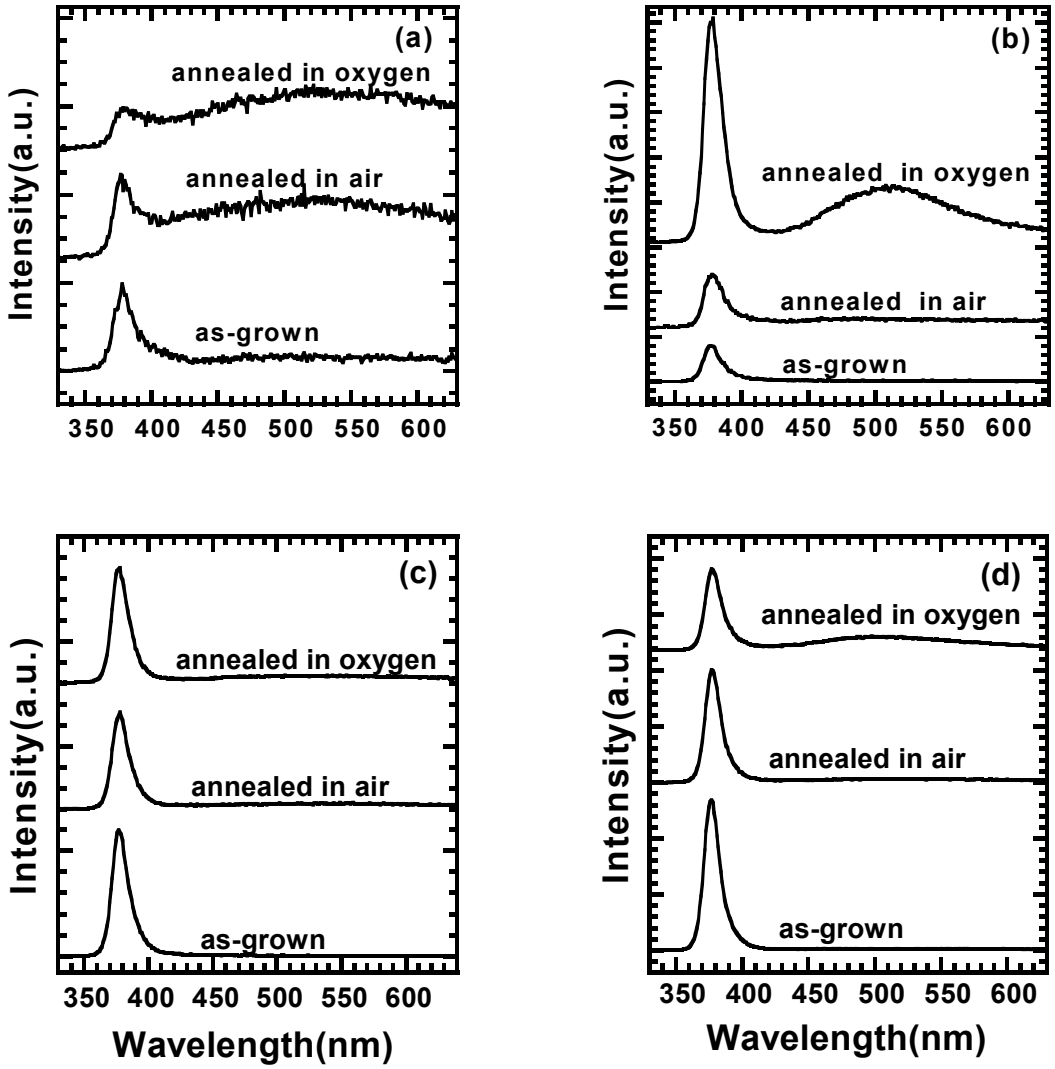

Fig 4-3. Room temperature CL spectra of ZnO samples annealed in air at 700°C for one hour, in oxygen at 750°C for one hour, grown at (a) 600°C, (b) 650°C, (c) 700°C and (d) 750°C.

Figure 4-4 shows the absorption spectra for pre-annealed and post-annealed ZnO samples grown at different temperatures. The absorption peak of the exciton is visible

near the absorption edge due to a large exciton binding energy of ~60meV at room temperature for high quality ZnO films shown in Figure 4-4-a.

The sharpness of excitonic peaks is improved for samples grown at 700^{o} C and 750^{o} C, annealed in air. This is consistent with improving the crystal quality of the thin film and is consistent with the improvements found in the CL spectra.

Upon annealing in oxygen environment, strong, sharp and clear excitonic peaks are shown in Figure 4-4-c. The unpolarized transmission spectrum is taken with the incident light normal to the surface and the strain between the ZnO thin film and the sapphire substrate are expected to impact the selection rules. The lower energy peak (λ~377 nm) consists of the A and B excitons broadened into one peak, while the high energy peak (λ~365 nm) is the "C" exciton. This is also consistent with low temperature spectra previously collected from thin ZnO films of sapphire.[10]

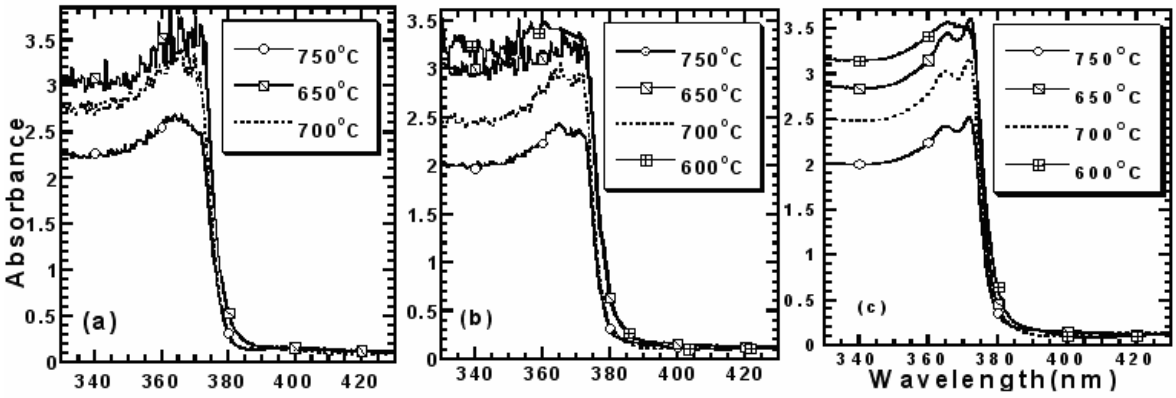

Fig 4-4. Absorbance spectra of ZnO samples (a) pre-annealed, (b) annealed in air at 700^{o}C for one hour, (c) annealed in oxygen at 750^{o}C for one hour at different growth temperatures.

Based on the data collected, we can conclude that the best temperature for the pulsed laser deposition of zinc oxide from a solid-phase target in oxygen ambient is approximately 700^{o}C. For higher quality films, film quality is further improved after thermally annealing in air and in oxygen, but for lower quality films, it's made worse. It

was found that the excitonic structure was useful in investigating and quantifying the effects of annealing on the quality of wide band gap thin films.

4.2 Pulsed electron deposited ZnO

The other method that was used in this study for the preparation of ZnO thin films on sapphire was pulsed electron deposition (PED). The experimental technique was described in Chapter 3.

Since the substrate temperature of 700^{o} C worked well in the pulsed laser deposition study, it was used again in the pulsed electron deposition study. This may not be ideal, however, since the PED technique typically uses higher oxygen pressures, and the combination of a high temperature and a higher oxygen pressure leads to a more oxidizing environment which leads to poor surface morphology. Nevertheless, the solution to this problem is not to lower the growth temperature for PED since the thermal energy is still needed for adatom mobility. The best solution is to mix the oxygen with argon prior to leaking the gas into the PED chamber. This slows down the oxidation of the film and allows the higher growth temperature.

Optical micrographs of the ZnO target before and after ablation can be seen in Figure 4-5. The surface morphology after growth shows a rippled appearance. This is indicative of the thermal effects induced by the relatively long electron pulse of ~100 ns. The surface morphology can be correlated to plasma plume uniformity. The tops of the bumps appear to have a metallic sheen when viewed under the optical microscope, while the valleys still have the color of the original ZnO target. Surface roughness of the post-

ablation target may also indicate a mixture of ablation and thermal evaporation.[11] This mixture of ejected phase is typically blamed for "chunks" appearing in the film, and is usually worse for pulsed electron deposition than it is for pulsed laser deposition.

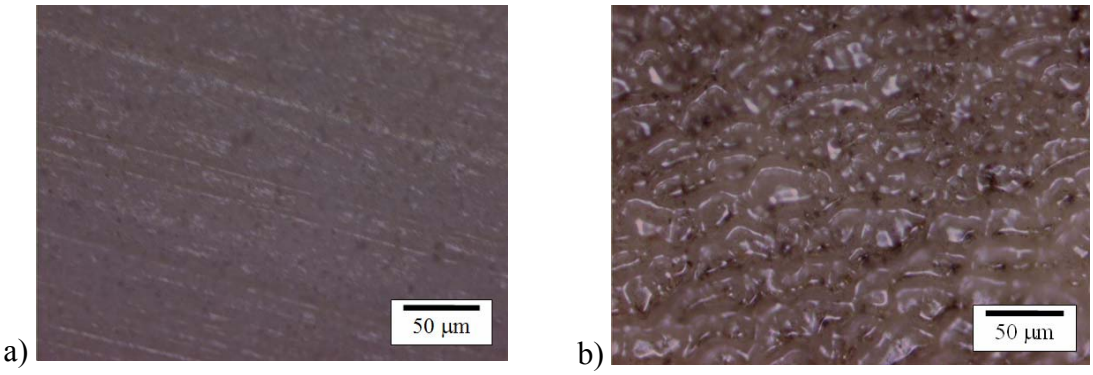

Fig. 4-5. Surface morphology of ZnO target a) before growth, and b) after growth of about 18,000pulses.

The films were first characterized by X-ray diffraction (XRD) and found to be single crystal, and strongly oriented in the (000l) direction. The over-all appearance of the Θ-2Θ spectrum (Figure 4-6) is comparable to that of films grown through PLD that were shown to be epitaxial, and of high crystalline quality through transmission electron microscopy (TEM) studies.[2]

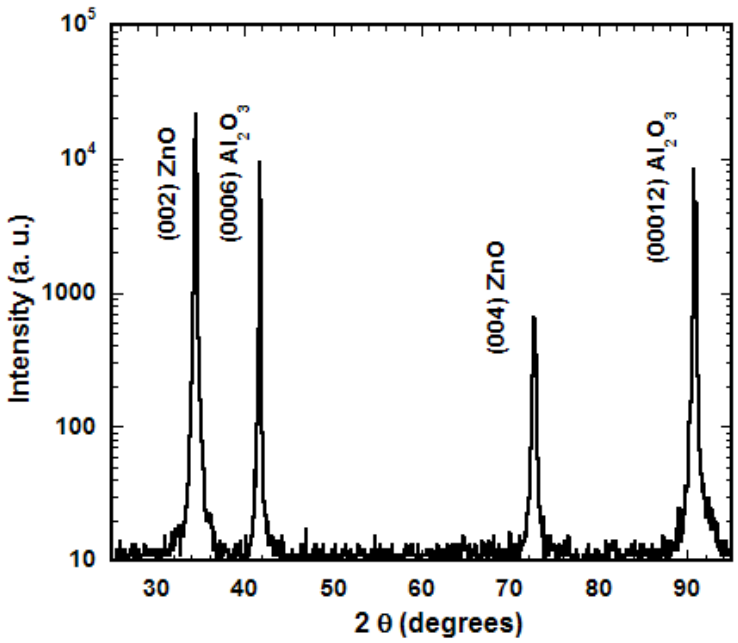

Fig. 4-6. θ-2θ X-ray diffraction spectrum, plotted on a log scale, from the 250 nm thick ZnO film deposited through pulsed electron deposition (PED) method.

Cross-sectional samples were observed under high resolution transmission electron microscopy (HR-TEM). Figure 4-7-a shows the epitaxial growth of of ZnO on sapphire through pulsed electron deposition. The epitaxial quality is very good, comparable to that of the sapphire itself. Several stacking faults are observed in both the film and substrate. The inset of Figure 4-7-a is the selected area diffraction (SAD) of the low magnification image. The sharpness of the diffraction spots confirms epitaxial growth. Low magnification images (not shown) indicate surface roughness due to both chunk formation, and three-dimensional growth mode. Figure 4-7-b shows the Fourier filtered image of the high resolution micrograph, which illustrates the domain matching epitaxial[4] relationship between ZnO and sapphire. Half planes of sapphire clearly terminate at the interface every seven lattice planes throughout the epitaxial growth.

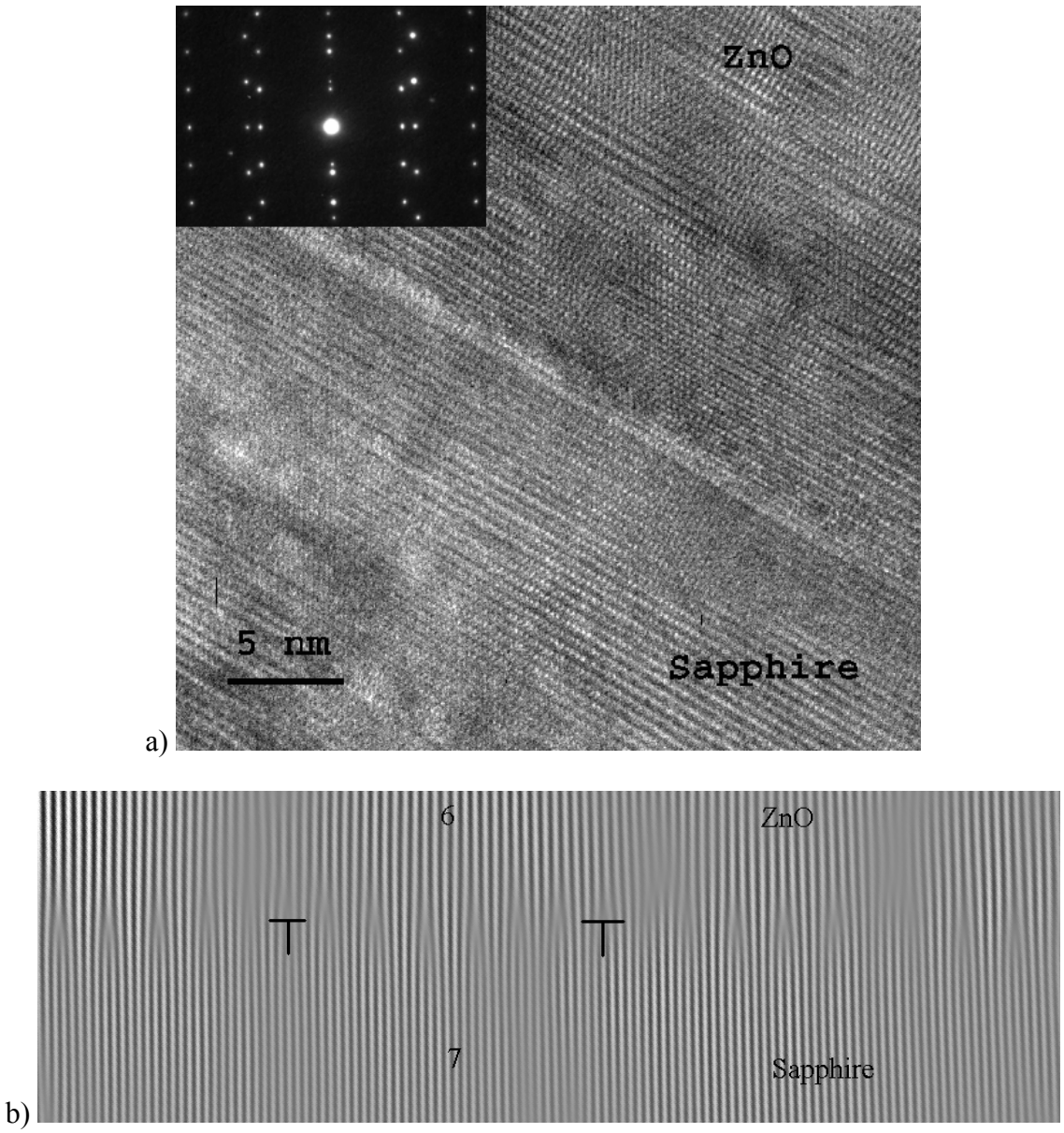

Fig. 4-7. a) High resolution transmission electron micrograph (HR-TEM) of ZnO grown on sapphire through the pulsed electron deposition technique, with an inset of the selected area diffraction (SAD) taken from the low magnification image, and b) the Fourier filtered image demonstrating the domain matching epitaxial relationship between the film and the substrate.

Room temperature cathodoluminescence of the sample is shown in Figure 4-8. A sharp peak in the emission at 3.272 eV (378 nm), with a full-width at half-maximum (FWHM) of 154 meV is present indicating band edge emission.

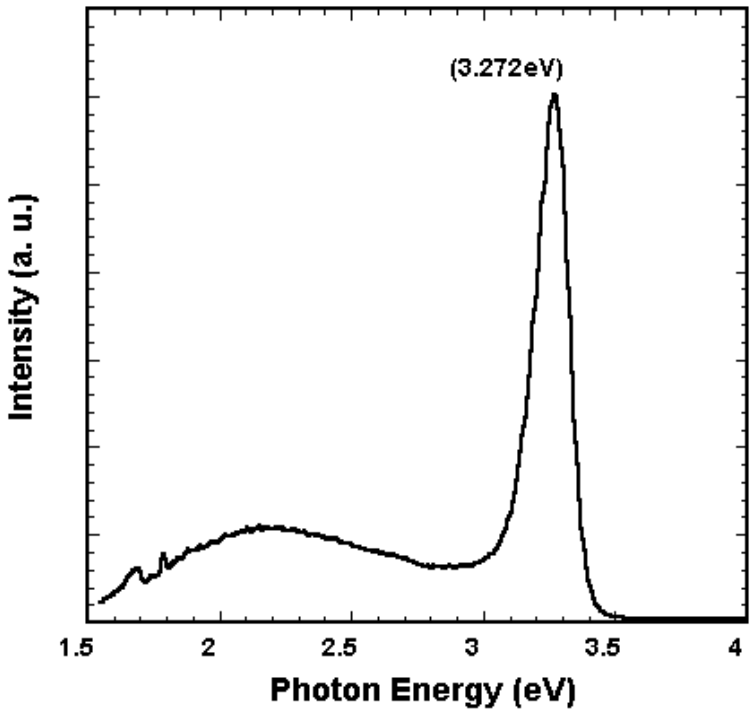

Fig. 4-8. Room temperature cathodoluminescence spectrum of ZnO film prepared through pulsed electron deposition (PED) method.

Optical transmission/absorption measurements were taken on a dual-beam Perkin-Elmer Lambda 5 ultraviolet-visible infrared spectroscopy-near infrared (UV-VIS-NIR) absorption spectrophotometer. The room temperature optical absorption is shown in Figure 4-9. The A and B excitons are visible as one peak, since the spectrum is taken at room temperature, and the individual peaks have merged, due to thermal broadening.[12] The broad peak just below the band edge is the result of a Fabry-Perot oscillation due to the index mismatch of the ZnO and sapphire substrate. The transmission was greater than 80 percent across the visible and NIR portion of the spectrum. Optical absorption was also performed on the same sample at liquid nitrogen temperature (77 K). For this

spectrum, (Figure 4-9-b), we can see clear separation between the A and B excitonic absorption peaks. The C excitonic peak is present, but broader and less distinct.

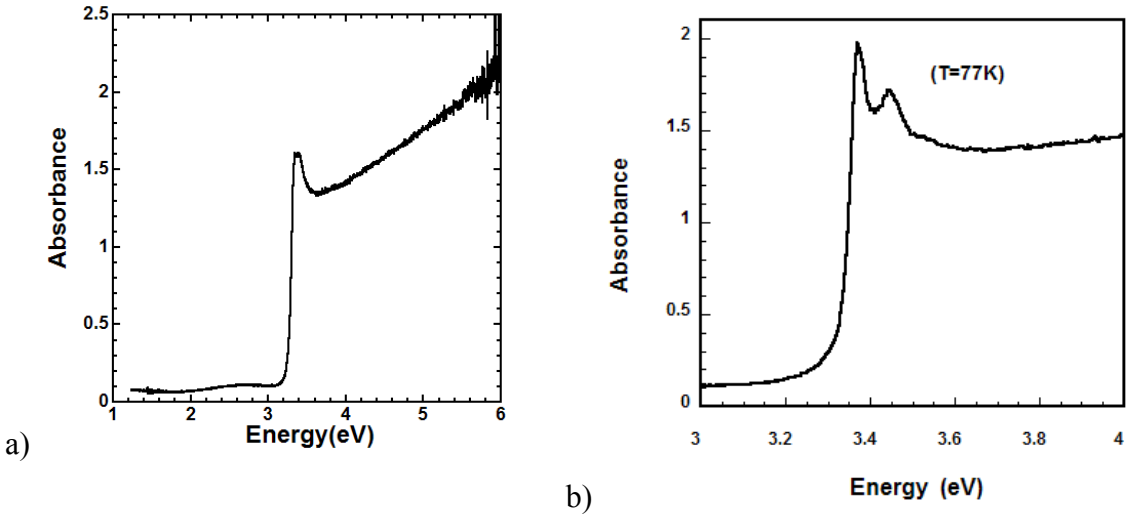

Fig. 4-9. Optical absorbance at a) room temperature, and b) liquid nitrogen temperature, of ZnO film prepared through pulsed electron deposition (PED) method. The A and B excitons are clearly visible as one peak at room temperature, while they have separated at 77 K. The peak below the band edge at RT is a single Fabry-Perot oscillation, due to the index mismatch between the film and substrate.

In conclusion, x-ray diffraction, cathodoluminescence, optical transmission and absorption have been used to characterize ZnO films grown on sapphire (0001) substrates, through pulsed electron deposition (PED). The films are shown to be of high crystalline and optical quality. There are, however, issues that still need to be resolved regarding oxidation and surface morphology.

4.3 Resistivity versus temperature for pure ZnO

Electrical characterization on the pure ZnO samples, grown through pulsed laser deposition, was begun with resistivity versus temperature. The experimental set-up is explained in Chapter 3.

As the temperature of the ZnO films is lowered, the carrier concentration is reduced. This is due to the lack of thermal energy in the crystal, which is needed to ionize dopant atoms or defects that provide the *n*-type carriers in pure ZnO. However, the carrier mobility is improved, due to the reduction in phonon-electron scattering in the crystal. Throughout the temperature range from 0 K to 400 K, falling carrier concentration dominates, and the resulting resistivity versus temperature spectrum for a semiconductor shows an upward trend for lowering temperatures. This is true for "classical" semiconductors, such as silicon and GaAs.

The exact nature of this trend depends on the type of semiconductor material, and various models have been proposed to describe the relationship. The exact nature of the temperature dependence depends on the microstructure. When ZnO forms, three-dimensional growth islands come together to form threading dislocations. With the assumption that defect scattering at threading dislocations dominates the mobility of electrons in the crystal, and that threading dislocations are electrically identical to grain boundaries, it is natural to choose a model from studies on polycrystalline ZnO. Kamins[13] and Seto[14] have proposed a model for polycrystalline materials that suggests carrier mobility dominated by trapping at grain boundaries. This model seems to work

well for our samples, suggesting that threading dislocations in epitaxial ZnO are electrically similar to grain boundaries in polycrystalline material.

In both the polycrystalline case, and in the threading dislocation case, the disruption in the lattice can be modeled as small potential barriers. Figure 4-10 shows how potential barriers are formed at dislocations through charge build up from trapped carriers. These potential barriers impede flowing carriers, and dominate their mobility. In the case where the trapping energy, E_t, lies below the Fermi level, E_f, we have:

$$\sigma_D = \frac{q^2 L N_d}{(2\pi m_e^* kT)^{1/2}} \exp(-E_a / kT)$$

and

$$E_f - (E_t + E_b) >> kT$$

In the case where the trapping energy, E_t, lies above the Fermi level, E_f, we have:

$$\sigma_D = \frac{4qL}{Q_t}\left(\frac{\varepsilon E_b k^5}{\pi m_e^* N_d}\right)^{1/2} (2\pi m_e^* / h^2)^3 T^{5/2} \exp(-E\alpha / kT)$$

and

$$(E_t + E_b) - E_f >> kT .$$

In these expressions σ_D is the dislocation scattering dominated conductivity, L is the average distance between dislocations, and E_b is the energy barrier induced in the conduction band for n-type material.

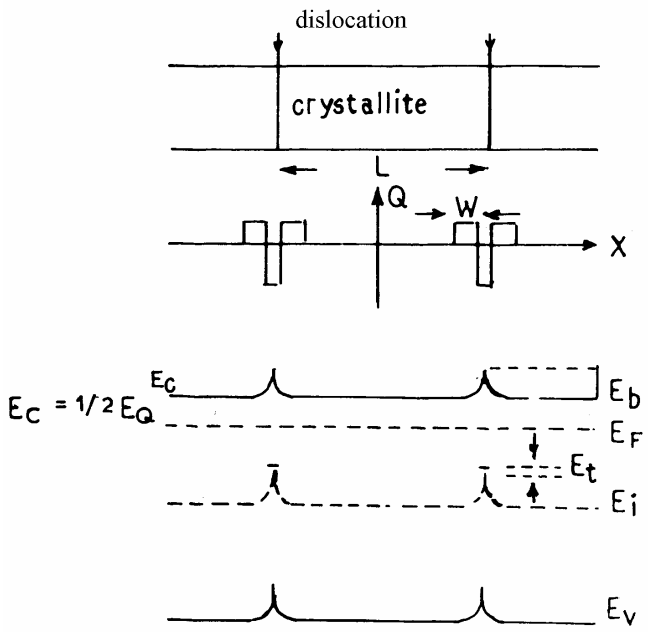

Fig. 4-10. Grain structure, charge distribution and energy band diagram for dislocation trapping model.[15]

When the raw data is manipulated such that ln ($\sigma_D/T^{2.5}$) is plotted versus 1000/T, in the temperature range between 200 K and 300 K, as shown in Figure 4-11, a very good straight line fit is achieved with an R^2 value of 0.9994. This indicates that for our samples, the trapping energy, E_t, lies above the Fermi level, E_f. The model where the trapping energy lies below the Fermi level is shown as the inset, and has a lower R^2 value of 0.9846. This indicates that there are perhaps still some trapping levels below the Fermi level. This is likely due to the fact that these were undoped ZnO films and the Fermi level was not so close to the conduction band as it was for the studies of *n*-type doped ZnO films in the cited studies. Thus there is room in the band gap both above and below the Fermi level for trapping states to exist, and there need not be only one trapping mechanism.

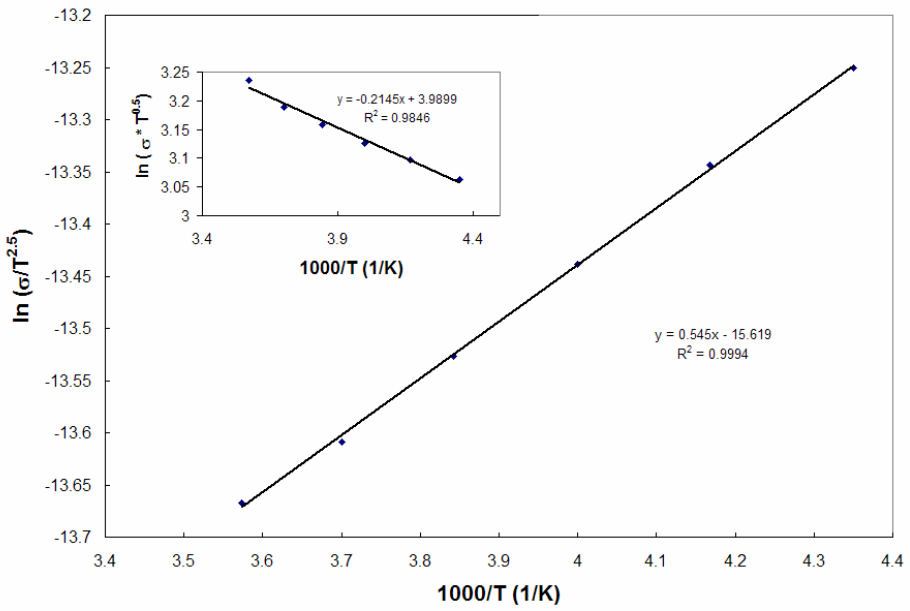

Fig. 4-11. Resistivity versus temperature plotted as a function of conductivity versus 1000/T. The inset shows a slightly inferior model.

4.4 Isoelectronic Te in ZnO

The major thrust of this study was to investigate the effect of adding the isoelectronic impurity, tellurium, into the ZnO thin films. The basic idea of research on isoelectronic impurities was introduced in Chapter 2, but here the focus will be more specifically on tellurium in II-VI compounds, and the results from this study.

Goede, et al., performed several studies on the isoelectronic impurity, Te, in II-VI semiconductor compounds.[16-19] The major focus of Goede's work was the role Te plays in trapping excitons. The trapped excitons were responsible for distinct bands in the low-temperature photoluminescence, which was suggested to be of application interest in electroluminescence devices. The mechanism by which the excitons were said to be bound to the tellurium had to do with electronegativity differences. The tellurium is less

electronegative than the host element, so it was said to bind holes. Then due to coulombic interactions, the holes were said to bind electrons, forming an exciton.

Fan, et al., also investigated the effect Te had on the nitrogen solubility in ZnSe.[20] The major focus of the work was on preparing *p*-type ZnSe, and it was shown that the Te increased the nitrogen concentration, but the free hole concentration dropped with Te concentration, indicating hole binding at Te sites.

The initial motivation of the present work was to enhance the *p*-type dopability of ZnO by adding the impurity, Te.[21] There were several reasons for trying this, and they are summarized as follows:

1. Intuition suggests an alloy between ZnO, which is naturally *n*-type, and ZnTe, which is naturally *p*-type, could provide a template, which might be easier to dope either *n*-type or *p*-type.
2. Because of the electronegativity differences, ZnTe is more covalent than ZnO, and the improved covalent nature of the material may improve hole mobility.
3. Because of the lower electron affinity of ZnTe, and the Anion correlation rule,[22] the addition of Te will raise the valence band of the ZnO more than it raises the conduction band. This may lead to better acceptor ionization efficiencies, and improve the ohmic behavior of metallization to *p*-type ZnO. (See Figure 4-12.)
4. The vapor pressure of Te is lower than that of oxygen, and the resulting alloy may have better anion stoichiometry, which will reduce the problem of oxygen vacancies in ZnO.[23]

5. The larger radius of the Te atom may induce Zn interstitial formation which has been suggested to form a *p*-type dopant complex for arsenic dopants in ZnO.[24]

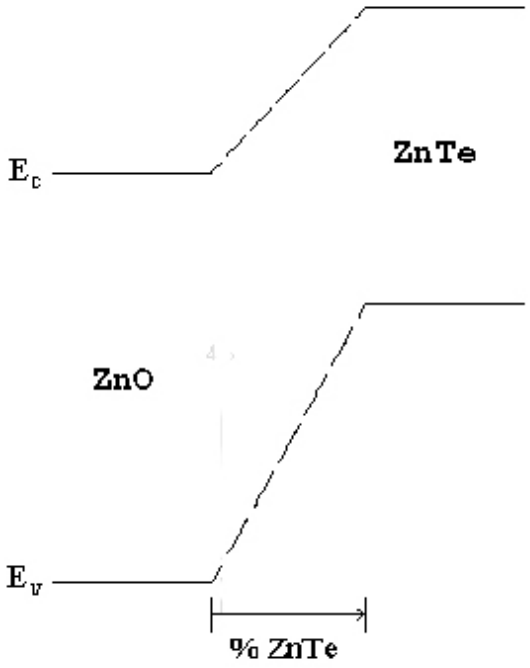

Fig. 4-12. The band gaps of ZnO and ZnTe, compared to the vacuum level, illustrating the effect to the conduction band and valence band of ZnO with the inclusion of ZnTe.

The last point deserves closer inspection. The problem of ZnO being naturally *n*-type has been largely attributed to oxygen vacancies; whereas, the tendency of ZnTe to be *p*-type is attributed to Zn vacancies. As was explained in Chapter 2, the reason for the vacancies is that the lighter of the two constituent elements in a compound semiconductor tends to evaporate out of the material, leaving a stoichiometry imbalance that has the effect of leaving the material either *n*-type or *p*-type as grown. If this be the case, then at least theoretically, it should be possible to grow an alloy of two compound semiconductors, such that the alloy has a perfect balance of cations to anions, and is

therefore electrically intrinsic, and would provide a good template for making bipolar devices.

Consider the compound semiconductor, with cation, C, and anion A. If the material is anion-deficient, as is ZnO, we can write something like:

$$C_1 A_{0.9999}$$

to express the true stoichiometry. If then, we had two different compound semiconductors, one of them anion-deficient, and the other cation-deficient we could write:

$$C_1^1 A_m^1 \text{ and } C_n^2 A_1^2$$

with the resulting alloy composition x, we would then have:

$$C_x^1 C_{n(1-x)}^2 A_{mx}^1 A_{1-x}^2$$

and we could solve for the x value that balances the stoichiometry as:

$$x = \frac{1-n}{(1-n)+(1-m)}$$

which could also be expressed as a deficiency, in atoms per cm^3, divided by the sum of two deficiencies. Obviously if the deficiencies are the same then x must equal 0.5, but if they differ by an order of magnitude or two we have:

$$x = \frac{10^{18}}{10^{18}+10^{19}} \approx 9\%$$

or

$$x = \frac{10^{17}}{10^{17}+10^{19}} \approx 1\% .$$

Such an imbalance in the deficiencies could be induced through the proper growth conditions, and would allow one of the two materials to dominate.

Two practical problems with this approach are the relatively low sublimation temperature of ZnTe (~500^{o} C), and the relatively low solubility of ZnTe in ZnO. The lower growth temperature can also reduce the number of oxygen vacancies in the ZnO. However, small percentages of ZnTe could be used to balance the cation to anion stoichiometry in the material, and the material would still be mostly ZnO, with the desirable properties of ZnO preserved.

In thermal annealing studies of CdTe and ZnO, Brune, et al., suggest that the Te and the O systems are virtually insoluble.[25] This, however, is based on equilibrium annealing, and that is not the case for pulsed laser deposition (PLD). Since PLD is a very non-equilibrium process, materials that might otherwise be insoluble, do not have the thermal energy needed to separate out into separate phases, and can be alloyed.

Some of the initial films of ZnO grown with Te impurities were characterized to determine the incorporation of Te in the crystal lattice. Figure 4-13-a shows the excitonic absorption peak for two ZnO:Te films as compared to a pure ZnO film. In alloy films one expects the exciton peak to be alloy-broadened, and that was observed for higher concentrations of Te. Also, for higher concentration films, it is shown in Figure 4-13-b that the A exciton was diminished, as compared with the B exciton. For smaller concentrations, a measurable, and repeatable, shift in the A excitonic peak position is observed for the ZnO:Te film as compared to pure ZnO films grown at the same temperature. Linearly interpolating between the band gaps of ZnO (3.35) and ZnTe (2.39), a shift of the exciton peak of about 30 meV provides a rough estimate of about 3 to 4% Te incorporation. However, as will be shown, there is good reason to doubt this.

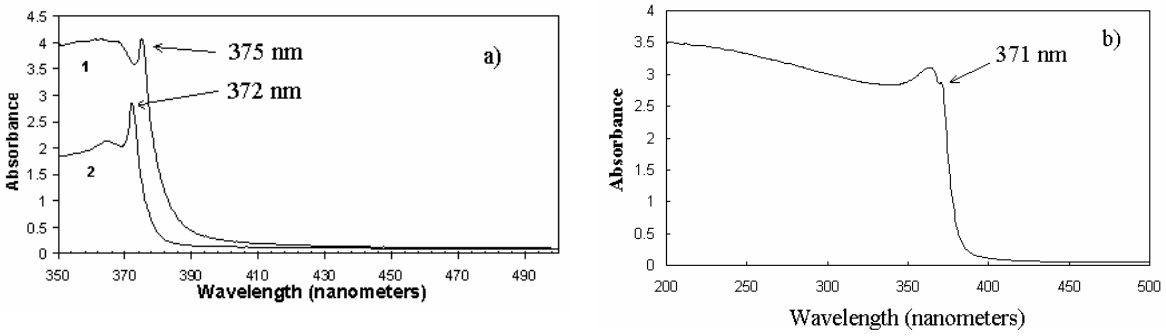

Fig. 4-13. Optical absorption spectrum for ZnO:Te (a.1), and pure ZnO (a.2), grown at similar substrate temperatures and ZnO:Te (b), grown at a slightly higher temperature.

However, such high Te concentrations are doubtful, especially considering later studies. The large shift in exciton position may be due to deviations from Vegard's Law, or strain in the crystal. A suitable estimate of the band gap bowing parameter for this system was not attempted, due to the small concentration. It is also likely that the ZnO/ZnTe system is a persistence-type system, and amalgamation-type excitonic peak shifts are less probable.[17]

Also, there are other explanations for the broadening of the exciton peak, besides alloy broadening. Goede, et al., attribute exciton broadening to exciton binding, and the resulting electron-phonon interactions.[18]

Cathodoluminescence with an accelerating voltage of 5 keV was obtained. In Figure 4-14-a-1, a peak of 378 nm for pure zinc oxide was obtained. In Figure 4-14-a-2, we see that the addition of a small amount of Te shifted the luminescence to 380 nm, and increased the defect luminescence below the band gap. In Figure 4-14-b, we see that the introduction of large amounts of Te shifted the band edge luminescence to ~382 nm, but with this amount of Te, the below band edge emission dominated the spectrum.

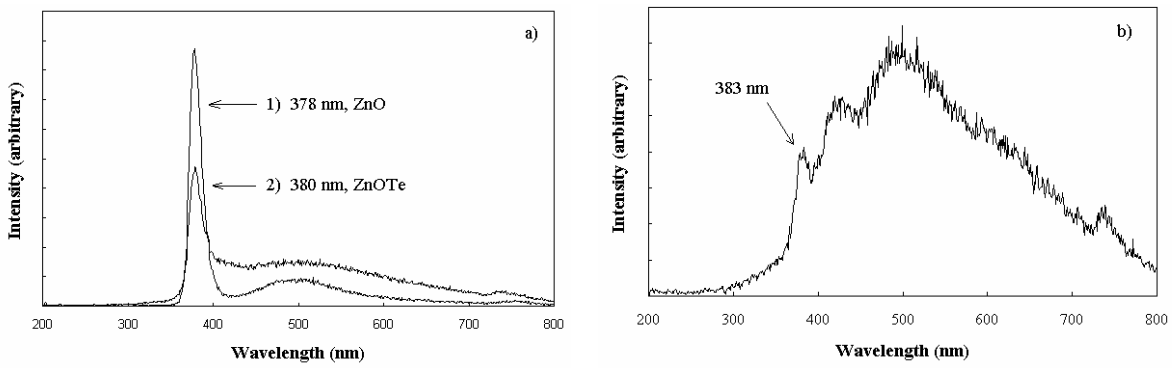

Fig. 4-14. Cathodoluminescence for (a-1) ZnO, (a-2) a lower concentration of Te in ZnO:Te, and (b) a higher concentration of Te in ZnO:Te.

X-ray diffraction (XRD) and transmission electron microscopy (TEM) were also used to confirm film quality. Figure 4-15-a shows a typical XRD spectrum for ZnO:Te grown on sapphire (0001). No appreciable shift in x-ray peaks is observed in ZnO:Te films as compared to pure ZnO films, probably owing to the low-resolution of the system. The (0002) peaks for ZnO:Te are comparable in intensity and sharpness to the (0002) peaks of pure ZnO, but the (0004) peaks are usually diminished in intensity. The cross-sectional TEM micrograph of Figure 4-15-b shows a sharp interface between the ZnO:Te film and sapphire, with single-crystal epitaxial growth.

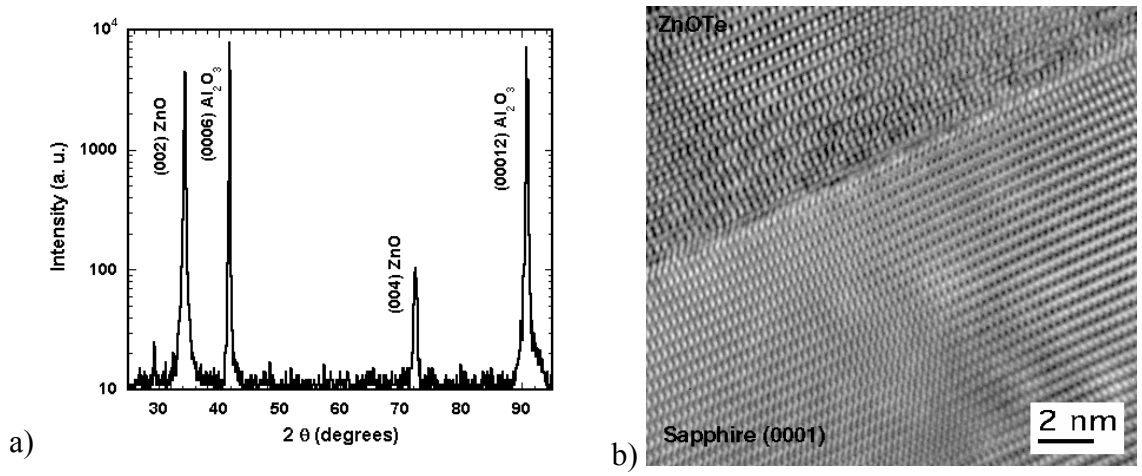

Fig. 4-15. Typical θ-2θ X-ray diffraction (XRD) spectrum for ZnO:Te films grown on sapphire (0001), (a), and high resolution cross-sectional transmission electron micrograph (HRTEM) of the ZnO:Te/Sapphire interface.

X-ray photoelectron spectroscopy (XPS) was also performed on the samples to verify the chemical state of the component elements. An XPS scan was performed on the surface of the samples, and then repeated for the bulk of the film, after a short *in situ* sputtering of about 15 Å off of the surface of the film with Ar^+ ions. Figure 4-16-a shows the change in the oxygen XPS spectrum for the ZnO:Te films from the surface to the bulk. Strong O_2 oxygen peaks are observed at the surface, whereas in the bulk they are absent. In the bulk, only oxides corresponding to metal oxides are found.

A similar trend is found for the tellurium peaks in the XPS spectrum. Figure 4-16-b shows the presence of a tellurite or tellurate peak on the surface of the film, which is absent in the bulk. The bulk shows only the desired telluride state for tellurium. This data, combined with the data for oxygen, suggests that the bulk of the film has only tellurides and metal oxides, as desired, while only the surface of the film still has tellurites and tellurates, as would be expected when the film is exposed to the atmosphere.

This verifies that the tellurium in ZnTe does not revert to the +4 or +6 oxidation state in the presence of ZnO. The undesired compounds, zinc tellurate and zinc tellurite, $ZnTeO_4$ and $ZnTeO_3$, are only observed on the surface, if at all. This is also supported in Pashinkin's report that ZnO and ZnTe do not react to form Zn and TeO_2.[26]

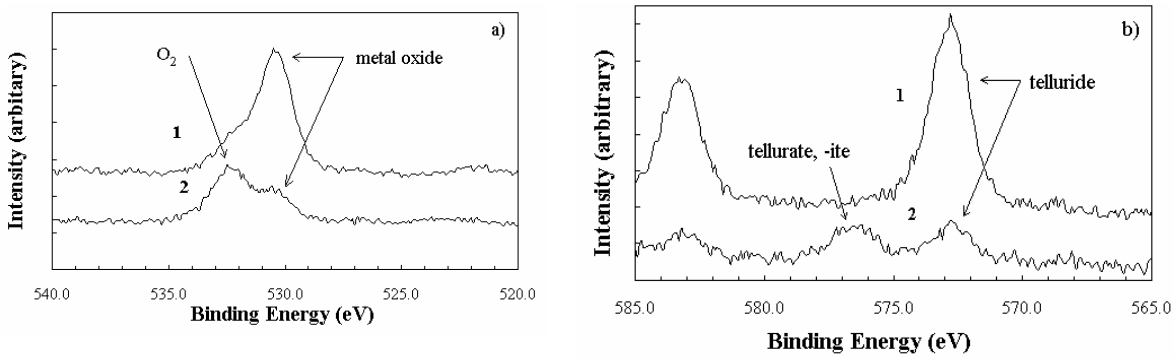

Fig. 4-16. XPS spectrum oxygen peaks for the ZnO:Te films taken both in the bulk (a-1), and on the surface (a-2), and tellurium peaks taken both in the bulk (b-1), and on the surface (b-2).

Rutherford backscattering/channeling (RBS/C) was also performed. A 2.3 MeV He^{++} ion beam and a standard solid-state detector positioned at 160° to detect the backscattered ions was used for this purpose. In Figure 4-17-a, we see ion channeling was obtained for pure ZnO, and indicated a X_{min} value of around 5%, as compared to the ideal value of 3%. In Figure 4-17-b, we see that ion channeling was not achieved for the ZnO:Te films probably due to poor crystal quality at the surface. (In situ sputtering was not attempted prior to RBS/C measurements, and there was no capping layer on the film. Thus considering the tellurites and tellurates discovered through XPS it's not unreasonable to expect more ion scattering near the surface.) Estimates of Te concentration from RBS measurements were not in agreement with other methods, probably due to non-uniformities in the film.

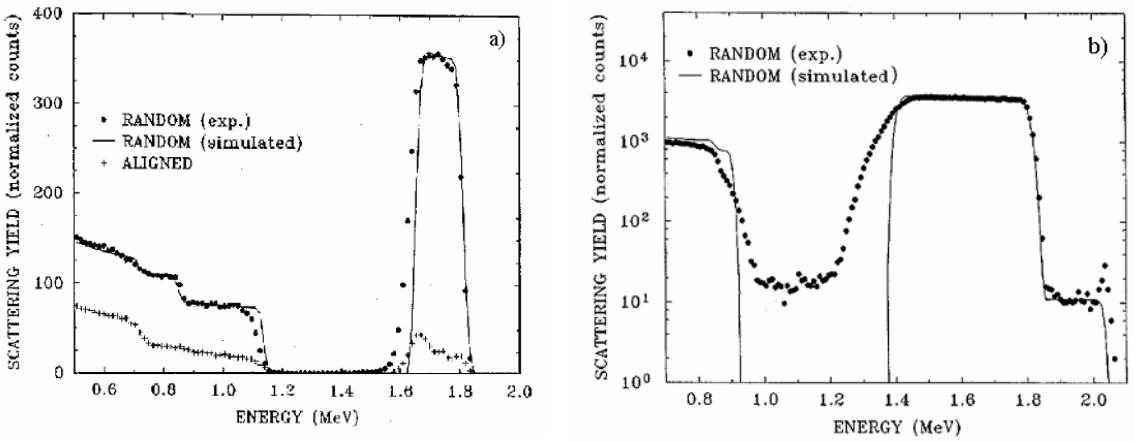

Fig. 4-17. Rutherford backscattering/channeling (RBS/C) spectrum for pure ZnO, (a), and for ZnO:Te, (b), indicating channeling for the pure ZnO, but not for the ZnO:Te.

A Magne-Tron M-700 Resistivity/Conductivity Test System was used to obtain resistivity and carrier type information on the ZnO:Te films. Tests indicated a higher resistivity for ZnO:Te films, as compared with pure ZnO. And the carrier type was inconclusive, as compared to the decisively *n*-type as-grown ZnO films. These findings were also supported by hot-point probe measurements, which indicated slightly *p*-type behavior for some of the films. This suggests that the mere inclusion of ZnTe, without any conventional dopants, has already made a significant improvement to the electrical properties of the films, providing a more intrinsic template upon which *n*- or *p*-type films may be created.

4.5 Nitrogen doping of ZnO with a Kaufman ion source

To achieve nitrogen doping in ZnO films a Kaufman ion source was employed. The experimental technique is introduced in Chapter 3.

A Kaufman ion source accelerates N_2^+ ions towards the sample surface during growth, and because of the impact energy, the N_2 molecules are broken into elemental nitrogen upon impact with the first few monolayers of the sample.

The energy loss rate of ions, during ion implantation, is expressed as:

$$\frac{dE}{dx} = -N[S_n(E) + S_e(E)]$$

where N is the atomic density of the target, and $S_n(E)$ and $S_e(E)$ are the nuclear and electronic components, respectively, of the stopping energy of the ions, as a function of acceleration energy E.[27] Thus, the range of penetration of the ions can be computed as:

$$R = \int_0^R dx = \frac{1}{N}\int_0^{E_0} \frac{dE}{S_n(E) + S_e(E)}$$

Due to the low acceleration energies of the Kaufman source, nuclear stopping power should dominate. This is good, because nuclear stopping power is mostly responsible for damage, and this damage energy is needed to dissociate the molecular nitrogen into atomic species. The ion and the sample differ only by their frame of reference, so while damage energy is normally associated with damage to the crystal, it can also be viewed as damage energy available to the impinging molecule.

The maximum energy transfer per collision is expressed as:

$$E_{Trans} = \frac{4m_1m_2}{(m_1 + m_2)^2} E$$

and the nuclear stopping energy can be estimated as:

$$S_n(E) = 2.8\times10^{15}\frac{Z_1Z_2}{(Z_1^{2/3}+Z_2^{2/3})^{1/2}}\frac{m_1}{m_1+m_2}eVcm^2$$

where finally the energy loss rate of the ions, when nuclear stopping dominates, is written as:

$$\frac{d\mathrm{E}}{d\mathrm{x}}|_N = \frac{\mathrm{N}\pi^2}{2}e^2a\frac{Z_1Z_2m_1}{(m_1+m_2)}$$

where m_1 and Z_1 refer to the ion and m_2 and Z_2 refer to the substrate atomic mass and atomic number. For N_2 implantation into ZnO, the stopping power is approximately 194 eV/nm. Thus for each monolayer, there will be enough stopping power to equal approximately ten times the N_2 bond strength of 9.8 eV/molecule. And with an ion beam of approximately 1 keV we can clearly see that the ions will penetrate several monolayers into the film, and that each monolayer of penetration provides an abundant amount of energy for breaking the N_2 bond.

This method should then incorporate atomic nitrogen into ZnO films, where the nitrogen is free to find substitutional sites. The nuclear damage that induces the dissociation of the molecular nitrogen should not have too much of a negative effect on crystal quality of the ZnO films, since the impact is occurring at high temperature, and the damage very quickly anneals out of the film.

The challenge of calibrating the ion source is finding the right combination of growth conditions that provides enough energy to atomize the nitrogen, and enough nitrogen to dope the sample, but not so much of either to sputter the film itself. It was observed that a suitable beam current was typically around 3.9 mA, with a beam voltage of 1200 V. This somewhat low beam current was achieved by lowering the cathode

current until the discharge current was a little under 0.2 A. It was also observed that the proper functioning of the neutralizer filament was necessary to keep the beam focused on the sample. Films that were grown without the neutralizer did not receive adequate nitrogen flux.

One feature observed in most of the ZnO films grown with the Kaufman-type ion source was that the exciton resonance was retained. Figure 4-18 shows a comparison between several typical absorption peaks for ZnO grown both with the ion source, and without the ion source. The absorbance has been normalized to the above-band minimum found in all samples. A possible explanation for the improvement of the absorbance peak is that the ion beam induced doping (IBID) process improves film atomic density. However, the line width of the A and B excitons did not appear to improve proportionally with increase of absorption.

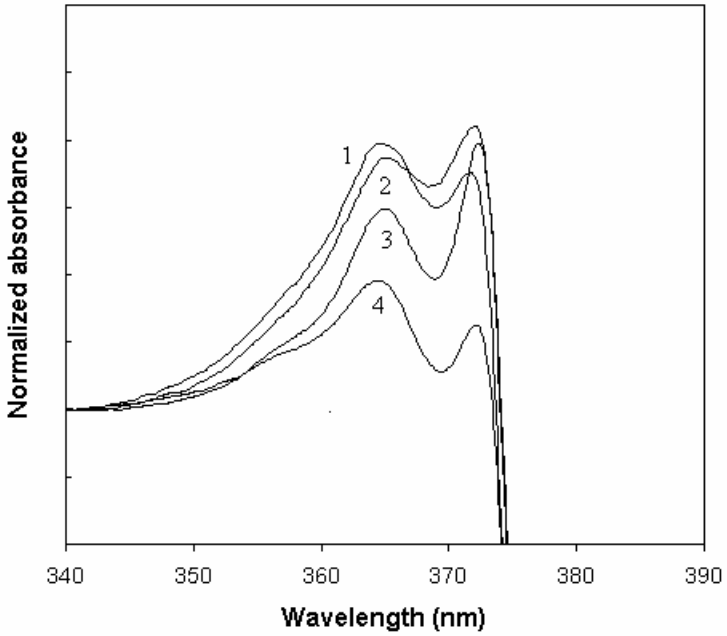

Fig. 4-18. Typical absorption spectrum of (1) and (2) ZnO films grown with IBID, and (3) and (4) ZnO films grown without IBID.

Figure 4-19, however, shows that cathodoluminescence is not improved. For cathodoluminescence a measurable and repeatable reduction in luminescent efficiency, and an increase in sub-band emission (as compared to peak emission), were observed in the films grown with IBID. This is due to the addition of nitrogen in the samples, which increases defect density and reduces luminescent efficiency. These additional defects are not observed in optical absorption, due to the low density of states of defects.

a) b)

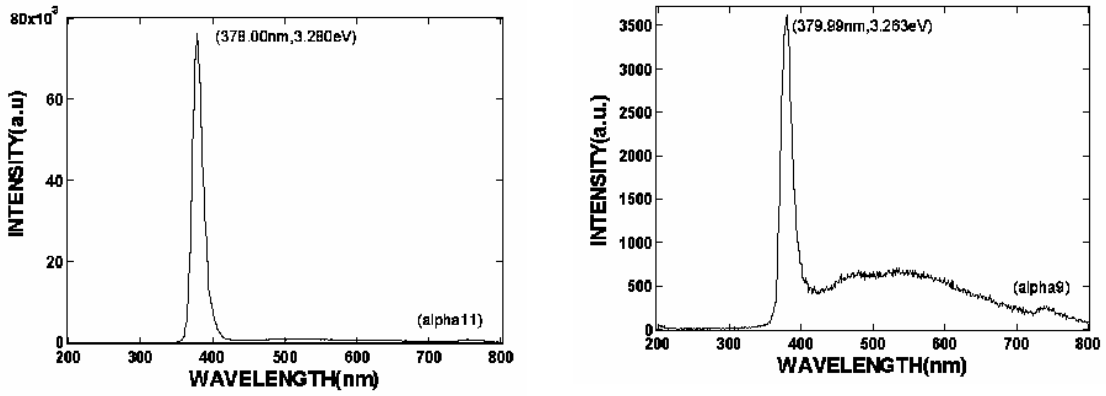

Fig. 4-19. Typical cathodoluminescence spectrum of (1) ZnO grown without IBID, and (2) ZnO grown with IBID.

Figure 4-20 shows a comparison of the low magnification cross-sectional transmission electron micrographs (TEM) of a film grown without IBID to a film grown with IBID. Both films were grown at the higher temperature of around 700^{o} C, without Te. Most noticeably, we see that the film grown with IBID is significantly thinner. This is most likely due to sputtering of the ZnO film during ion bombardment. (Two TEM samples were prepared for both samples, and taken from different parts of the original samples. Both times, similar results were found.) Dislocations were characterized using the **g**·**b** technique, and the film grown with IBID was somewhat higher in screw dislocations, whereas dislocations in the film grown without IBID were mostly mixed.

This seems to indicate that a lower flux of N_2^+ ions, and at a lower energy, would produce thicker films with less screw dislocations. The higher proportion of screw dislocations in the ion bombarded sample may explain the poor cathodoluminescence efficiency, as screw dislocations are often blamed for poor performance in optical devices.

For the film grown without IBID, at the interface, the dislocation density begins at around 10^{10} cm^{-2} and through reactions, goes down to about 10^8 cm^{-2} near the surface. For the film grown with IBID, the dislocations are mostly of one type, so they do not react, and the dislocation density remains constant at around 10^9 cm^{-2}.

a)

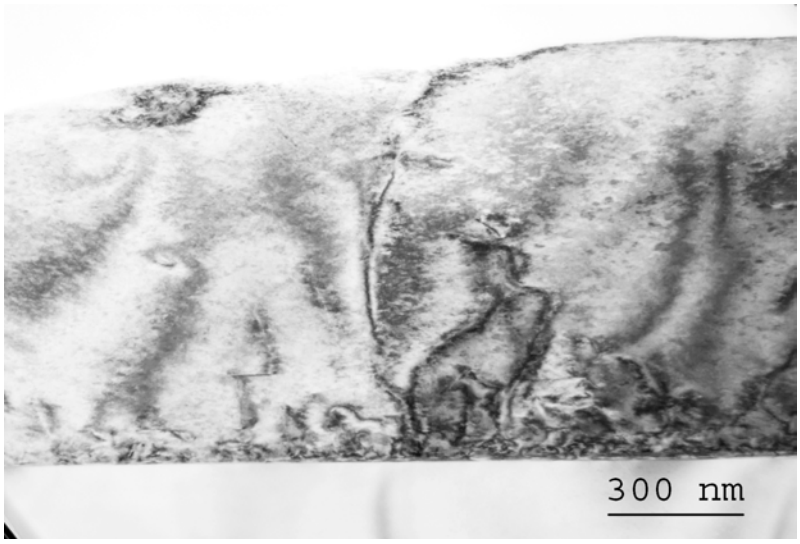

b)

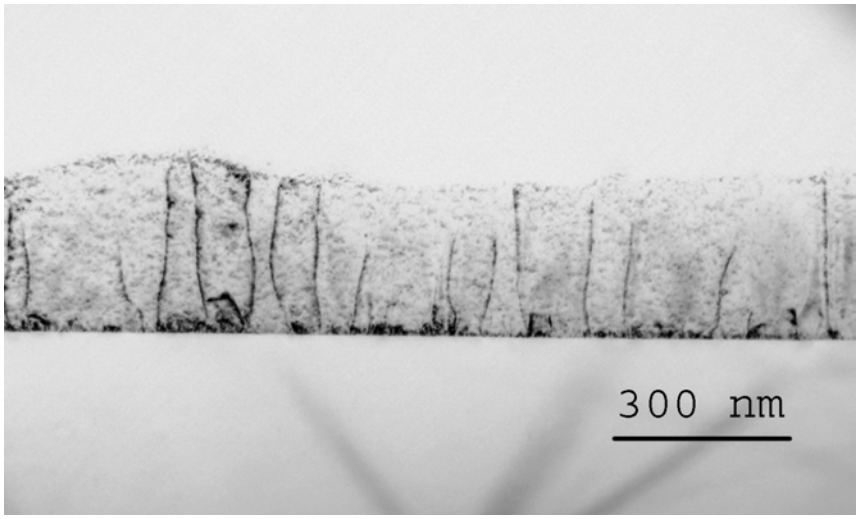

Fig. 4-20. Low magnification, cross-sectional transmission electron micrographs (TEM) of a) ZnO sample grown on sapphire (0001) without IBID, and b) ZnO sample grown on sapphire (0001) with IBID.

A hot-point probe was used after each growth to determine if the films tended to be *p*-type or *n*-type, and for the films that tended to be *p*-type, a van der Pauw Hall effect measurement system was used to more completely characterize the electrical properties of the films. For the films grown without the Kaufman-type ion source IBID, but still with a nitrogen ambient, the films were still mostly *n*-type**,** but their resistivities

(corrected for film thickness) were typically much higher than ZnO films grown without any nitrogen whatsoever. For the films grown with not only nitrogen, but with the Kaufman-type ion source IBID, the resistivities were, on average, double that of the first type of films, and the carrier type was no longer usually *n*-type. Finally, the films co-doped with tellurium demonstrated measurable, and repeatable *p*-type behavior with carrier concentrations in the 10^{17} cm^{-3} range, and mobilities around 0.01 cm^2/Vs. This carrier concentration is as good, or better, than any reported so far.[28] The mobility, however, is not reasonable.

Atomic force microscopy (AFM) studies were carried out on the films grown both with IBID and without IBID. Figure 4-21 shows a comparison of the two results. The Kaufman ion beam bombardment has given one sample a smoother appearance than the sample grown without ion bombardment. However, in both cases the RMS value of the surface roughness was about the same, 12 nm. This is probably due to sputtering from the ion bombardment, and the differences in surface adatom mobility induced by the kinetic energy imparted by the impinging ions.

a) b)

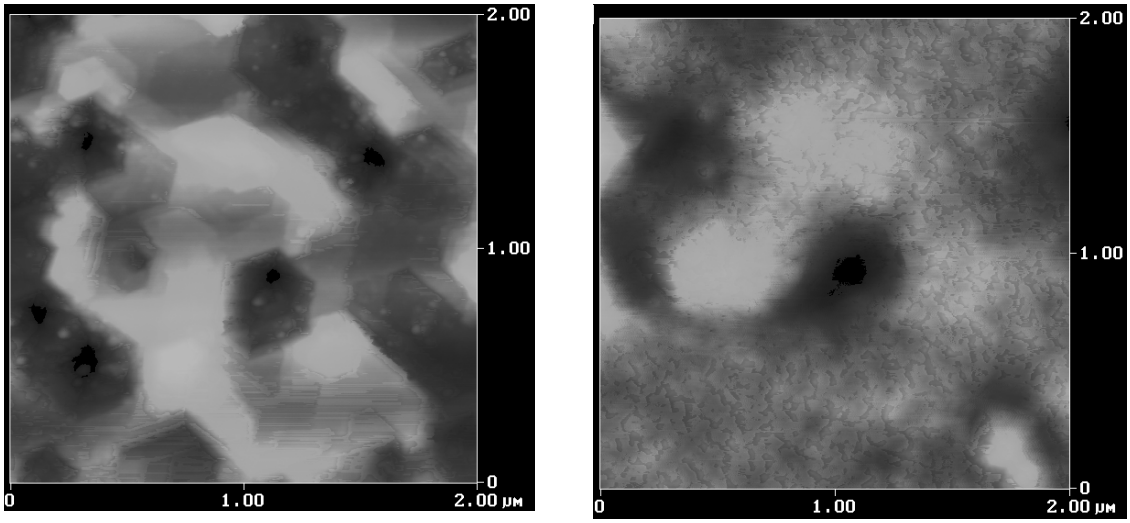

Fig. 4-21. Atomic force micrograph (AFM), taken in tapping mode of a) ZnO film grown without IBID, and b) ZnO sample grown with IBID.

To verify the nature of the *p*-type behavior, secondary ion mass spectroscopy (SIMS) was performed on the samples using a Cameca IMS-6f instrument operating with a Cs^+ primary beam at 14.5 keV impact energy. The ZnN^- profile as a function of depth is shown in Figure 4-22, along with the reference sample used for calibrating concentration. The uniform N concentration of $\sim 10^{21}$ cm^{-3}, when compared to the measured hole concentration of $\sim 10^{17}$ cm^{-3}, indicates a doping efficiency of 0.01%. This suggests, through a simple calculation, that if the nitrogen is indeed the source of *p*-type behavior, it is showing an ionization energy in the 200 meV regime, which is a reasonable value in agreement with expectations.

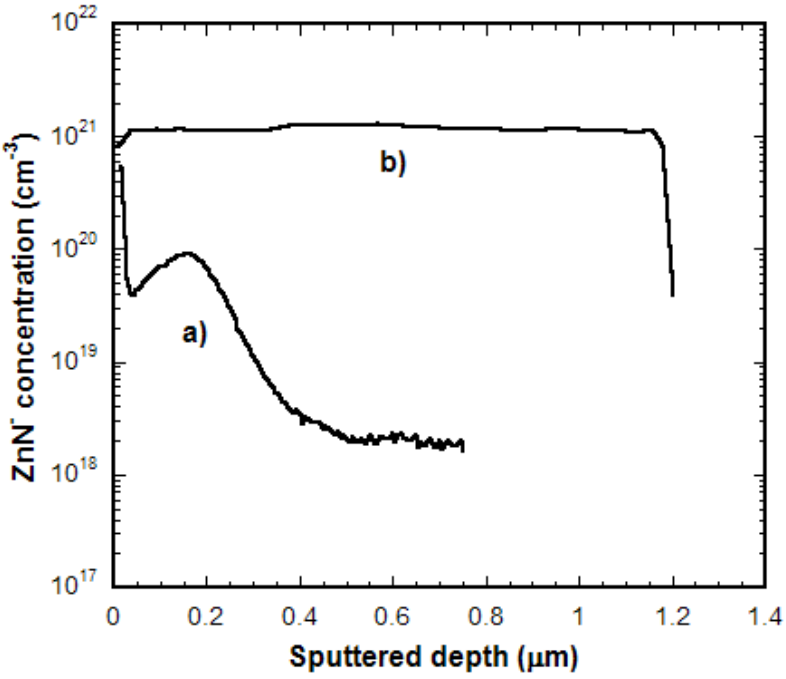

Fig. 4-22. SIMS profile showing nitrogen concentration of a) reference sample, and b) ZnO films grown with IBID and co-doped with tellurium.

The very high nitrogen concentration achieved through Kaufman ion source IBID is due both to the non-equilibrium processing of pulsed laser deposition, which allows equilibrium solubility limits to be exceeded, and also to the use of tellurium, which enhances nitrogen solubility in II-VI semiconductors.[20]

4.6 Low-temperature processing of ZnO:Te films

In a previous section, it was shown that the best temperature for growing ZnO films through PLD is around 700° C. This is not possible, however, for Te doped films, since ZnTe sublimates at around 500° C. ZnO:Te films grown above 500° C are virtually indistinguishable from pure ZnO films.

Because of this, some of the earlier ZnO:Te films were grown between 450^{o} C and 500^{o} C. The problem, however, was that these films had poor crystal structure, including low angle brain boundaries.

The next step was to consider a growth strategy that employed a high temperature buffer layer of pure ZnO grown directly onto the sapphire substrate, prior to the growth of the lower temperature ZnO:Te. In Figure 4-23, we see a schematic of this process illustrating the desired outcome. With the higher temperature buffer layer, it will be easier to begin the growth, where domain matching epitaxy, and a dislocation tangle can form, providing a relatively low dislocation template upon which the lower temperature ZnO:Te film can be grown. This strategy of using a high temperature buffer layer of ZnO to grow low temperature ZnO has been reported by others.[29-31]

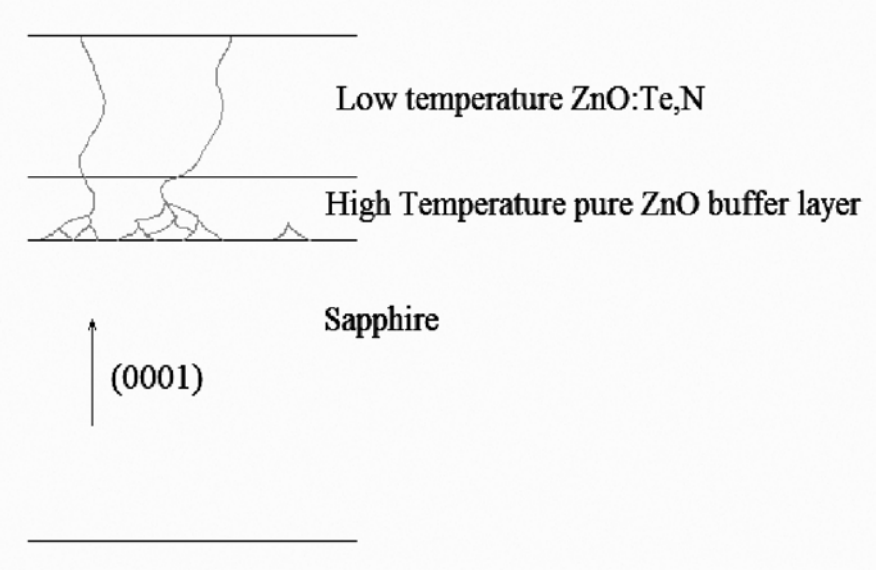

Fig. 4-23. Schematic diagram illustrating the use of high-temperature buffer layers in low-temperature processing of ZnO thin films.

An important question to consider in this study is the role the dopants themselves are playing in the resulting crystal structure of the films. We observed for the ZnO:Te

films grown between 450^{o} C and 500^{o} C that there was a poor crystal structure, but it is impossible to conclude from that information alone that it is the low growth temperature that is causing the poor crystal structure. It may also have been the dopants. Thus, it was necessary for this study to compare films grown both with and without the two-step growth method, and films grown both with and without dopants. Figure 4-24 shows the results of the TEM study. All four possibilities are illustrated with a representative sample. For the sake of thoroughness, the experiment was repeated for each of the four possibilities, and the results were consistent.

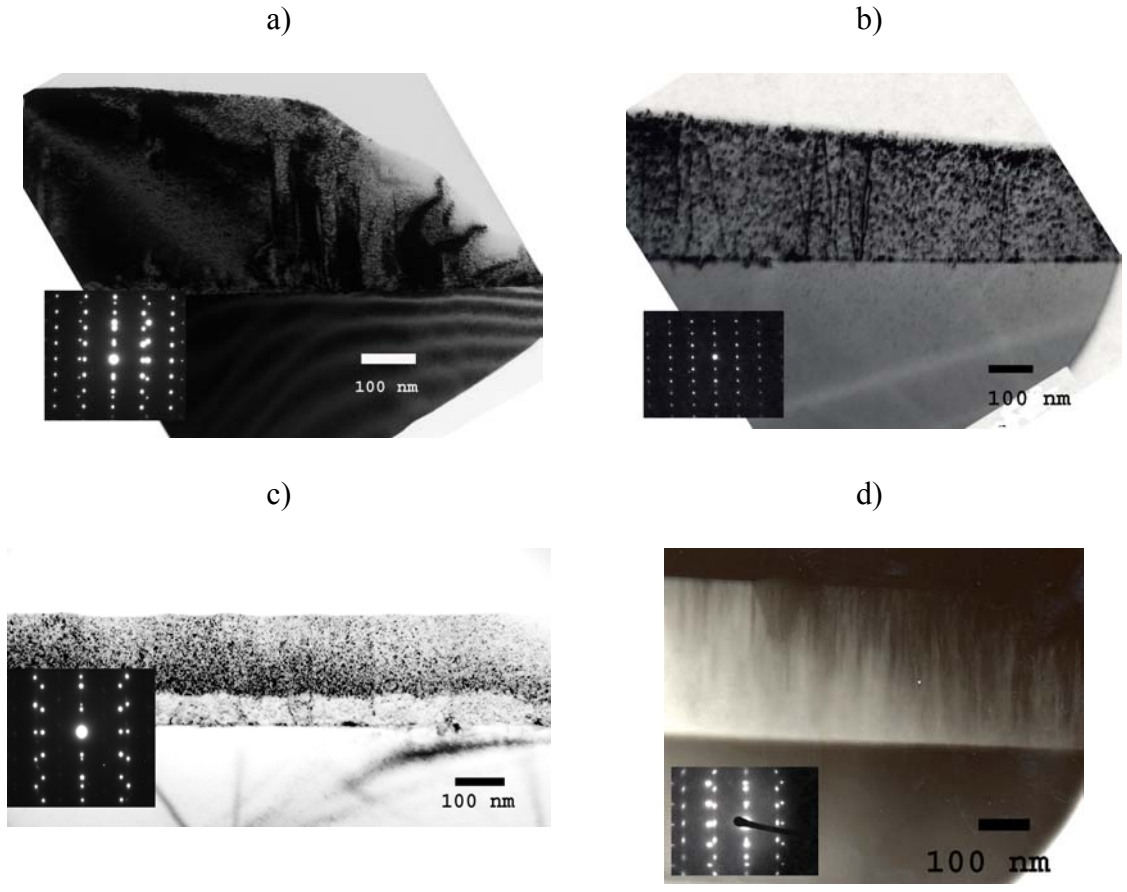

Fig. 4-24. Low magnification transmission electron microscopy (TEM) study of the possible growth conditions, including a) ZnO film grown with the two-step method undoped, b) ZnO film grown at low temperature undoped, c) ZnO film grown with the two-step method and co-doped with nitrogen and tellurium, and d) ZnO film grown at low temperature and co-doped with nitrogen and tellurium.

The results of the study are described in Figure 4-25. For the undoped films, there was fairly good crystal quality for both the two-step grown material, and the low temperature material. There was a slight improvement, however, with the use of the two-step method. In fact, the dislocation density and over-all crystal quality of the two-step grown undoped ZnO was competitive with the best high temperature pure ZnO films. There is a different situation for the doped films. The two-step growth method demonstrates a much more dramatic improvement over low temperature growth, for films doped with Te and N. The low angle grain boundaries are absent for the two-step grown material, and the diffraction pattern shows sharp definite diffraction spots. Contrast is observed between the undoped, high temperature buffer layer, and the doped, low temperature layer. Because of this contrast, it is difficult to see in the micrographs the threading dislocations propagating to the surface of the film, but they are indeed there, as they were observed in the microscope.

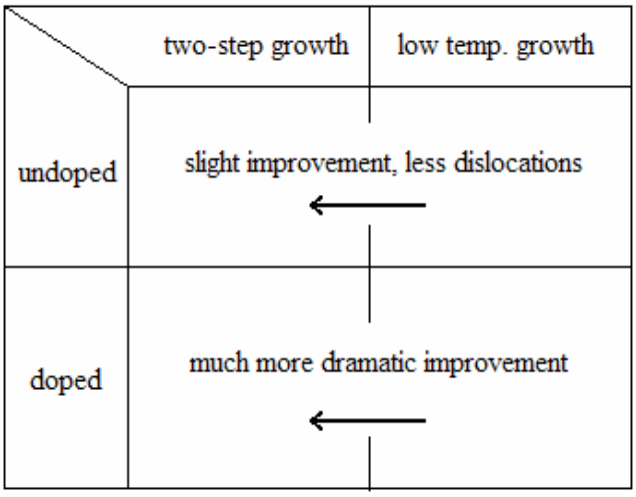

Fig. 4-25. Results summary of growth technique comparison.

Thus, the two-step growth strategy is essential for growing ZnO:Te films. This strategy is beneficial, not only because it allows the incorporation of Te, but also, as has been suggested,[32] low temperature ZnO has less oxygen vacancies, and is easier to dope *p*-type. Thus, the anion-balanced stoichiometry that was proposed in a previous section in this chapter is facilitated through the two-step growth process, since less oxygen vacancies will mean that less ZnTe is needed in the films to create a balance.

4.7 Laser annealing of ZnO:Te films

Due to the problems observed in this study in failing to achieve good RBS ion channeling effects in the ZnO:Te, as compared with pure ZnO, attempts were made at laser annealing these films to improve the ratio of substitutional to interstitial Te atoms. The effectiveness of this technique was examined through optical absorption, which demonstrated improvements in the substitutional Te in ZnO:Te, as evidenced by a shift in band-edge and improvements in excitonic spectra. Also, it is observed that this same laser annealing procedure can be applied to pure ZnO, and to ZnO:N, to improve their over-all optical properties.

One consequence of ZnTe being unstable above 500^{o} C is the fact that it then becomes impossible to use conventional annealing methods on the films above these temperatures. This is a severe limitation, given the importance of annealing in forming *p*-type films.[33]

It is, however, possible to use rapid thermal annealing (RTA) or laser annealing (LA) on these films. The reason is because the Te atoms are so heavy, that in the very

short time the sample is heated, there is not enough time for them to evaporate out of the film. For this study, laser annealing has been employed.

The experimental procedure was described in Chapter 3. An ultraviolet (248 nm) KrF excimer laser was used to pulse anneal the ZnO. ZnO has a very high optical absorption for ultraviolet wavelengths, and the penetration depth is not expected to be more than a few 10's of nanometers for the laser annealing process. Nevertheless, the heat produced by this shallow absorption should penetrate much deeper, at least as much as 100 nm.

In a previous section, a 3 nm shift, from pure ZnO, in band-edge absorption, is reported for ZnO:Te films. Figure 4-26 shows an increase in this band-edge shift, by 0.2 nm from laser annealing a ZnO:Te film. Assuming linearity, this represents a 7% improvement in tellurium incorporation. This experiment was repeated with similar results each time.

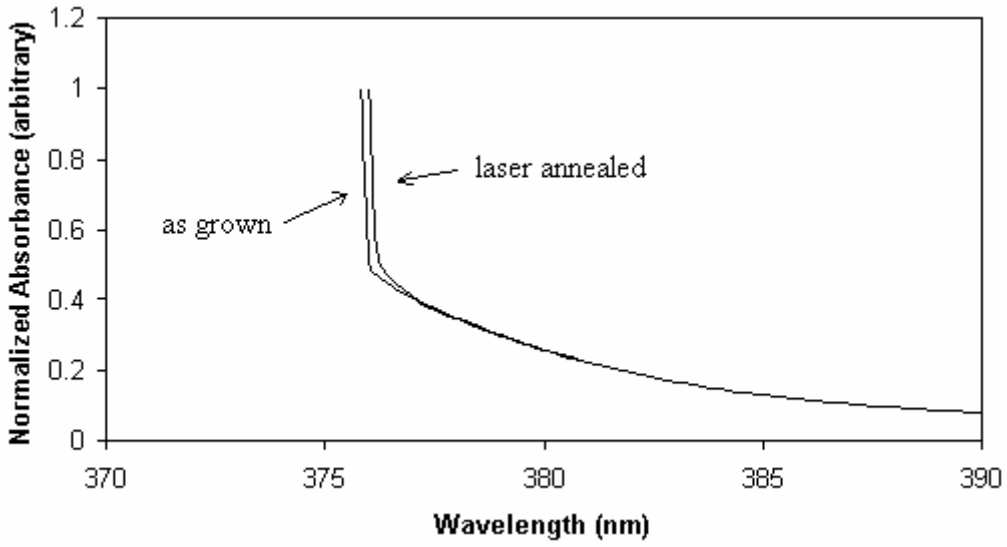

Fig. 4-26. Shift in band-edge optical absorption for ZnO:Te films after laser annealing. (Absorbance has been normalized for comparison.)

This experiment was repeated for pure ZnO samples, and, as is shown in Figure 4-27, a small improvement in exciton intensity was observed in the post-annealed samples. Also, there was an increase in above-band absorbance. (No shift in the position of the band-edge was observed for pure ZnO, reinforcing the conclusion that the band-edge shift observed in the ZnO:Te was indeed due to better Te incorporation.) This improvement in exciton intensity is probably due to an improvement in the crystal structure of ZnO which then improves electron and hole mobility, enhancing the probability of exciton formation.

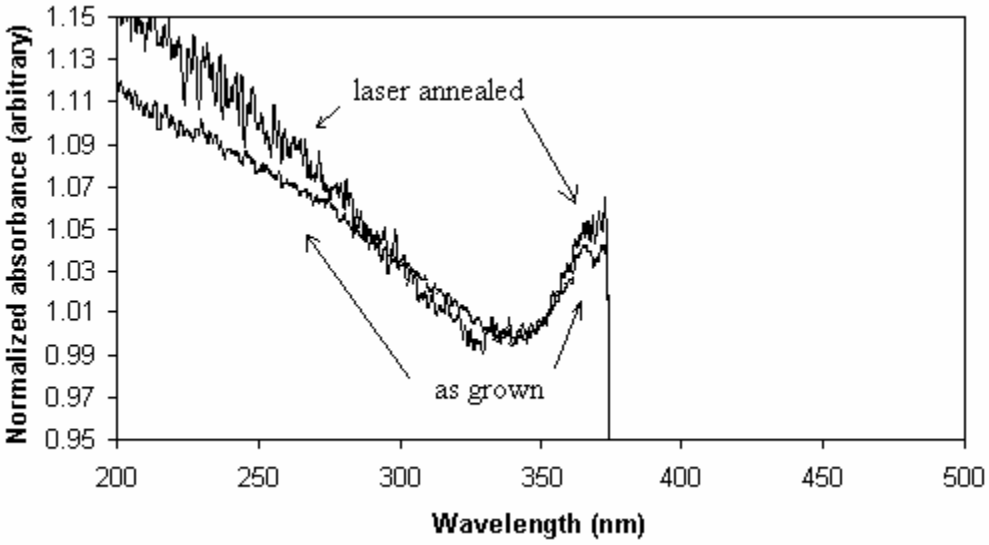

Fig. 4-27. Enhanced exciton intensity in pure ZnO after pulsed laser annealing.

The experiment was then repeated on nitrogen-doped ZnO. If the dosage is too high, the Kaufman ion source nitrogen bombardment sometimes results in considerable exciton broadening effects. These broadening effects were not improved under pulsed laser annealing. However, Figure 4-28 shows sub-band absorbance was reduced, and above-band absorbance was increased. This is also probably a result of improved crystal structure, and a reduction in mid-gap states. It is interesting to note, in Figure 4-28, that

the improvement does not increase by much after a second laser annealing. This demonstrates that changes in optical absorption spectra are not the result of sublimation thinning. The second laser anneal used many more laser pulses than the first laser anneal, on the order of 1000, and if sublimation thinning were a significant issue, then the effects would have been all that much more pronounced, and they were not.

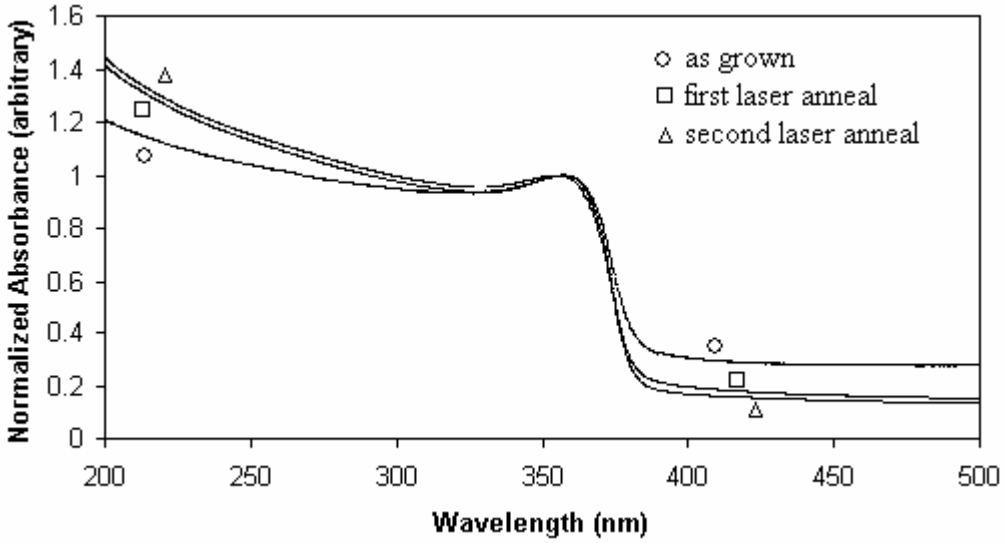

Fig. 4-28. The effects of the first laser anneal, consisting of only a few pulses, and a second laser anneal, consisting of about 1000 pulses, on the optical absorption of a ZnO:N film.

Through UV laser annealing, optical properties in the films are improved, and, in the case of pure ZnO, this improvement is attributed to improved crystal structure; whereas in the case of ZnO:Te, it is attributed to improved Te incorporation. The improvements were very modest, however, and no electrical improvements were observed, so the study was limited only to a few samples.

4.8 Resistivity and photoconductivity

Four-point needle probe resistivity experiments were performed on the samples, while they were held in darkness. As was indicated in Chapter 3, the outer needle probes produced a current in the sample, while the inner needle probes measured the induced voltage. The resulting resistivity was then measured according to the equation:

$$\rho = 2\pi s F(\frac{V}{I})$$

where s is the spacing between the probes, and F is a correction factor.[34] If the sample is thin compared to s, but s is small compared to the width of the sample, the correction factors are all equal to 1, and this expression simplifies to:

$$\rho = 4.532 t \frac{V}{I} ohm \cdot cm$$

where t is film thickness.

Accurate and repeatable resistivity measurements were made for all of the samples. In order to explain these resistivities, estimates of nitrogen and tellurium concentrations had to be made. This was done by comparing the SIMS data for two of the samples, to the ion beam current conditions in the Kaufman ion source, in order to estimate the nitrogen concentration; and to estimate the tellurium concentration, the SIMS data for two of the samples was compared to the color of the film. Tellurium doped ZnO has a distinctive brownish color that is darker with Te concentration.

The tellurium atoms, themselves, are not acceptor impurities, but insofar as they are able to compensate oxygen vacancies, and make the films less *n*-type, they can be treated as acceptor impurities, mathematically. Thus we can write:

$$n_{Te} = n_{pure} - eN_{Te}$$

where n_{Te} is the electron concentration after tellurium doping, n_{pure} is the electron concentration before tellurium doping, e is the efficiency of the tellurium, and N_{Te} is the concentration of tellurium.

Thus, it is expected that the resistivity should go up with tellurium concentration, and that is what is observed in Figure 4-29, up to a tellurium concentration of about 0.5%. The breakdown that occurs at around 0.5% is most likely due to solubility issues, which are either causing precipitates to form, or otherwise impeding the efficiency of the tellurium.

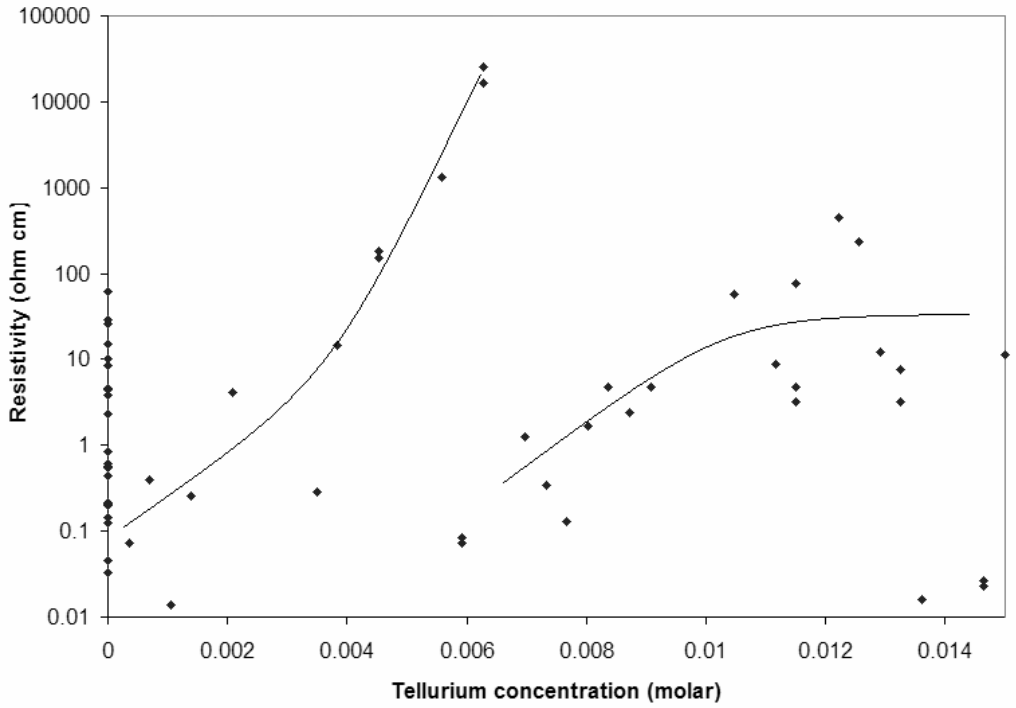

Fig. 4-29. Resistivity versus total tellurium concentration for ZnO films do-doped with nitrogen and tellurium. The points are actual samples grown, and the lines are drawn to show the trend.

There doesn't seem to be a logical trend in the resistivity versus nitrogen concentration graph, but in Figure 4-30, the resistivity versus total dopants graph is

shown, which shows a general upward trend. For the samples that appear to make a straight line at the top of the graph, the resistivity had to be estimated, because it was too high for the instrument to measure.

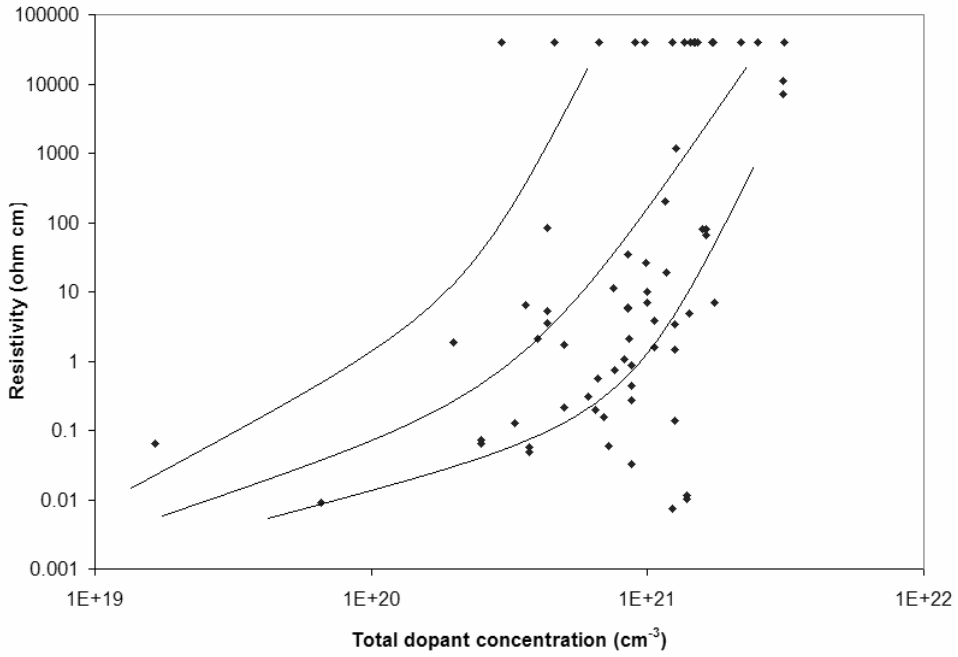

Fig. 4-30. Resistivity versus total dopant concentration for ZnO films co-doped with nitrogen and tellurium. The points are actual samples grown, and the lines are drawn to show the trend.

Very little work has been done on the photoresponse of ZnO under the influence of dopants.[35-39] However, the study of non-equilibrium carrier transport properties, such as photoconductivity, is of vital importance if *p*-type behavior, and bipolar devices, are ever to be achieved.[40] The knowledge gained would not only be useful in understanding the doping and electrical characteristics of ZnO, but the direct application to the formation of solar-blind UV photodetectors would be desirable as well.[41,42]

The photoconductive response of these films is assumed to be extrinsic, since the mobility of holes is much lower than the mobility of the electrons. This would be true for any ZnO film, but it is even more true for these films, since the tellurium impurities have

been blamed for binding holes, and leading to poor *p*-type conductivity.[20] This is useful to know, because it implies that any deep level peaks observed in the photoconductive spectrum are almost certainly due to transitions from deep levels above the valence band into the conduction band. (This is not always discernible from photoluminescence spectra, for example, where it is just as likely a transition can be due to deep levels from either band.)

Since photoconductivity measures changes in conductivity, and those changes are due to increased carrier concentration, the best photoconductors are those which are formed from nearly intrinsic materials. This use of the word "intrinsic" here is not to be confused with "intrinsic" versus "extrinsic" photoconductivity. They have completely different meanings in the two contexts.

Since the photoconductivity is *n*-type, we can write:

$$photosensitivity = \frac{I_{light}}{I_{dark}} = \frac{\sigma_{light} E}{\sigma_{dark} E} = \frac{n_o + \Delta n}{n_o} = \frac{n_o + G\tau}{n_o}$$

by which it is clear that as the equilibrium carrier concentration, n_o, goes down, the photosensitivity goes up. Photosensitivity has been defined here as being a function of G, which is going to depend on how much light is shining on the sample. Therefore, the units of photosensitivity are arbitrary, and it is only used as a means of comparing samples to one another, which have all been illuminated by the same amount of light.

Photosensitivity, as it is defined here, can be related to resistivity by:

$$\rho = \frac{1}{q\mu n_o}$$

since they both have n_o in common. In Figure 4-31, the photosensitivity of various samples is plotted against their resistivity. Also, in Figure 4-31, various theoretical

curves have been plotted indicating how the trend should appear for various mobilities. In the model, Δn is chosen to be 10^{16} cm^{-3}.

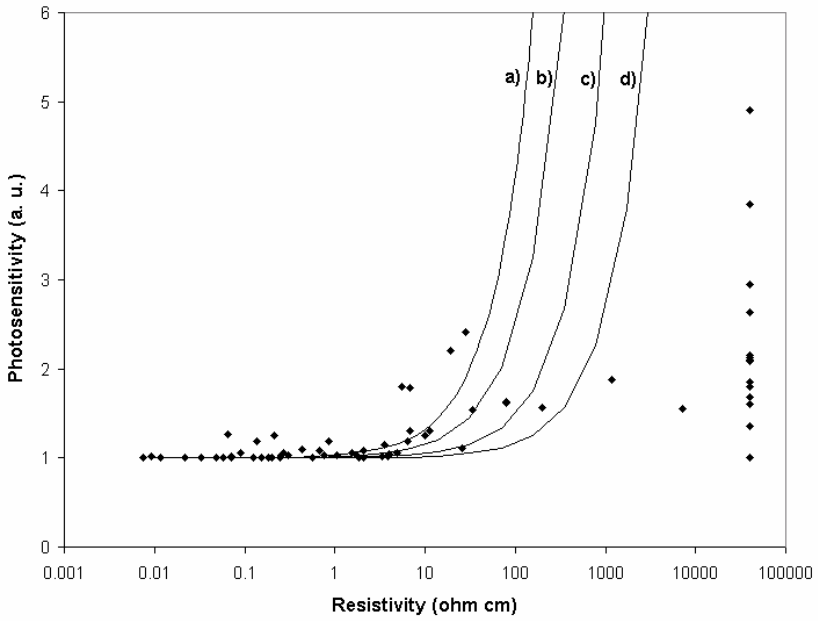

Fig. 4-31. The photosensitivity measured for various co-doped samples versus the resistivity, plotted with the theoretical curves for carrier mobilities corresponding with a) 20 cm^2/Vs, b) 9 cm^2/Vs, c) 3 cm^2/Vs, and d) 1 cm^2/Vs.

Similarly, photosensitivity can be related to dopant concentration, if the dopants are treated equally, and assigned some value for their doping efficiency. In Figure 4-32, the photosensitivity of various samples has been plotted versus their total dopant concentration. Again using the equation:

$$n_{Te} = n_{pure} - eN_{Te}$$

a connection can be made between the dopant concentration and photosensitivity, through n_{Te}, which is the same as n_o in the photosensitivity equation. These curves are also plotted in Figure 4-32 with the empirical data. In the model, n_{pure} is chosen as 5×10^{17} cm^{-3}, and Δn is chosen as 3×10^{16} cm^{-3}. This is not the same Δn used in the model for photosensitivity versus resistivity, but then these models are only being chosen for

illustration, and the exact values are only within the order of magnitude of what is reasonable.

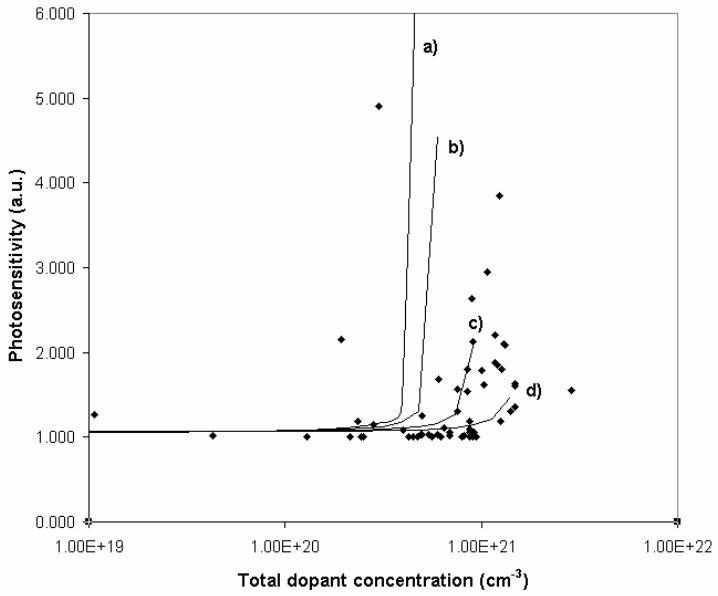

Fig. 4-32. The photosensitivity measured for various co-doped samples versus the total dopant concentration, plotted with the theoretical curves for a) 0.001 doping efficiency, b) 0.0008 doping efficiency, c) 0.0005 doping efficiency, and d) 0.0003 doping efficiency.

In Figure 4-33, photosensitivity, for samples co-doped with nitrogen, is plotted as a function of tellurium concentration. There is a definite maximum at a tellurium concentration of 0.5%. This is the same concentration at which a maximum in resistivity was observed in Figure 4-29. Again, this reinforces the conclusion that there is a solubility limit at 0.5% tellurium, and that the enhanced photosensitivity is related to the increased resistivity.

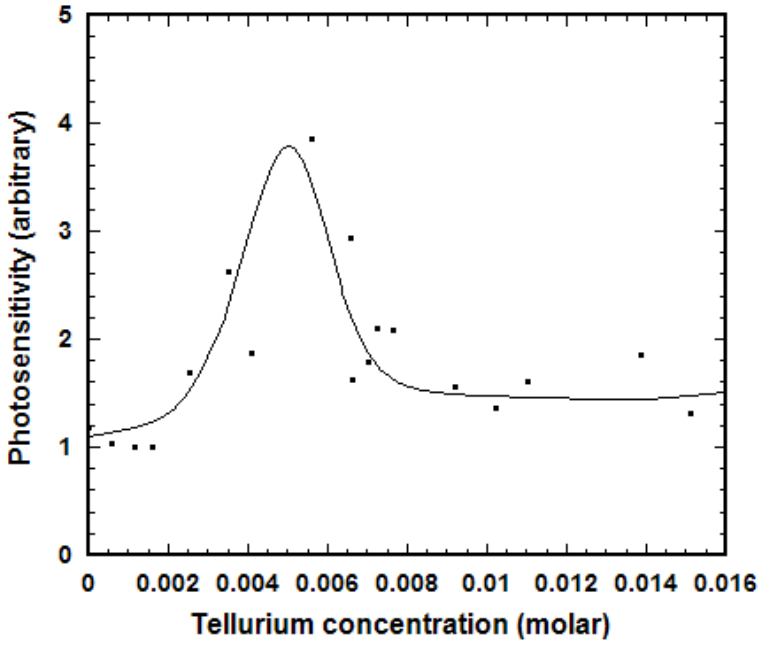

Fig. 4-33. Photosensitivity, taken as the ratio of light current to dark current, of N-doped ZnO films, for various Te concentrations.

Figure 4-34 shows photoconductivity as a function of wavelength for a typical sample doped with tellurium, and for a typical pure ZnO sample. Here, photoconductivity has been defined as the ratio of light current to dark current at a particular wavelength of light. Thus, photosensitivity, which is measured for polychromatic light, can be thought of as the area under the curve of the photoconductivity spectrum. The wavelength dependent data shows a tall band edge photoconductivity for the tellurium doped samples, which verifies band edge enhancement. The bump at 760 nm is most likely due to a grating issue, since 760 nm is exactly twice the wavelength for band edge photoconductivity at 380 nm.

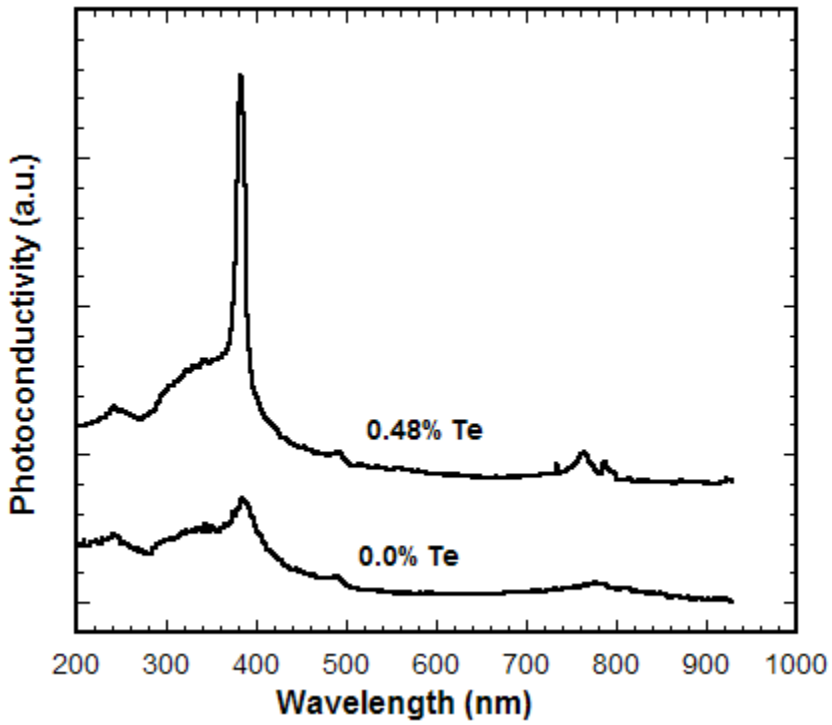

Fig. 4-34. Photoconductive response, as a function of wavelength, for N-doped ZnO films with tellurium concentrations of 0.0 and 0.48 at. %.

Figure 4-35 compares the optical absorption spectrum of a tellurium doped sample to the photoconductivity spectrum of the same sample. Not surprisingly, the band edge in photoconductivity appears at longer wavelengths than optical absorption, and beyond the band edge, photoconductivity falls off, while optical absorption remains strong.[43] The reason for this is that optical absorption is more closely related to density of states, whereas photoconductivity measures not only density of states, but their usefulness in conductivity. Deep level photoconductivity is observed very strongly at 460 nm. However, it is either not apparent in optical absorption, or is obscured by interference fringes.

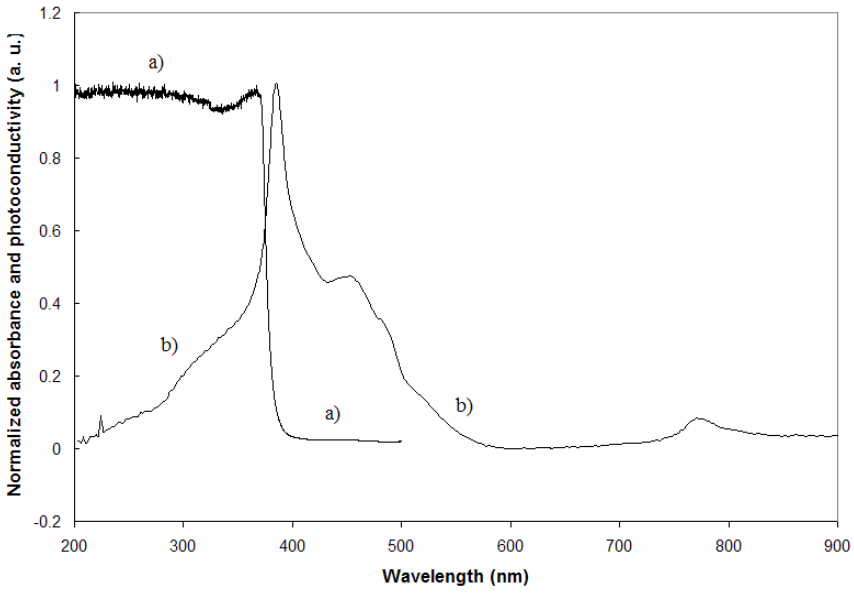

Fig. 4-35. A normalized comparison between a) optical absorption, and b) photoconductivity for the same sample.

It has been suggested that the electronegativity difference between tellurium and the anions in other II-VI compounds is responsible for the tellurium being a trap for holes in II-VI compounds doped with the isoelectronic impurity tellurium.[16-18] If this be the case, it could help explain some of the results of this study. While the tellurium is helping fill the oxygen vacancies of ZnO, and thereby helping establish a good hole concentration in *p*-type material, the tellurium might be trapping those holes, and leading to poor mobility. This could explain the Hall effect results, mentioned in a previous section, that indicated hole concentrations of 10^{17} cm^{-3}, and mobilities of 0.01 cm^2/Vs. Also, it is possible the tellurium is enhancing this photoconductivity by trapping holes, and slowing down the recombination process. Thus in the equation:

$$photosensitivity = \frac{n_o + G\tau}{n_o}$$

photosensitivity might be enhanced not only by making n_o smaller, but also by making τ larger. The only way to confirm or deny this would be to carry out a study on carrier life-times in the doped and undoped films. This is the main point of the next section on photoluminescence.

Another important conclusion from the photoconductivity study is about electron mobility. In the photoconductive process, electron hole pairs are generated, and because of the tremendous difference in mobility, the resulting photoconductivity is mainly *n*-type conductivity. Through non-equilibrium carrier transport phenomena, it has been shown that electron mobility and hole mobility can be independent of each other. The poor hole mobility of marginally *p*-type samples, did not correlate with a similarly poor electron mobility. If that had been the case, photoconductivity would not have been observed. This is important, because it gives the researcher the ability to differentiate between a poor mobility that may be due to poor crystal structure, and a poor mobility that is only due to trapping for that particular carrier type.

4.9 Photoluminescence

Finally, a photoluminescence study was carried out on a few select samples. A sample of pure ZnO was chosen as a control sample. To separate the nitrogen and tellurium contributions to the photoluminescence behavior of the co-doped samples, a sample each of tellurium and nitrogen doping was chosen. Also, a sample with much more than the ideal amount of tellurium doping was chosen. And finally, a sample that was co-doped with nitrogen and tellurium was chosen. For each of the five samples, care

was taken to make sure that each of them was a good representative of its group. The aim of the study was to determine if there was band edge luminescence and stimulated emission for both the undoped and doped samples, and also to determine recombination lifetimes for the different samples.

Firstly, steady-state, room temperature photoluminescence was measured as a function of wavelength for the various samples. The results of these measurements are shown as Figure 4-36. As expected, the strongest near band edge luminescence was found in the pure ZnO sample. Deep level luminescence was stronger in the ZnO:Te sample than it was in the ZnO:N sample, and the deep level peak was shifted from 650 nm in the ZnO:N sample to 550 nm in the ZnO:Te sample. This is due to the different energy levels of the mid-gap states the two different dopants introduce into the band gap of ZnO. For the co-doped sample, near band edge luminescence was significantly weaker.

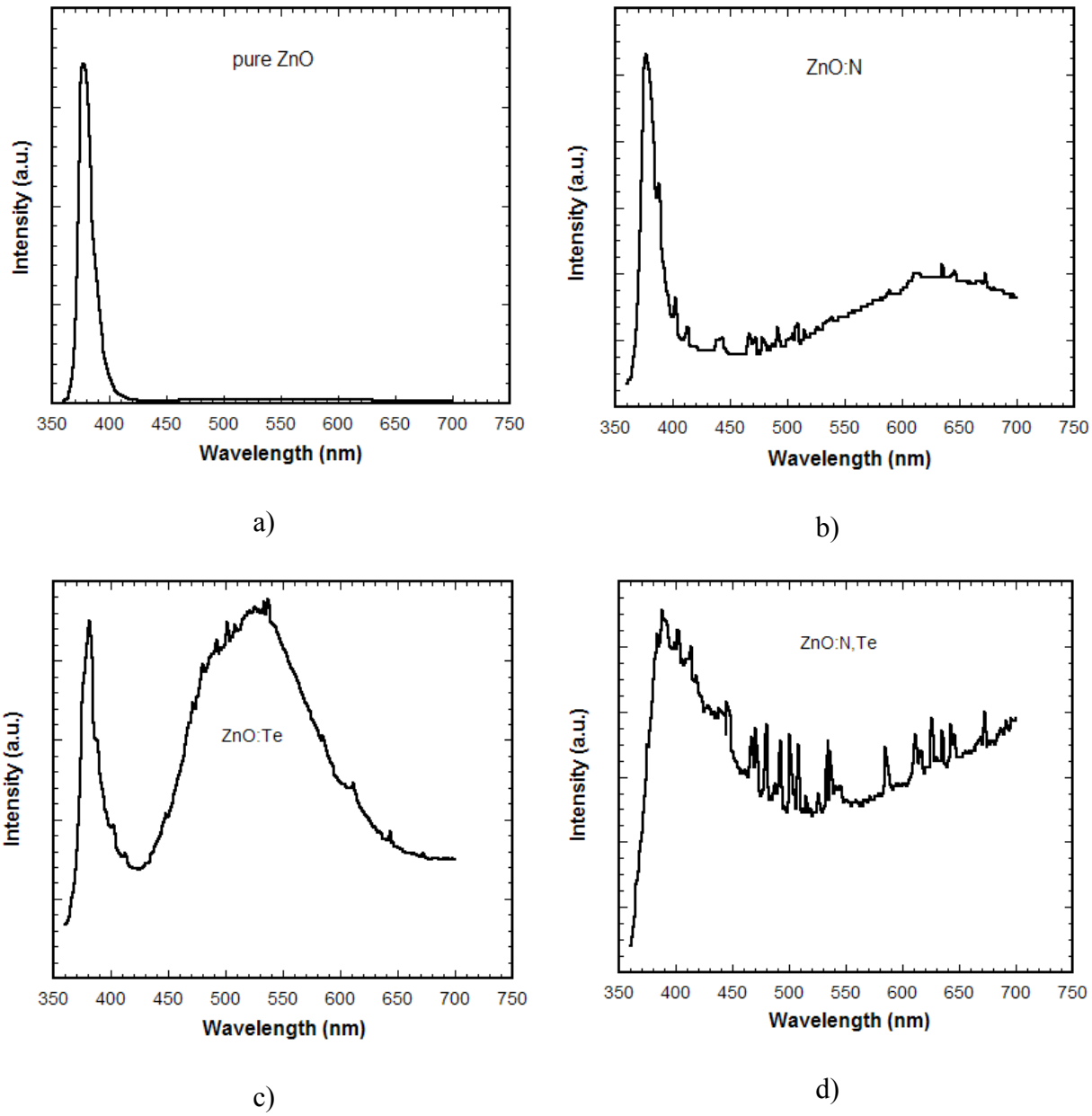

Fig. 4-36. Steady-state, room temperature photoluminescence for a) pure ZnO, b) ZnO doped with nitrogen, c) ZnO doped with tellurium, and d) ZnO co-doped with N and Te.

The time-resolved photoluminescence spectra were taken for several samples, using a streak camera, and spectrally integrated near the band edge. Not surprisingly, the sample which showed the longest carrier life-time was the pure ZnO sample. An exponential curve fit from the raw data produced a value of 132 ps for τ. The assumption

that decay in photoluminescence should exhibit the same time-dependent behavior as decay in excess carrier concentration is based on the assumption that luminescent intensity should always be proportional to excess carrier concentration. The data is shown in Figure 4-37. The co-doped sample demonstrated a decay time not greater than 30 ps. The jitter in the laser system limits the resolution of the system. The streak camera had a resolution of around 30 ps, and this is the value produced from the curve fit for all of the doped samples. This result supports the conclusion that the tellurium is making the films more intrinsic, since the smaller τ suggests n_o must be getting smaller to make the photosensitivity smaller in the equation introduced in the previous section:

$$photosensitivity = \frac{n_o + G\tau}{n_o}$$

This assumes that the generation rate is the same for both cases, which should hold true since the excitation intensity and absorption coefficient are similar. The fact that the inclusion of dopants shortens excess carrier life-time is not surprising, in light of the higher deep level emission. Deep level emission is evidence of the introduction of alternate recombination processes, which often shortens carrier lifetimes.

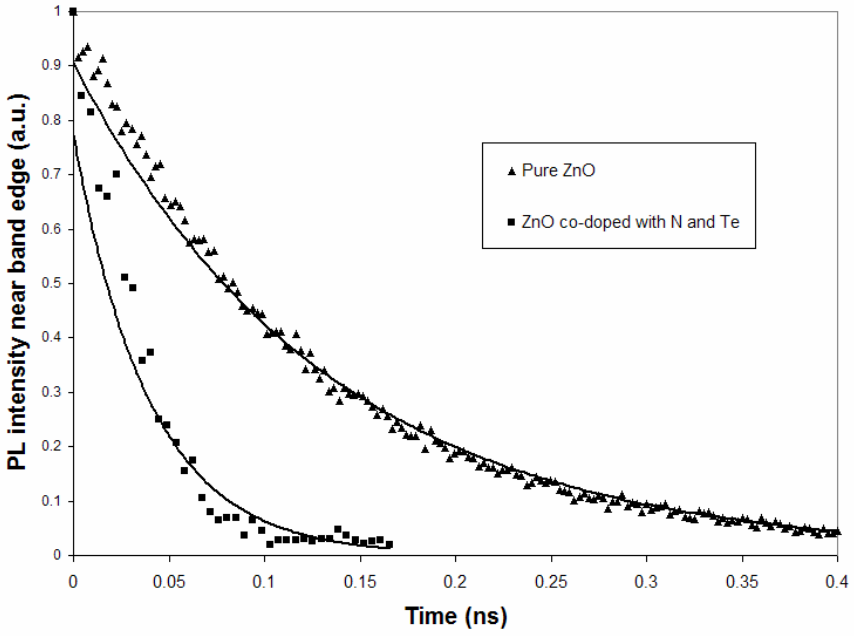

Fig. 4-37. Time-resolved photoluminescence, spectrally integrated near the band edge, for a pure ZnO sample, showing an average recombination time of 132 ps and a co-doped ZnO:N,Te sample, showing an average recombination time no greater than 30 ps.

Intense ultraviolet emission was observed for both doped and undoped samples. As pumping power was increased the luminescence red-shifted to around 390 nm from the original, near band edge luminescence of around 380 nm and began to dominate the spectrum for both samples shown in Figure 4-38. The origin of the photoluminescence is attributed to the formation of electron hole plasma due to the extremely high pumping powers used. The electron hole plasma model explains the high gain and non linear dependence of the optical intensity as a function of pumping power as well as the broadening of the peak with increased excitation intensity.[44,45]

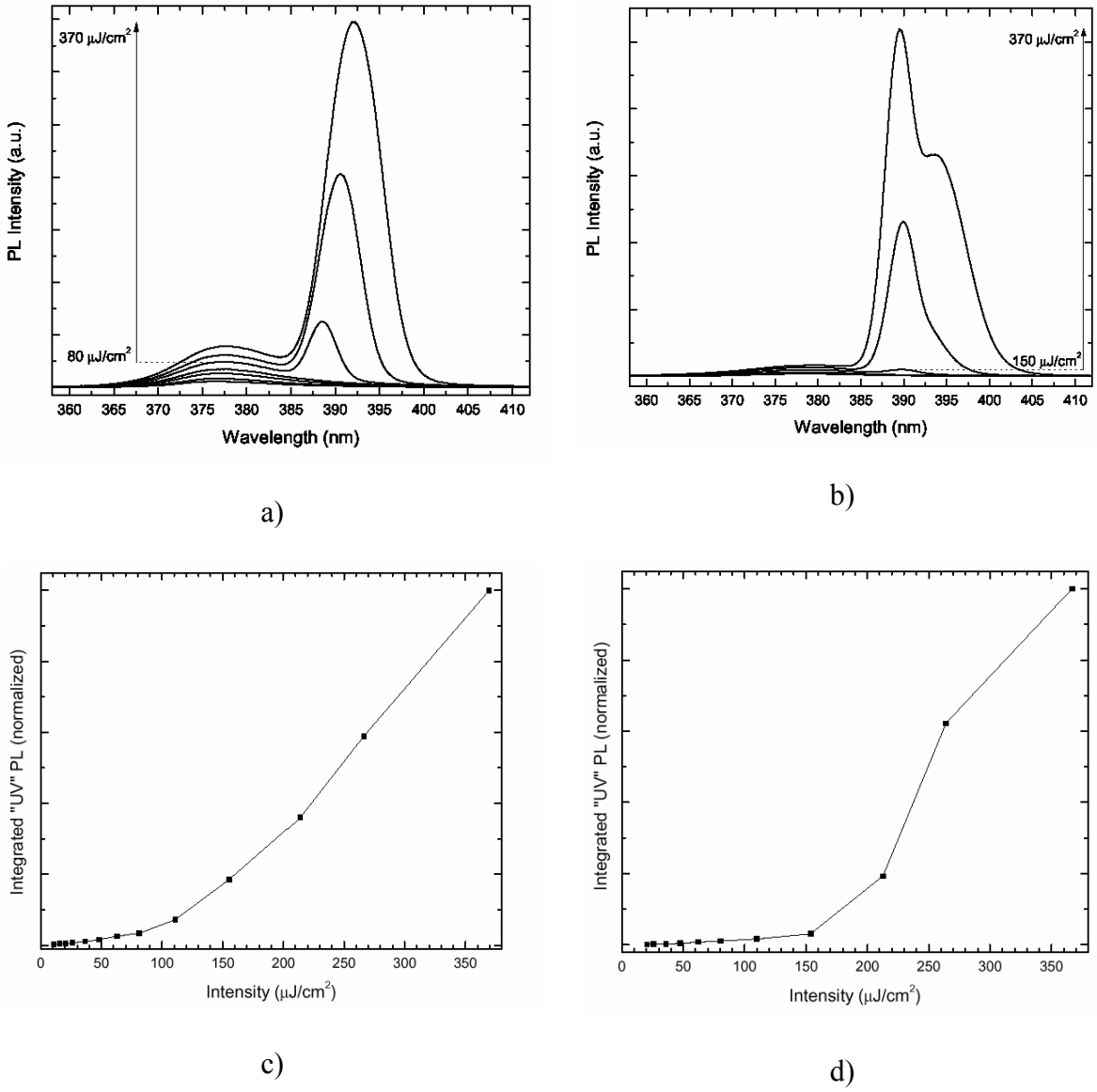

Fig. 4-38. Spectrally-resolved, stimulated emission, for pumping powers ranging from 80 μJ/cm^2 to 370 μJ/cm^2, for a) pure ZnO, and b) tellurium doped ZnO. The threshold curves for c) pure ZnO, and d) tellurium doped ZnO are also shown.

There was no observed exciton-exciton scattering emission in either the pure ZnO or ZnO:Te samples, only a smooth transition between free exciton (FE) emission and electron-hole plasma (EHP). Exciton-exciton scattering has only been observed in ZnO by other groups with samples of the highest quality.[46]

One feature that was only observed in the Te doped samples was the presence of a shoulder on the long wavelength side of the emission peak. This peak did not shift with optical pumping power. The origin of the peak is not clear, but may be associated with a trapping state that is not saturated except under intense excitation conditions.

The two-pump method was employed to investigate the time-dependence of non-linear photoluminescence behavior. The results of the technique known as femtosecond excitation correlation (FEC) are shown in Figure 4-39. The data are spectrally resolved, and normalized to twice the one pump intensity. The pump intensities were deliberately chosen to be above threshold for stimulated emission. Four curves on each graph represent four different pump pulse separation times. The ZnO:Te sample (Figure 4-39-b) shows the greatest non-linear response with a peak in the stimulated emission of almost 15 times twice the one pump case for when the two pumps are at 0 ps separation. This is reasonable because at 0 ps separation, the sample receives the largest power density of above threshold excitation. The ZnO sample (Figure 4-39-a) is actually sub-linear for various wavelengths, and stimulated emission shows the greatest super-linearity when the pump separation is 33 ps. The sub-linear response at 0 ps separation may be due to saturation of power. A deeply red-shifted bump in the 0 ps curve near 410 nm is postulated to be due to coulombic repulsion in the electron-hole plasma (EHP) in the highly pumped material. These characteristics for pure ZnO have been observed by most pure ZnO samples grown in other laboratories and by other methods.

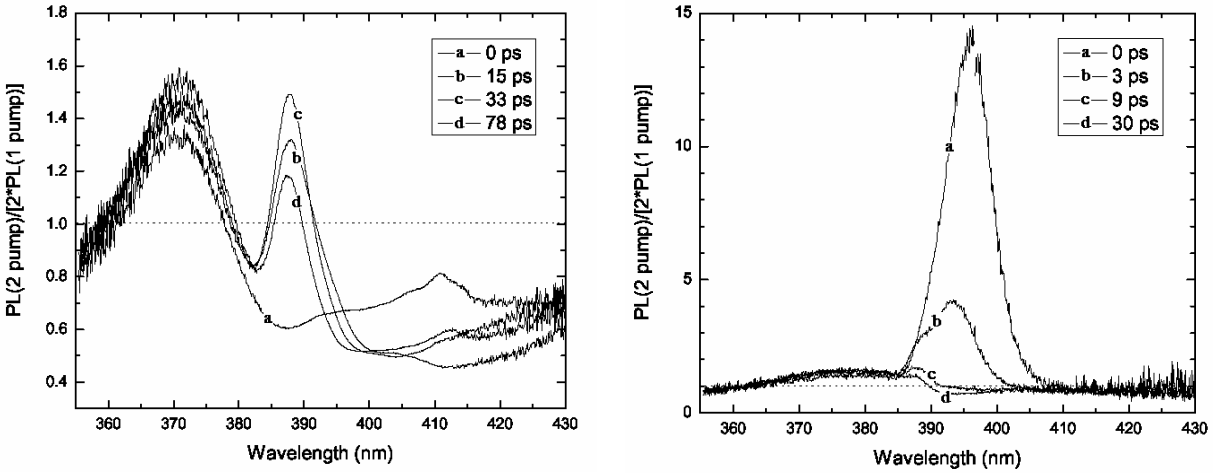

Fig. 4-39. Femtosecond excitation correlation (FEC) showing the intensity of the two pump photoluminescence, normalized to twice the one pump intensity, and for various pump separation times, for a) the undoped ZnO sample, and b) the ZnO:Te sample.

For samples that are heavily doped with tellurium, as seen in Figure 4-40, there is an interesting shoulder in the steady-state photoluminescence spectrum. The shoulder is not observed for this particular sample in photoconductivity. However, there is a similar shoulder observed in the photoconductive spectrum of a different sample, as shown in Figure 4-35. Both samples are doped heavily with tellurium, to concentrations much greater than the optimum. It has been suggested that this shoulder may be due to ZnTe precipitates forming in the ZnO matrix. However, with its band gap of around 2.25 eV, ZnTe would be expected to luminesce at around 550 nm. The shoulders for these two samples appear at around 450 nm, which corresponds to a photon energy of 2.75 eV. It may still be due to ZnTe precipitates, but ZnTe nanodots in a ZnO matrix forms a Type II band alignment, and the recombination process would likely involve an electron in the ZnO conduction band falling into a valence band state in the ZnTe nanodot, which is shifted in energy, due to the small dimensions. What remains unexplained, however, is

why it is visible in photoconductivity only for one sample, and not another, but remains visible in photoluminescence for that sample.

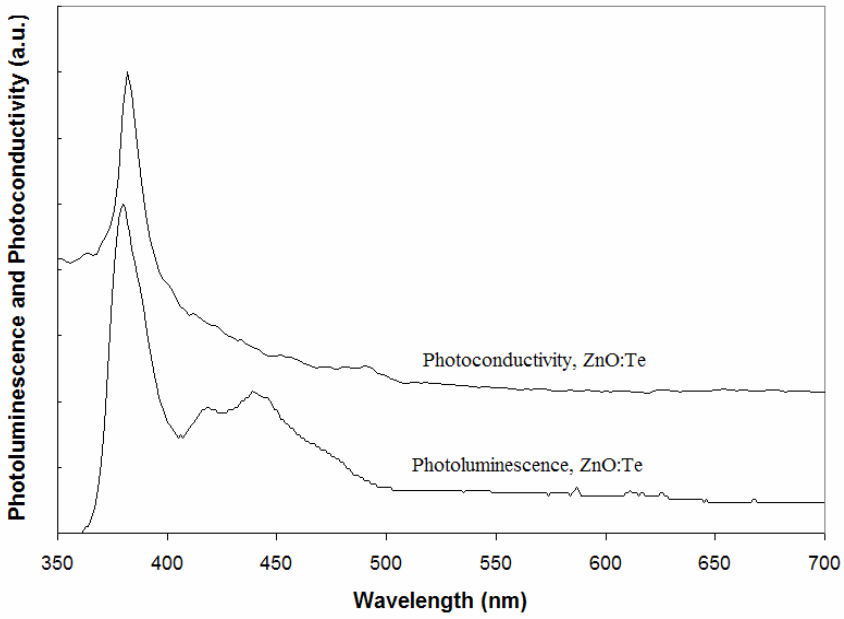

Fig. 4-40. Comparison between the photoconductive and photoluminescence spectra of a heavily tellurium doped ZnO sample, showing the presence of a deep level peak at around 440 nm in the photoluminescence, which is absent in the photoconductivity.

Thus, it has been shown through photoluminescence that the doped samples still luminesce, and can be excited into stimulated emission. It has also been shown that the doped samples have faster recombination lifetimes than the undoped samples. The reason for the shorter lifetimes is defects. At low tellurium concentrations, these are most likely point defects, but at higher concentrations, there may be precipitate formation. The faster recombination lifetime limited the density of the electron-hole plasma. Thus large red shifts in the stimulated emission were not observed and the stimulated emission was more tightly confined and correlated with input optical power.

4.10 Gallium oxide

Single-crystal, thin films of β-Ga_2O_3 on c-plane (0001) sapphire (α-Al_2O_3) substrates were grown by Pulsed Electron beam Deposition (PED). The growth technique is described in Chapter 3, and as indicated, the substrate temperature was found to be optimal when maintained at 850^o C during growth, and the oxygen pressure in the chamber was maintained at 17 mTorr.

The primary focus of this study is that single-crystal (epitaxial) thin films can be grown via domain matching epitaxy[4] on substrates with large lattice misfit and having totally different crystal symmetry. Here, epitaxy is defined as the films having a fixed orientation relationship with the substrate rather than the same orientation relationship, as proposed in the conventional epitaxial framework.

The as-grown films had very high electrical resistance, (~10^6 ohms), indicating good oxygen incorporation. The films were characterized by x-ray diffraction (XRD), (Figure 4-41) and for the films grown above 650^o C, found to be single crystal, and strongly oriented in the $[\bar{2}01]$ direction. This growth mode has been reported by others,[47] and it is attributed to the Ga and O monolayers stacking in this direction.[48]

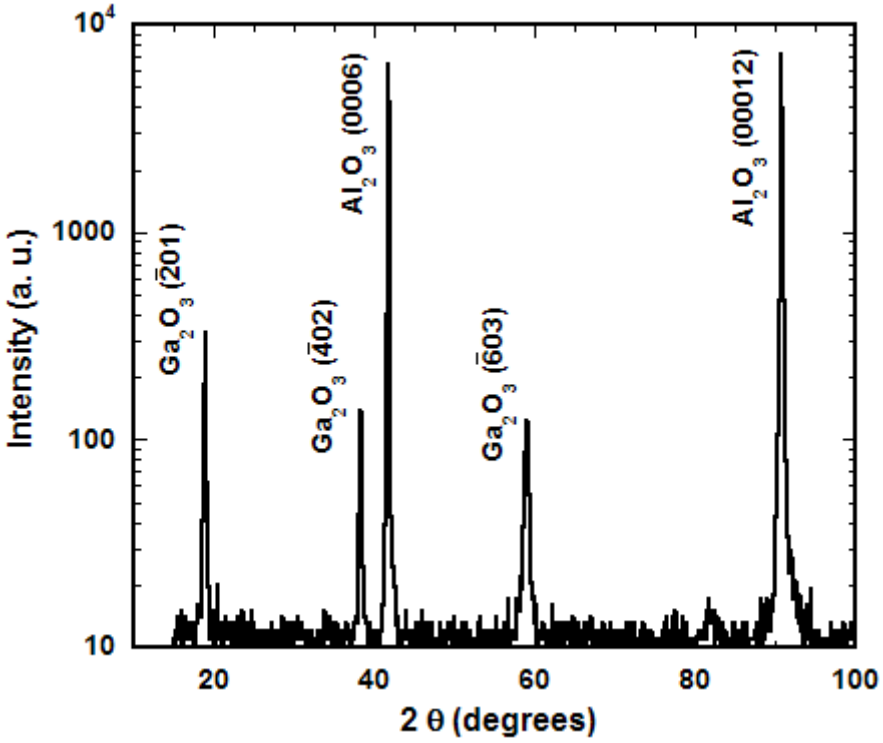

Fig. 4-41. θ–2θ x-ray diffraction spectrum of a sample of β-Ga_2O_3 deposited through pulsed electron deposition (PED) method.

High resolution transmission electron microscopy (HR-TEM) (Figure 4-42) was performed on the sample grown at 850° C. The interface is atomically sharp, and no interfacial reaction is evident. The film is epitaxial with the in-plane orientation to be (010) β-Ga_2O_3 // (01$\bar{1}$0) α-Al_2O_3, and (201) β-Ga_2O_3 // (2$\bar{1}\bar{1}$0) α-Al_2O_3. This orientation has also been reported,[47] and is shown schematically in Figure 4-43. The growth mode is suggested to be domain matching epitaxy, since it is shown that 4 lattice planes of β-Ga_2O_3 in the [010] direction match very closely with 3 lattice planes of sapphire in the [01$\bar{1}$0] direction, and 2 lattice planes of β-Ga_2O_3 in the [201] direction match very closely with 3 lattice planes of sapphire in the [2$\bar{1}\bar{1}$0] direction. The resulting lattice mismatches are -1.6% and +3.13% respectively, which is accommodated by the domain variation principle.[4]

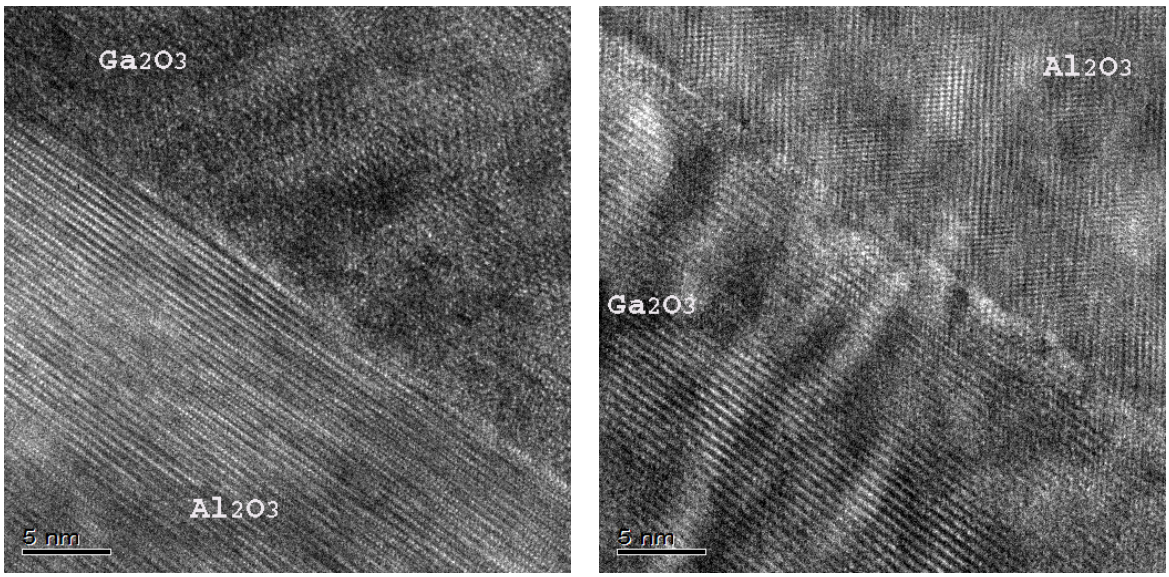

a) b)

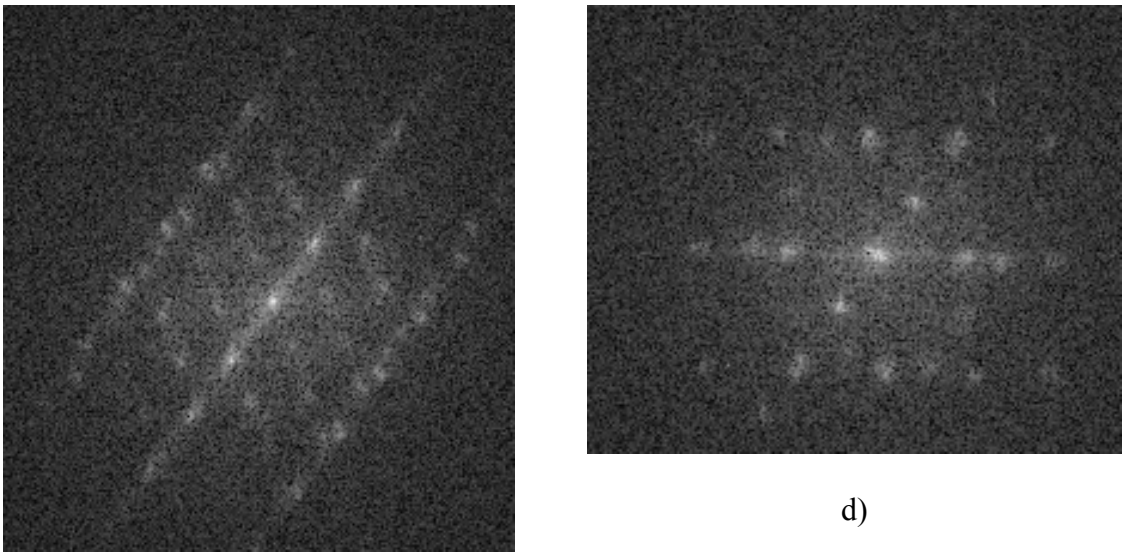

c) d)

Fig. 4-42. High-resolution transmission electron micrographs (HR-TEM) of β-Ga_2O_3 on α-Al_2O_3, where a) is taken from the $(2\bar{1}\bar{1}0)$ zone of sapphire, and b) is taken from the $(01\bar{1}0)$ zone of sapphire. Also shown is c) the FFT taken from the $(2\bar{1}\bar{1}0)$ zone, and d) the FFT taken from the $(01\bar{1}0)$ zone.

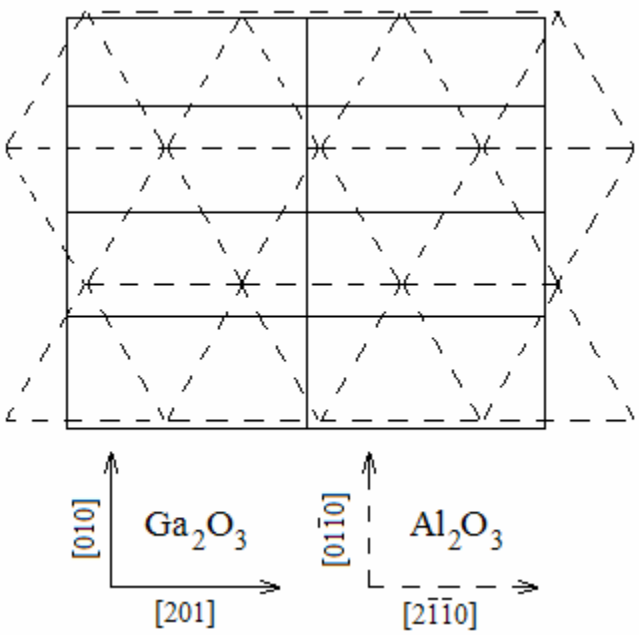

Fig. 4-43. Diagram showing the in-plane crystallographic orientation of β-Ga_2O_3 on α-Al_2O_3, where the [010] direction in β-Ga_2O_3 is parallel with the [01$\bar{1}$0] direction in α-Al_2O_3, and the [201] direction in β-Ga_2O_3 is parallel with the [2$\bar{1}\bar{1}$0] direction in α-Al_2O_3. The lattices of film and substrate are deliberately offset slightly for clarity.

In the DME framework, integral multiples of lattice planes match across the film-substrate interface. If the misfit lies in between the integral multiples, then the residual misfit is accommodated by the principle of domain variations where two domains alternate with a certain frequency to achieve zero residual misfit. It is very interesting to conclude from these results that the epitaxial growth of films can occur on substrates having a different symmetry. This is so, because although β-Ga_2O_3 and α-Al_2O_3 have completely different crystal symmetries in the growth direction, the need for two-dimensional periodicity in epitaxial growth is still satisfied, within the DME framework. It should be noted that epitaxy in the DME paradigm is defined as the film having a fixed orientation rather than the same orientation as the substrate.

Optical transmission measurements were taken on a dual-beam Perkin-Elmer Lambda 5 spectrophotometer. The room temperature optical transmission is shown in Fig. 4 for films grown at various temperatures. There is a general trend towards increased band edge absorption for higher growth temperatures. This is most likely due to improved stoichiometry and crystal structure, which minimize defect related absorption phenomena. When the data is plotted as absorbance squared versus photon energy, the x-intercept of the sample grown at 750^{o} C demonstrates an optical band gap of 4.76 eV, and the x-intercept of the sample grown at 850^{o} C demonstrates an optical band gap of 4.96 eV. These are near the expected value.[49,50] Samples grown below 650^{o} C (Fig. 4-c and d) were not epitaxial, (as observed through XRD), and as such, produced absorption band edges which were dominated by band tailing. The low, below-band transmission percentages for the samples grown at 950^{o} C and 1050^{o} C were due to rough surface morphology, which lowered the apparent transmission of the films in the visible spectrum by scattering light. The high oxygen pressures required for the PED growth process (~17 mTorr), combined with such high growth temperatures, led to a highly oxidizing environment, which produced rougher three-dimensional growth. Samples grown at lower temperatures are smoother, and have better transparency in the visible spectrum, but it is only the samples grown at temperatures around 750^{o} C or 850^{o} C that produce a smooth, as well as epitaxial film with reasonable absorption band edges.

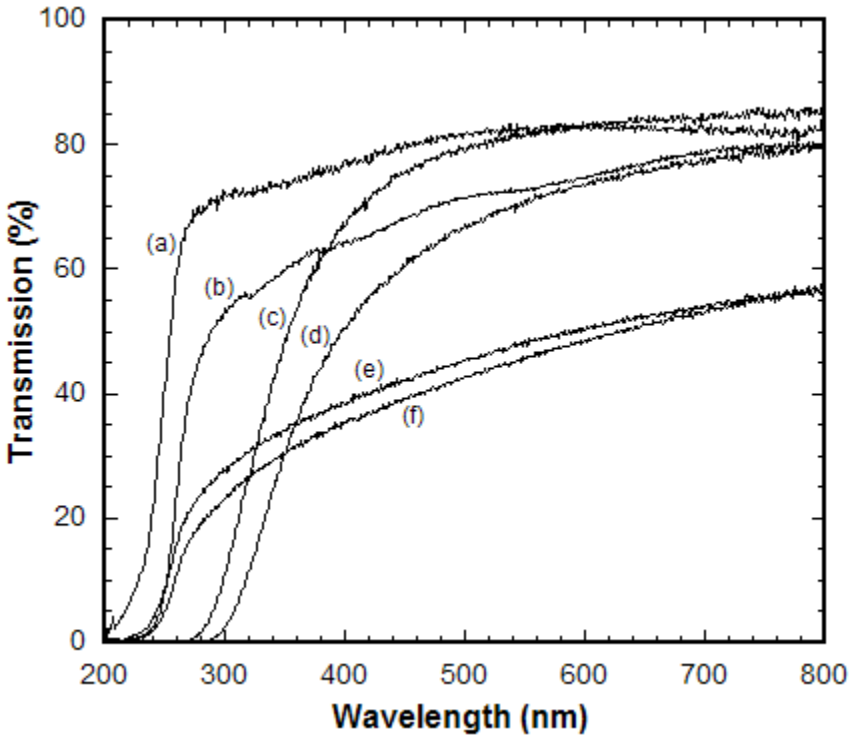

Fig. 4-44. Optical transmission at room temperature of β-Ga_2O_3 films prepared through pulsed electron deposition (PED) method with substrate temperatures during growth of a) 850° C, b) 750° C, c) 450° C, d) room temperature, e) 950° C, and f) 1050° C.

X-ray diffraction, high-resolution transmission electron microscopy (HR-TEM), and optical transmission have been used to characterize β-Ga_2O_3 films grown on sapphire (0001) substrates, through pulsed electron deposition (PED). The films are shown to be single crystal with a fixed orientation relationship with the substrate. The β-Ga_2O_3, having a monoclinic structure, can be grown on α-Al_2O_3, a structure of totally different symmetry, as long as there is integral multiples of planar matching between the film and the substrate, and two-dimensional periodicity is achieved in the growth plane. The growth temperature has been optimized at 850° C, where the film is demonstrated to be both epitaxial, and relatively smooth.

4.11 References

1. A. L. Cai, J. F. Muth, M. J. Reed, H. L. Porter, C. Jin, and J. Narayan, "Effect of growth temperature and annealing on ZnO," presented at Quantum Confined Semiconductor Nanostructures, Dec 2-5 2002, Boston MA, United States, 2002.
2. J. Narayan, K. Dovidenko, A. K. Sharma, and S. Oktyabrsky, "Defects and interfaces in epitaxial ZnO/α-Al_2O_3 and AlN/ZnO/α-Al_2O_3, heterostructures," *Journal of Applied Physics*, vol. 84, pp. 2597-2601, 1998.
3. S. H. Bae, S. Y. Lee, B. J. Jin, and S. Im, "Growth and characterization of ZnO thin films grown by pulsed laser deposition," *Applied Surface Science. First Vacuum and Surface Sciences Conference of Asia and Australia (VASSCAA-1), 1999*, vol. 169-170, pp. 525-8, 2001.
4. J. Narayan and B. C. Larson, "Domain epitaxy: A unified paradigm for thin film growth," *Journal of Applied Physics*, vol. 93, pp. 278-285, 2003.
5. S.-H. Lim, J. Washburn, Z. Liliental-Weber, and D. Shindo, "Transmission electron microscopy of threading dislocations in ZnO films grown on sapphire," *Journal of Vacuum Science Technology A*, vol. 19, pp. 2601, 2001.
6. F. Vigue, P. Vennegues, S. Vezian, M. Laugt, and J.-P. Faurie, "Defect characterization in ZnO layers grown by plasma-enhanced molecular-beam epitaxy on (0001) sapphire substrates," *Applied Physics Letters*, vol. 79, pp. 194, 2001.
7. D. C. Reynolds, D. C. Look, B. Jogai, J. E. Van Nostrand, R. Jones, and J. Jenny, "Source of the yellow luminescence band in GaN grown by gas-source molecular

beam epitaxy and the green luminescence band in single crystal ZnO," *Solid State Communications*, vol. 106, pp. 701-704, 1998.

8. M. K. Ryu, S. H. Lee, M. S. Jang, G. N. Panin, and T. W. Kang, "Postgrowth annealing effect on structural and optical properties of ZnO films grown on GaAs substrates by the radio frequency magnetron sputtering technique," *Journal of Applied Physics*, vol. 92, pp. 154, 2002.
9. K. Vanheusden, C. H. Seager, W. L. Warren, D. R. Tallant, and J. A. Voigt, "Correlation between photoluminescence and oxygen vacancies in ZnO phosphors," *Applied Physics Letters*, vol. 68, pp. 403-405, 1996.
10. J. F. Muth, R. M. Kolbas, A. K. Sharma, S. Oktyabrsky, and J. Narayan, "Excitonic structure and absorption coefficient measurements of ZnO single crystal epitaxial films deposited by pulsed laser deposition," *Journal of Applied Physics*, vol. 85, pp. 7884-7887, 1999.
11. V. Craciun, N. Bassim, R. K. Singh, D. Craciun, J. Hermann, and C. Boulmer-Leborgne, "Laser-induced explosive boiling during nanosecond laser ablation of silicon," presented at Proceedings of the European Materials Research Society 2001 Symposium, Jun 5 2001, Strasbourg, 2002.
12. J. F. Muth, J. H. Lee, I. K. Shmagin, R. M. Kolbas, H. C. Casey, Jr., B. P. Keller, U. K. Mishra, and S. P. DenBaars, "Absorption coefficient, energy gap, exciton binding energy, and recombination lifetime of GaN obtained from transmission measurements," *Applied Physics Letters*, vol. 71, pp. 2572-2574, 1997.
13. T. I. Kamins, "Hall Mobility in Chemically Deposited Polycrystalline Silicon," *Journal of Applied Physics*, vol. 42, pp. 4357-4365, 1971.

14. J. Y. W. Seto, "The electrical properties of polycrystalline silicon films," *Journal of Applied Physics*, vol. 46, pp. 5247-5254, 1975.

15. M. Jain, *II-VI Semiconductor Compounds*, 1st ed: World Scientific Publishing Company, 1993.

16. O. Goede, W. Heimbrodt, T. Lau, G. Matzkeit, and B. Selle, "Optical and RBS Studies of ZnS:Te Thin Films," *Physica Status Solidi A*, vol. 94, pp. 259, 1986.

17. O. Goede, W. Heimbrodt, and R. Muller, "$CdS_{1-x}Te_x$ as Persistence-Type Semiconductor Mixed Crystals," *Physica Status Solidi B*, vol. 105, pp. 543-550, 1981.

18. O. Goede and W. Heimbrodt, "Isoelectronic Impurity Te in $CdS_{1-x}Se_x$ Mixed Crystals," *Physica Status Solidi B*, vol. 110, pp. 175-182, 1982.

19. D. Hennig, O. Goede, and W. Heimbrodt, "Koster-Slater Model for Isolated and Paired Isoelectronic Te Impurities in II-VI Semiconductors," *Physica Status Solidi B*, vol. 113, pp. K163-K167, 1982.

20. Y. Fan, J. Han, R. L. Gunshor, J. Walker, N. M. Johnson, and A. V. Nurmikko, "The Study of Nitrogen Doping in ZnSe and ZnSe:Te," *Journal of Electronic Materials*, vol. 24, 1995.

21. H. L. Porter, C. Jin, J. Narayan, A. L. Cai, J. F. Muth, and O. W. Holland, "Structural, optical and electrical properties of the novel semiconductor alloy $ZnO_xTe_{(1-x)}$," presented at Quantum Confined Semiconductor Nanostructures, Dec 2-5 2002, Boston MA, United States, 2002.

22. J. W. Mayer and S. S. Lau, *Electronic Materials Science: For Integrated Circuits in Si and GaAs*, 1st ed. New York, NY: Macmillan Publishing Company, 1990.

23. N. K. Abrikosov, V. F. Bankina, L. V. Poretskaya, L. E. Sheliova, and E. V. Skudnova, *Semiconducting II-VI, IV-VI, and V-VI Compounds*, 1st ed. New York: Plenum Press, 1969.

24. S. Limpijumnong, S. B. Zhang, S.-H. Wei, and C. H. Park, "Doping by large-size-mismatched impurities: The microscopic origin of arsenicor antimony-doped p-type zinc oxide," *Physical Review Letters*, vol. 92, pp. 155504-1, 2004.

25. A. Brune and J. B. Wagner Jr., "Studies of virtually insoluble systems with large interfacial area: CdTe-ZnO," *Solar Energy Materials and Solar Cells*, vol. 77, pp. 113-124, 2003.

26. A. S. Pashinkin, "Partial pressure diagrams of the systems metal-tellurium-oxygen," *Izvestiya Akademii Nauk SSSR*, vol. 11, pp. 1650-1653, 1976.

27. J. D. Plummer, M. Deal, and P. B. Griffin, *Silicon VLSI Technology*, 1st ed. Upper Saddle River, NJ: Prentice Hall, 2000.

28. D. C. Look and B. Claftin, "P-type doping and devices based on ZnO," *Physica Status Solidi B-Basic Research*, vol. 241, pp. 624-630, 2004.

29. M. Joseph, H. Tabata, H. Saeki, K. Ueda, and T. Kawai, "Fabrication of the low-resistive p-type ZnO by codoping method," presented at Yanada Conference LIV. 9th International Conference on Shallow-Level Centers in Semiconductors, Sep 24-27 2000, Awaji Island, Hyogo, 2001.

30. S. Muthukumar, C. R. Gorla, N. W. Emanetoglu, S. Liang, and Y. Lu, "Control of morphology and orientation of ZnO thin films grown on SiO_2/Si substrates," 2001.

31. H. Tabata, M. Saeki, S. L. Guo, J. H. Choi, and T. Kawai, "Control of the electric and magnetic properties of ZnO films," *Physica B: Condensed Matter*, vol. 308-310, pp. 993-998, 2001.

32. B. M. Ataev, V. V. Mamedov, A. K. Omaev, and B. A. Magomedov, "Epitaxial ZnO films grown by RF-assisted low-temperature CVD method," *Materials Science in Semiconductor Processing*, vol. 6, pp. 535-537, 2003.

33. "MRS Workshop Explored Zinc Oxide Research," in *Materials Research Society Bulletin*, vol. 38, 2003, pp. 314.

34. D. K. Schroder, *Semiconductor Material and Device Characterization*, 2nd ed. New York, NY: John Wiley & Sons, Inc., 1998.

35. P. Sharma, K. Sreenivas, and K. V. Rao, "Analysis of ultraviolet photoconductivity in ZnO films prepared by unbalanced magnetron sputtering," *Journal of Applied Physics*, vol. 93, pp. 3963-3970, 2003.

36. J. C. Simpson and J. F. Cordaro, "Photocapacitance and photoconductance of Bi-doped ZnO," *Journal of Applied Physics*, vol. 69, pp. 4011, 1991.

37. A. N. Gruzintsev, V. T. Volkov, and E. E. Yakimov, "Photoelectric properties of ZnO films doped with Cu and Ag acceptor impurities," *Semiconductors*, vol. 37, pp. 259-262, 2003.

38. N. R. Aghamalyan, E. K. Goulanian, R. K. Hovsepyan, E. S. Vardanyan, and A. F. Zerrouk, "Effect of lithium impurity on the opto-electrical properties of zinc oxide films," *Physica Status Solidi a-Applied Research*, vol. 199, pp. 425-430, 2003.

39. Y. W. Heo, K. Ip, S. J. Pearton, and D. P. Norton, "The near band-edge emission and photoconductivity response of phosphorus-doped ZnO thin films grown by

pulsed laser deposition," *Physica Status Solidi a-Applied Research*, vol. 201, pp. 1500-1509, 2004.

40. J. W. Tomm, B. Ullrich, X. G. Qiu, S. Y., A. Ohtomo, M. Kawasaki, and H. Koinuma, "Optical and photoelectrical properties of oriented ZnO films," *Journal of Applied Physics*, vol. 87, pp. 1844, 2000.

41. D. Basak, G. Amin, B. Mallik, G. K. Paul, and S. K. Sen, "Photoconductive UV detectors on sol-gel-synthesized ZnO films," *Journal of Crystal Growth*, vol. 256, pp. 73-77, 2003.

42. P. Schreiber, T. Dang, T. Pickenpaugh, G. Smith, P. Gehred, and C. Litton, "Solar blind UV region and UV detector development objectives," *Proceedings of SPIE - The International Society for Optical Engineering. Proceedings of the 1999 Photodetectors: Materials and Devices IV, Jan 27-Jan 29 1999*, vol. 3629, pp. 230-248, 1999.

43. R. H. Bube, *Photoconductivity of Solids*, 1st ed. New York, NY: Robert E. Krieger Publishing Co., Inc., 1960.

44. U. Ozgur, A. Teke, C. Liu, S.-J. Cho, H. Morkoc, and H. O. Everitt, "Stimulated emission and time-resolved photoluminescence in rf-sputtered ZnO thin films," *Applied Physics Letters*, vol. 84, pp. 3223-3225, 2004.

45. X. Q. Zhang, I. Suemune, H. Kumano, J. Wang, and S. H. Huang, "Surface-emitting stimulated emission in high-quality ZnO thin films," *Journal of Applied Physics*, vol. 96, pp. 3733-3736, 2004.

46. D. M. Bagnall, Y. F. Chen, Z. Zhu, T. Yao, M. Y. Shen, and T. Goto, "High temperature excitonic stimulated emission from ZnO epitaxial layers," *Applied Physics Letters*, vol. 73, pp. 1038-1040, 1998.

47. H. Ohta, M. Orita, M. Hirano, K. Ueda, and H. Hosono, "EPITAXIAL GROWTH OF TRANSPARENT CONDUCTIVE OXIDES," *International Journal of Modern Physics B*, vol. 16, pp. 173-180, 2002.

48. S. Geller, "Crystal Structure of β-Ga_2O_3," *The Journal of Chemical Physics*, vol. 33, pp. 676-684, 1960.

49. H. H. Tippins, "Optical Absorption and Photoconductivity in the Band Edge of β-Ga_2O_3," *Physical Review*, vol. 140, pp. A316-A319, 1965.

50. M. R. Lorenz, J. F. Woods, and R. J. Gambino, "Some electrical properties of the semiconductor β-Ga_2O_3," *Journal of Physics and Chemistry of Solids*, vol. 28, pp. 403-404, 1967.

5.0 Conclusion

Zinc oxide has received much attention in recent years due to its potential for applications in a variety of ultraviolet (UV) opto-electronic devices.[1-2] It has a wide band gap of 3.437 eV at low temperature, a high exciton binding energy of 60 meV, a high radiation resistance, and it responds well to wet etching.[3] In terms of commercial success, however, zinc oxide has lagged behind another wide band gap material, gallium nitride, because of difficulty in fabricating *p*-type ZnO with good conductivity.

Very little work has been done on the photoresponse of ZnO under the influence of dopants.[4-8] However, the study of non-equilibrium carrier transport properties, such as photoconductivity, is of vital importance if *p*-type behavior, and bipolar devices, are ever to be achieved.[9] The knowledge gained would not only be useful in understanding the doping and electrical characteristics of ZnO, but the direct application to the formation of solar-blind UV photodetectors would be desirable as well.[10-11]

Past work on isoelectronic tellurium in II-VI semiconductor compounds has focused on enhancing nitrogen solubility and *p*-type dopability,[12-13] and enhancing luminescence through exciton binding.[14-17] The present work demonstrates the enhancement of the photoconductive response of ZnO with tellurium.

Since photoconductivity measures changes in conductivity, and those changes are due to increased carrier concentration, the best photoconductors are those which are formed from nearly intrinsic materials. Mathematically we write:

$$photosensitivity = \frac{I_{light}}{I_{dark}} = \frac{\sigma_{light} E}{\sigma_{dark} E} = \frac{n_o + G\tau}{n_o}$$

by which it is clear that as the equilibrium carrier concentration, n_o, goes down, the photosensitivity goes up.

By co-doping with nitrogen and tellurium, intrinsic ZnO with a very high resistivity is achieved. This intrinsic ZnO has a very high photoconductive response, when compared to its dark conductivity, because of the low background carrier concentration.

There also exists the possibility that the photosensitivity is enhanced, not because n_o has gone down, but because τ has gone up. In the above equation, if we assume G does not change—that is to say, we assume the generation rate is not a function of doping concentration—it is also possible an increased τ could result in an increased photosensitivity.

Time resolved photoluminescence (TRPL) studies on the films have shown the opposite to be the case. TRPL has shown that excess carrier lifetimes are much shorter in the presence of either nitrogen or tellurium. This is not surprising, in light of what is known about other semiconductors, such as silicon, where certain impurities are known as "lifetime killers". The addition of impurities, as well as the lower growth temperatures, has increased the defects and introduced mid-gap states which provide a greater variety of non-radiative recombination mechanisms in the crystal. These mid-gap states are clearly visible in the steady-state photoluminescence spectra.

Since it is clear that τ has gone down, one could argue that n_o has not only gone down, but it has gone down by a large amount, to compensate for the fact that τ has also gone down, while photosensitivity has gone up. Again, we are assuming the generation rate remains constant.

This is good news, not only because it strengthens the argument that the films are more intrinsic, but also because the shorter excess carrier lifetimes can be used to build higher speed photoconductive communication devices. Thus, ZnO films co-doped with tellurium and nitrogen are not only more sensitive solar-blind photoconductors, but they are also much faster photoconductors. Excess carrier lifetimes of around 30 picoseconds allow the upper limit of operation speed for a photoconductive communication device to be much greater than one fabricated from pure ZnO, which has an excess carrier lifetime of around 130 picoseconds.

Since the films are highly resistive, and have a low dark current, any photoconductive devices built from these films will have low power consumption, and low heat build up. This is an added benefit for integrated devices, because sapphire is a poor conductor of heat, and heat build up would both increase the background carrier concentration, and shorten the lifetime of the device. The increased carrier concentration would increase the dark current, and make the device less sensitive. Besides speed, sensitivity and long life are the two most important figures of merit for a commercial device.

Several innovative techniques were employed in the fabrication of these films. Also, a number of tests were performed on the films to confirm that certain desirable properties were preserved, and to confirm the conclusions that were derived from initial investigations.

The studies performed on doping issues were carried out on films grown through pulsed laser deposition (PLD). However, some pure ZnO films were grown through pulsed electron deposition (PED) to demonstrate another possible method for carrying

out ZnO research. The films grown through pulsed electron deposition (PED) showed good epitaxial quality, through x-ray diffraction (XRD) and transmission electron microscopy (TEM), but issues related to surface roughness still need to be resolved.

In order to achieve nitrogen doping of ZnO films, a Kaufman ion source was employed. Since the Kaufman ion source accelerates N_2^+ ions at the sample at around 1 kV of potential, it is assumed that impact with the ZnO film will dissociate N_2 molecules into atomic nitrogen.

Another side effect of nitrogen bombardment during growth is sputtering of the film, and lower effective growth rate. This issue was resolved by adjusting the beam current of the Kaufman ion source until a suitable growth rate, and nitrogen flux was achieved. Another parameter that is important to optimize is neutralizer current, since the neutralizer can focus and defocus the beam, which effects the nitrogen flux at the sample.

A study was carried out using low magnification transmission electron microscopy (TEM) to characterize the effect of the nitrogen beam on film quality. Through $\mathbf{g}\cdot\mathbf{b}$ analysis, it was shown that the nitrogen bombarded samples have more screw dislocations, whereas the control samples had more mixed dislocations. As a result of the nitrogen bombarded samples having mostly screw dislocations, there was less reaction of dislocations, and a relatively constant density of dislocations throughout the thickness of the film.

Doping with tellurium was achieved by mixing a small amount of ZnTe in the ZnO target material, prior to pressing and sintering. ZnTe is unstable above ~500^o C, so the final concentration of tellurium in the films was very much a function of growth

temperature. Films grown at 400^{o} C and lower has much higher tellurium concentrations than films grown at 450^{o} C and higher.

A study was carried out to find the optimal growth temperature for pure ZnO grown through PLD. High-resolution x-ray diffraction (HR-XRD) rocking curves were performed on a series of samples grown at different temperatures. It was found that the optimal growth temperature for pure ZnO grown through pulsed laser deposition (PLD) is around 700^{o} C. Therefore, the necessity to use lower growth temperatures to prepare ZnO:Te films raised a number of issues.

The lower growth temperatures had the positive effect of improving oxygen stoichiometry. At the lower temperature, there is less thermal energy to eject oxygen atoms from the growing films, and the resulting stoichiometry of the film is better balanced. This is also observed in the growth of *p*-type GaN, where crystal growers typically lower growth temperatures slightly to improve nitrogen incorporation.

Another benefit from the lower growth temperature is there is less thermal mechanism for ZnTe precipitate formation. Taking advantage of the highly non-equilibrium nature of pulsed laser deposition (PLD), it is possible to grow single crystal films at lower growth temperatures, (than through other methods). As such, conventional, equilibrium solubility limits can be exceeded, and ZnO:Te films grow epitaxially, although the ZnO/ZnTe system is generally considered a "virtually insoluble" system.[18]

It is the tendency for II-VI compounds doped with isoelectronic tellurium to form tellurium clusters.[17] This is observed in the statistical likelihood of tellurium atoms to be second-nearest neighbors, on anion sites, at a somewhat higher than random rate.

However, as long as these clusters are small, (i.e. a few atoms), they are expected to remain in the ZnO lattice, and are not expected to form precipitates.

The biggest challenge with respect to the lower growth temperature is in epitaxial growth. There is a tendency, at lower temperatures, and especially in the presence of dopants, for ZnO films to become polycrystalline, textured films. Since the films are textured, the x-ray diffraction (XRD) may still be very good. It is only through transmission electron microscopy (TEM) that epitaxial growth can truly be confirmed.

To improve the likelihood of epitaxial growth, high temperature buffer layers of pure ZnO were used, prior to growth of doped films, to provide a better template for the doped films to grow on. This was useful, because the beginning of growth process is the most critical for forming a single crystal interface. It is during the early stages of growth that domain matching epitaxy takes place, and subsequently, dislocation tangles can react with each other to form single crystal ZnO. It is important during this early stage of growth that enough thermal energy be available for defect diffusion, so that the necessary processes can occur. Beyond the dislocation tangle, less thermal energy is necessary for subsequent film growth. As such, the strategy of growing a high temperature buffer layer, followed by a lower temperature doped film is a viable strategy for incorporating tellurium dopants into the ZnO films.

Low magnification transmission electron microscopy (TEM) was carried out on films both with and without the high temperature buffer layer, and with and without the inclusion of dopants. Through defect analysis, it was shown that the high temperature buffer layers did, indeed, improve crystal quality. The effect was more dramatic for the doped films than for the undoped films. Undoped films had a pretty good crystal quality

with or without the buffer layers, but doped films without buffer layers had poor crystal quality.

With the use of optical absorption and cathodoluminescence studies it was possible to determine at what tellurium concentration the films began to lose their desirable optical properties. Too much tellurium was shown to quench excitonic absorption, as well as cathodoluminescence.

X-ray photoelectron spectroscopy was used to characterize the chemical nature of the ZnO:Te films. It is not expected that ZnO and ZnTe will react to form any TeO_x compounds,[19] but since the films were grown in an oxygen environment, it was still possible that the tellurium was oxidized, so XPS was used to confirm that this was not the case. XPS spectra were acquired for the surface of the film, and for in the bulk of the film, (through *in situ* sputtering). The surface of the film was found to have tellurites or tellurates, and oxygen in the O_2 state, but in the bulk of the film only tellurides and metal oxides were found.

Rutherford backscattering/channeling was performed on ZnO:Te films. Ion channeling was achieved for pure ZnO films, but not for ZnO:Te films. This suggests that there was a substantial amount of interstitial tellurium in the films.

To solve the problem of interstitial tellurium, it is natural to consider annealing the films. Conventional furnace annealing is out of the question, however, due to the fact that the tellurium in the films is not stable above 500^o C. This leaves only laser annealing or rapic thermal annealing as possible alternatives.

Laser annealing was attempted on several films using a pulsed excimer laser operating in the deep UV. The photons of laser light are not expected to penetrate very

deeply into the ZnO film. However, the heat generation from the pulse of energy should penetrate deep enough to make a difference for most of the film.

Laser annealing was shown, through optical absorption, to shift the band edge of the ZnO:Te films to a slightly lower energy, which would be expected if more tellurium were incorporated into the film. It was also shown that for films which had a small enough tellurium concentration to still have room temperature separation between A and B excitons, that the A and B excitons became stronger with laser annealing. Finally, it was observed that laser annealing lowered the deep level absorption, and increased the above band absorption, suggesting better quality films. The improvements observed from laser annealing were mostly the result of the first few pulses, and were not greatly increased with an increased number of pulses. This is consistent with the observation of others.[20]

Finally, studies were carried out on the pulsed electron deposition (PED) of beta-phase gallium oxide, β-Ga_2O_3. Gallium oxide is another transparent conducting oxide (TCO), which like ZnO, has a number of desirable opto-electronic properties. Epitaxial films of gallium oxide may provide a useful material for fabricating a number of devices in the deep UV, including waveguides, dielectrics, and conducting layers.[21]

Films of β-Ga_2O_3 grown on sapphire (0001) are strongly oriented in the $[\bar{2}01]$ direction, as evidenced through x-ray diffraction (XRD). This has been observed by others.[22-23] Through high resolution transmission electron microscopy (HR-TEM) we were able to demonstrate that the in-plane orientation was such that (010) β-Ga_2O_3 // $(01\bar{1}0)$ α-Al_2O_3, and (201) β-Ga_2O_3 // $(2\bar{1}\bar{1}0)$ α-Al_2O_3.[23] This was predicted, prior to performing the TEM, by using domain matching epitaxy as the model of crystal growth,

and showing that 4 lattice planes of β-Ga_2O_3 in the [010] direction match very closely with 3 lattice planes of sapphire in the $[01\bar{1}0]$ direction, and 2 lattice planes of β-Ga_2O_3 in the [201] direction match very closely with 3 lattice planes of sapphire in the $[2\bar{1}\bar{1}0]$ direction.

Film quality was also confirmed with optical transmission, which showed that the films transmitted around 80% of the light in the visible and near UV. This is important if the films are to be incorporated with optical devices made from materials such as ZnO or GaN, which would operate in the near UV. Finally, the optical band gap was shown to be 4.96 eV for the better films.

5.1 Future work

There are two major branches to suggestions for future work. One of the two branches involves future work on *p*-type ZnO, and the other branch involves future investigations on the samples already grown.

Firstly, considering work on fabricating *p*-type ZnO, the focus is mostly on growing new samples. However, it may be possible to pursue *p*-type ZnO studies from the strategy of annealing the samples already grown. This may be problematic, however, since the ZnTe in the samples is not stable above 500^{o} C, and non-equilibrium annealing strategies, such as rapid thermal annealing (RTA) and laser annealing, would need to be employed. Laser annealing has already been attempted, but the laser wavelength was 248 nm, which is very strongly absorbed by the ZnO, and has a very shallow penetration

depth. A longer wavelength may be useful in future studies on laser annealing of the samples.

Concerning the growth of new samples, it would probably be beneficial to carry out a study of purely nitrogen doped samples, compared to purely tellurium doped samples. This would help isolate the effects of the two dopants on the samples. In the present study, most of the samples were co-doped, and this made it difficult to understand the contributions each of the dopants were bringing to the crystal.

For example, with respect to nitrogen doping, it would be beneficial to perform more calibration studies with a Faraday cup to get a better idea of the flux rate of nitrogen impinging on the sample during growth. This flux rate should be a function of several parameters in the Kaufman ion source, and it would be useful to know exactly how much nitrogen the samples are getting as these parameters are adjusted. The Faraday cup that was used in the present study was fabricated in-house, and was probably not as reliable as a commercially obtained instrument.

For tellurium doping, a much needed improvement would be to achieve greater reliability in control and measurement of tellurium concentration. Tellurium concentration was very much a function of growth temperature, and if that could some how be calibrated, it would be a tremendous improvement. Also, it was difficult to measure the tellurium concentration without SIMS, and SIMS is an expensive technique. If a less expensive means of measuring tellurium (and nitrogen) concentration, such as some optical measurement, could be devised, it would give the researcher a more immediate understanding of the effects of each change in growth conditions.

Cleanliness is always an important consideration for studies on film doping. Any future work would likely take place in a chamber used by other researchers, growing other materials, and the impurities introduced by these other materials is a major challenge to over-come. For the present study, the best way to prevent cross-contamination was to reserve the chamber for several growths, and disregard the results from the first one or two growths. Thus, purity could be improved by coating the chamber with the first growth, and purging unwanted impurities by raising the substrate heater to bake them off. This technique is very time consuming, and not extremely effective. I would suggest future work on doping ZnO to be done in a chamber dedicated only to doping ZnO. This, of course, may not be practical, but is worth suggesting nevertheless.

And for the second branch of suggested future work, concerning investigations on the samples already grown, there is already work in progress to investigate their photoluminescence more carefully. This should hopefully produce more information about defect-related luminescence introduced by the nitrogen and tellurium dopants.

There is still a lot that is not known about these samples. For example, it is not precisely known why there is such a wide range of resistivities and photoconductivities for these samples. The models to predict these values span a wide range of possible mobilities and doping efficiencies. If there were some way to accurately measure carrier concentration and mobility, combined with a more accurate measurement of nitrogen and tellurium concentration, it could shed more light on the effect of the dopants on the samples.

Thus, the key focus of future studies on these samples should be on point defects, and the electrical properties of point defects. The point defects can include not only nitrogen and tellurium, but also to any interstitial complexes they form. Also, it would be useful to try to measure the concentration of oxygen vacancies, and compare it to the undoped case, to provide proof for the theory that the tellurium is filling oxygen vacancies. There are a variety of optical and electrical techniques that could be used to measure these defects, including DLTS, optical DLTS, and plasma resonance.

In addition to materials studies, device studies may also be carried out on the films already grown. As has been mentioned previously in this thesis, the photoconductors that could be built from these samples should have a high upper limit of modulation speed. It would be relatively easy to investigate this by patterning inter-digitated finger structures on the samples and measuring their speed with a fast optical signal. If the masks used to pattern these devices had a range of spacings between the inter-digitated fingers, it would also be interesting to study the transit time, compared to the excess carrier lifetime in the material.

5.2 References

1. D. C. Look and B. Claftin, "P-type doping and devices based on ZnO," *Physica Status Solidi B-Basic Research*, vol. 241, pp. 624-630, 2004.
2. D. P. Norton, Y. W. Heo, M. P. Ivill, K. Ip, S. J. Pearton, M. F. Chisholm, and T. Steiner, "ZnO: Growth, doping and processing," *Materials Today*, vol. 7, pp. 34-40, 2004.

3. D. C. Look, "Recent advances in ZnO materials and devices," *Materials Science and Engineering B-Solid State Materials for Advanced Technology*, vol. 80, pp. 383-387, 2001.

4. P. Sharma, K. Sreenivas, and K. V. Rao, "Analysis of ultraviolet photoconductivity in ZnO films prepared by unbalanced magnetron sputtering," *Journal of Applied Physics*, vol. 93, pp. 3963-3970, 2003.

5. J. C. Simpson and J. F. Cordaro, "Photocapacitance and photoconductance of Bi-doped ZnO," *Journal of Applied Physics*, vol. 69, pp. 4011, 1991.

6. A. N. Gruzintsev, V. T. Volkov, and E. E. Yakimov, "Photoelectric properties of ZnO films doped with Cu and Ag acceptor impurities," *Semiconductors*, vol. 37, pp. 259-262, 2003.

7. N. R. Aghamalyan, E. K. Goulanian, R. K. Hovsepyan, E. S. Vardanyan, and A. F. Zerrouk, "Effect of lithium impurity on the opto-electrical properties of zinc oxide films," *Physica Status Solidi a-Applied Research*, vol. 199, pp. 425-430, 2003.

8. Y. W. Heo, K. Ip, S. J. Pearton, and D. P. Norton, "The near band-edge emission and photoconductivity response of phosphorus-doped ZnO thin films grown by pulsed laser deposition," *Physica Status Solidi a-Applied Research*, vol. 201, pp. 1500-1509, 2004.

9. J. W. Tomm, B. Ullrich, X. G. Qiu, S. Y., A. Ohtomo, M. Kawasaki, and H. Koinuma, "Optical and photoelectrical properties of oriented ZnO films," *Journal of Applied Physics*, vol. 87, pp. 1844, 2000.

10. D. Basak, G. Amin, B. Mallik, G. K. Paul, and S. K. Sen, "Photoconductive UV detectors on sol-gel-synthesized ZnO films," *Journal of Crystal Growth*, vol. 256, pp. 73-77, 2003.

11. P. Schreiber, T. Dang, T. Pickenpaugh, G. Smith, P. Gehred, and C. Litton, "Solar blind UV region and UV detector development objectives," *Proceedings of SPIE - The International Society for Optical Engineering. Proceedings of the 1999 Photodetectors: Materials and Devices IV, Jan 27-Jan 29 1999*, vol. 3629, pp. 230-248, 1999.

12. Y. Fan, J. Han, R. L. Gunshor, J. Walker, N. M. Johnson, and A. V. Nurmikko, "The Study of Nitrogen Doping in ZnSe and ZnSe:Te," *Journal of Electronic Materials*, vol. 24, 1995.

13. H. L. Porter, C. Jin, J. Narayan, A. L. Cai, J. F. Muth, and O. W. Holland, "Structural, optical and electrical properties of the novel semiconductor alloy ZnO_xTe_{1-x}," presented at Quantum Confined Semiconductor Nanostructures, Dec 2-5 2002, Boston MA, United States, 2002.

14. O. Goede, W. Heimbrodt, T. Lau, G. Matzkeit, and B. Selle, "Optical and RBS Studies of ZnS:Te Thin Films," *Physica Status Solidi A*, vol. 94, pp. 259, 1986.

15. O. Goede, W. Heimbrodt, and R. Muller, "$CdS_{1-x}Te_x$ as Persistence-Type Semiconductor Mixed Crystals," *Physica Status Solidi B*, vol. 105, pp. 543-550, 1981.

16. O. Goede and W. Heimbrodt, "Isoelectronic Impurity Te in $CdS_{1-x}Se_x$ Mixed Crystals," *Physica Status Solidi B*, vol. 110, pp. 175-182, 1982.

17. D. Hennig, O. Goede, and W. Heimbrodt, "Koster-Slater Model for Isolated and Paired Isoelectronic Te Impurities in II-VI Semiconductors," *Physica Status Solidi B*, vol. 113, pp. K163-K167, 1982.

18. A. Brune and J. B. Wagner Jr., "Studies of virtually insoluble systems with large interfacial area: CdTe-ZnO," *Solar Energy Materials and Solar Cells*, vol. 77, pp. 113-124, 2003.

19. A. S. Pashinkin, "Partial pressure diagrams of the systems metal-tellurium-oxygen," *Izvestiya Akademii Nauk SSSR*, vol. 11, pp. 1650-1653, 1976.

20. J. Narayan, O. W. Holland, W. H. Christie, and J. J. Wortman, "Rapid thermal and pulsed laser annealing of boron fluoride-implanted silicon," *Journal of Applied Physics*, vol. 57, pp. 2709-2716, 1984.

21. N. Ueda, H. Hosono, R. Waseda, and H. Kawazoe, "Synthesis and control of conductivity of ultraviolet transmitting β-Ga_2O_3 single crystals," *Applied Physics Letters*, vol. 70, pp. 3561-3563, 1997.

22. M. Orita, H. Hiramatsu, H. Ohta, M. Hirano, and H. Hosono, "Preparation of highly conductive, deep ultraviolet transparent β-Ga_2O_3 thin film at low deposition temperatures," *Thin Solid Films*, vol. 411, pp. 134-139, 2002.

23 H. Ohta, M. Orita, M. Hirano, K. Ueda, and H. Hosono, "EPITAXIAL GROWTH OF TRANSPARENT CONDUCTIVE OXIDES," *International Journal of Modern Physics B*, vol. 16, pp. 173-180, 2002.